AD NUMBER

AD880494

LIMITATION CHANGES

TO:

Approved for public release; distribution is unlimited.

FROM:

Distribution authorized to U.S. Gov't. agencies and their contractors; Critical Technology; 30 NOV 1970. Other requests shall be referred to Advanced Research Projects Agency, DoD, The Pentagon, Washington, DC 20301. This document contains export-controlled technical data.

AUTHORITY

AFTAC ltr, 26 Mar 1975

ARPA Program Code No. 9F10

Acknowledgment: This research was supported by the Advanced Research Projects Agency, Nuclear Test Detection Office, under Project VELA-UNIFORM, and accomplished under the technical direction of the Air Force Technical Applications Center under Contract No. F33657-70-C-0100.

HIGHER MODE DETECTION STUDIES

STATISTICAL DISCRIMINATION

Technical Report No. 3

by
William H. Swindell

Stanley J. Laster, Program Manager
Area Code 214, 238-6521

TEXAS INSTRUMENTS INCORPORATED
Services Group
P.O. Box 5621
Dallas, Texas 75222

Contract No. F 33657-70-C-0311
Amount of Contract: $222,240
Beginning 25 August 1969
Ending 14 September 1970

Prepared for

AIR FORCE TECHNICAL APPLICATIONS CENTER
Washington, D. C. 20333

Sponsored by

ADVANCED RESEARCH PROJECTS AGENCY
Nuclear Test Detection Office
ARPA Order No. 624
AFTAC Project No. VELA/T/0702/B/ASD

30 November 1970

DISCLAIMER NOTICE

THIS DOCUMENT IS THE BEST QUALITY AVAILABLE.

COPY FURNISHED CONTAINED A SIGNIFICANT NUMBER OF PAGES WHICH DO NOT REPRODUCE LEGIBLY.

This document is subject to special export controls and each transmittal to foreign governments or foreign nationals may be made only with prior approval of Chief, AFTAC

Qualified users may request copies of this document from:

Defense Documentation Center
Cameron Station
Alexandria, Virginia 22314

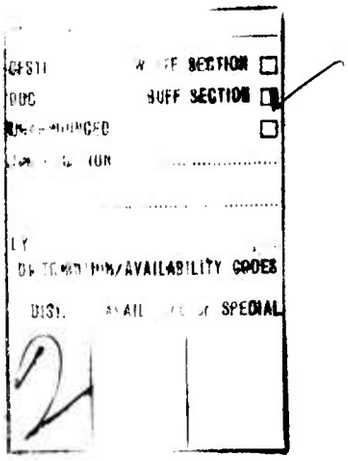

ARPA Program Code No. 9F10

Acknowledgment: This research was supported by the Advanced Research Projects Agency, Nuclear Monitoring Research Office, under Project VELA-UNIFORM, and accomplished under the technical direction of the Air Force Technical Applications Center under Contract No. F33657-70-C-0100.

HIGHER MODE DETECTION STUDIES

STATISTICAL DISCRIMINATION

Technical Report No. 3

by
William H. Swindell

Stanley J. Laster, Program Manager
Area Code 214, 238-6521

TEXAS INSTRUMENTS INCORPORATED
Services Group
P.O. Box 5621
Dallas, Texas 75222

Contract No. F 33657-70-C-0311
Amount of Contract: $222,240
Beginning 25 August 1969
Ending 14 September 1970

Prepared for

AIR FORCE TECHNICAL APPLICATIONS CENTER
Washington, D. C. 20333

Sponsored by

ADVANCED RESEARCH PROJECTS AGENCY
Nuclear Test Detection Office
ARPA Order No. 624
AFTAC Project No. VELA/T/0702/B/ASD

30 November 1970

ABSTRACT

This report presents results of applying a maximum entropy power spectrum analysis technique to detect higher order mode surface waves. The algorithm used partioned each seismogram into time gates representing average group velocities, and spectral analysis was used to determine the periods of the data in the gates. The technique was tested successfully on artificial seismograms containing the Rayleigh and three higher modes of surface waves, with and without additive noise. Maximum entropy power spectrum analysis techniques were applied to an ensemble of 29 long-period seismograms obtained from LASA beams. The long-period seismograms were of both continental and continental-oceanic paths. While several instances of possible higher mode waves were revealed by the analysis, no consistency was found in the occurrence of these modes. Major conclusions were that ME spectrum analysis provides finer details in seismogram spectra than are otherwise available and that it provides an effective method for computing group-velocity frequency curves.

TABLE OF CONTENTS

ILLUSTRATIONS

ILLUSTRATIONS (CONTD)

ILLUSTRATIONS (CONTD)

TABLES

SECTION I

INTRODUCTION AND SUMMARY

It has been suggested[1, 2] that the relative excitation of various modes of long-period surface waves would be useful in determining both the source function and the crustal structure along the propagation path. This report discusses the results of an experiment to use the maximum entropy power spectrum analysis technique[3, 4] as a means of detecting higher order mode surface waves in an ensemble of long-period seismograms obtained from LASA beams. The much higher resolution of the maximum entropy (ME) analysis offered the possibility of determining the presence of higher modes by revealing their characteristic spectral power usually obscured by the "window" effects of conventional Fourier analysis.

Generally speaking, higher mode surface wave energy detection and identification has been accomplished by visual examination of the seismogram, aided by travel time curves. This method is feasible only for small amounts of data and where the event signal-to-noise ratio is large. Higher modes have been observed fairly often when the propagation paths are purely continental and the crustal structure is regular.[5] However, paths combining oceanic and continental structure or which travel through areas which generate multipath effects such as the Kurile Islands yield more complicated seismograms which are less amenable to visual interpretation.

In attempts to automate mode detection so that large amounts of data can be routinely processed, three general types of algorithms have been used to detect and/or separate various higher order surface wave modes from seismograms. The first type uses a set of non-dispersive bandpass frequency filters to filter the entire seismogram. The maximums of the output envelope are plotted as a function of frequency and time.[6, 7]

The second type partitions the seismogram into time gates representing average group velocities and uses spectral analysis to determine the periods of the data in the gates.[7] The third type applies a dispersive wideband filter matched to the mode to be detected.[8] The maximum entropy analysis used for this report is of the second type.

Prior to application to real long-period data, the ME technique was tested on artificial seismograms containing the Rayleigh and three higher modes of surface waves, with and without additive noise. Results of these tests were excellent. The experimentally measured group velocities generally agreed well with the theoretical dispersion curve. It was determined that the ME technique was able to yield a good estimate of the group velocity dispersion down to a mode signal-to-noise ratio somewhere between 10 and 2. This limit was essentially imposed by the amount of time data used for each spectrum. Other results indicated that the LASA long-period data was oversampled considering the frequency response of the seismometers. Prior to analysis of that data, it was antialias filtered and decimated.

The ME analysis technique was applied to 29 vertical component seismograms taken from LASA beam outputs. These events included both continental and continental-oceanic paths. The ME analysis revealed several instances of possible higher mode waves; however, no consistency was found in the occurrence of these higher modes. The effects of multipath were clearly revealed by the maximum entropy technique.

In summary, the major conclusions drawn from the analysis are:

- The maximum entropy spectrum analysis technique reveals much finer details in the spectra of seismograms than is available by other methods of its type
- The ME analysis is capable of excellent estimates of the group velocities of wave modes down to a signal-to-noise ratio somewhere between 10 and 2

- Several instances of possible higher mode surface waves were found. These modes were identified as both first higher order shear mode and "leaking" mode. There was no consistency in the occurence of these modes however
- Events which were geographically close, say less than 30 kilometers, gave very similar group velocity curves. This was true for events from the Gulf of California and the Kurile-Kamchatka Trench

SECTION II

ANALYSIS PROCEDURES

The procedures used to analyze the data for this report were the following:

- The time series of the vertical component of the seismogram of each event was antialias filtered and decimated to provide a new folding frequency closer to the highest frequency of interest, 0.1 Hz
- The decimated seismogram was partitioned into a set of short, overlapping time gates of identical length. The amount of overlap depended on the epicentral distance from LASA
- The maximum entropy power spectrum of each time gate was computed and the spectrum was scanned for peaks
- The frequency, average travel time, and relative spectral power of each peak was plotted so as to build up a frequency vs group velocity curve for each event

The frequency-group velocity plots produced by this procedure are occasionally referred to later in this report as "dispersion" curves. It should be kept in mind that whenever an "experimental dispersion" or "dispersion" curve is mentioned, it refers to a group velocity curve rather than the usual frequency vs phase, group velocity dispersion curves.

The filtering and decimating the data prior to analysis was done to eliminate certain undesirable effects of maximum entropy spectral analysis when applied to highly non-white data. This is discussed in the next section.

All time gates were 25 data points long. This number corresponds to a real-time gate length of 100 seconds for the decimated

LASA data and 133.33 seconds for the theoretical data. The successive gates were overlapped to obtain redundancy between spectra. The shift in time between successive gates depended on the epicentral distance and varied between 10 seconds for events around 1900 km distance and 60 seconds for events 10,100 km away. The artificial data used 64-second displacements at a simulated distance of 5000 km.

The maximum entropy spectrum analysis technique is a relatively new concept and limited information about it is available.[3,4] The basis of this method is the design of a minimum-mean-squared-error prediction error filter on the time series data. If the assumption is made that the average product of the filter output with all previous values of output is zero, then the filter is also the optimum infinitely long prediction error filter and the output has a white spectrum. This corresponds to the maximum entropy assumption that the output has maximum entropy or uncertainty in that a longer filter would not increase the unpredicability of the output. The ME filter was designed to a length of 6 points. As the filter length is increased, the resulting ME spectrum peaks become both sharper and taller. Too long a filter relative to the length of data will introduce spurious peaks indicating decreasing spectral reliability. The 6-point filter allowed up to 5 spectral peaks to be displayed over the frequency range of zero to the sampling frequency without excessive worry about spurious peaks appearing.

Since here the assumption is implicitly made that the ME filter is the optimum prediction error filter, its output is assumed to be white and its frequency response is taken to be the reciprocal of the data spectrum. Thus taking the reciprocal of the filter response yields the estimated spectrum of the data.

When the ME spectrum was scanned and a peak in the spectral density was found, the spectrum in its neighborhood was least-mean-square fitted to a curve of the form

$$P(f) = \frac{a_o}{1 + \frac{4}{b_o^2}(f - f_o)^2}$$

where a_o is the maximum power spectral density of the peak, f_o is the frequency of the peak, and b_o is the -3dB bandwidth of the peak. In turn, this equation, when integrated, provides an estimate of the actual power in the detected spectral line. This technique, suggested by John Burg, leads to more stable estimates than are obtained by simply using the maximum power spectral density.

The travel time of any particular peak was taken to be the difference in time between the event origin and the midpoint of the time gate. After all spectral peaks had been found for an event, the powers were converted to decibels relative to the power of the strongest peak for the event. The peak was then plotted as a circle on the frequency travel-time plot with a number written in the circle signifying its relative power. For example, a "0" would indicate a relative power of 0 dB to -10 dB, a "1" would indicate a relative power of -10 dB to -20 dB and so on.

SECTION III

RESULTS OF TESTS ON THEORETICAL DATA

Unexpected and puzzling results in the form of unusual spectra occurred during initial testing of the maximum entropy spectrum analysis technique, casting suspicion on the validity of the technique. To determine whether or not these spectral peaks were artifacts, a series of tests were made on theoretically generated seismograms of precisely known modal content. In addition to validating the ME method, these tests also attempted to measure its efficacy under various signal-to-noise conditions.

The theoretical modal seismograms, generated under a previous contract, had been synthesized from the solution of the equations describing propagation in a single layer on an infinite half-space. Details of the original work are contained in the published report.[9] Since the original seismograms were direct simulations of an existing analog model, scaling of the physical parameters of the layer model was done to make it a reasonable model, within the scaling constraints, of the earth. The scaling used was to let 1 cm (model) correspond to 20 km (real earth) and 1 microsecond correspond to 4/3 second. This results in the model given in Table III-1.

Table III-1

PHYSICAL PARAMETERS FOR SCALED MODEL

P velocity (km/sec)	S velocity (km/sec)	Density Ratio	Thickness (km)
5.75	3.21	1.0	40
8.23	4.86	--	--

This model is not as close to a typical continental crust as one might desire because (1) the crustal velocity is somewhat too low, (2) the crustal thickness is somewhat too small, and (3) the mantle density

should be larger than the crustal density. Nonetheless, the model was adequate for the desired purpose.

The vertical seismograms of four modes: M_{11}, M_{21}, PL_{21}, and PL_{22} were computed for distances from 1 000 km to 9400 km at 400 km increments. The PL_{21} and PL_{22} modes are the first and second order leaking modes, while the M_{11} and M_{21} modes are the Rayleigh and first higher order shear modes.

The seismograms of the modes at a distance of 5000 km were chosen for analysis since at that distance the modes were sufficiently dispersed to give reasonably good separation in time. The four individual modes were summed to give a composite seismogram.

The individual modal and the composite traces were convolved with a zero-phase filter intended to simulate the response of a long-period seismometer.

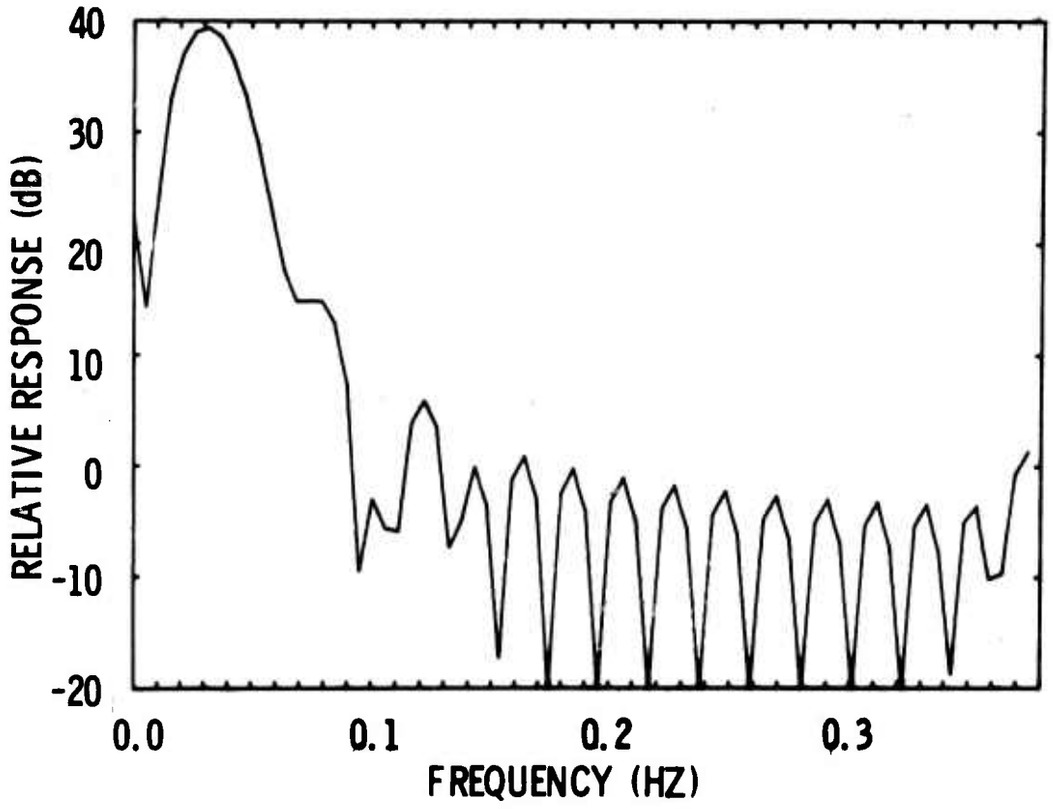

Figure III-1. Frequency Response of Simulated Seismometer Filter

The LASA long period seismometers have peak response nominally around 0.04 Hz. When a filter whose response imitated the seismometer was applied to the theoretical data, the resulting seismograms were not at all realistic in appearance since the high-frequency response of filter did not drop off quickly enough. In order to have a filtered seismogram similar in appearance to real LASA seismograms, the filter response was scaled in frequency so that the peak response was lowered to 0.03 Hz. The frequency response of the modified seismometer filter is shown in Figure III-1.

In addition to the pure event signal, the composite was mixed with random noise which was also filtered by the seismometer response. Signal-to-noise ratios of 50:1, 10:1, and 2:1 (maximum zero-to-peak signal/rms noise) were computed.

Initial results on these seismograms produced experimental group velocity dispersion curves where the spectral peaks had excessive scatter about the expected dispersion curves computed from the model parameters. It was realized that the scatter was caused by the pure seismograms being bandlimited and almost noise-free. The seismograms themselves were originally bandlimited to a maximum of 0.092 Hz through their excitation functions, leaving a wide spectral band of essentially no power. The ME algorithm, by designing a filter which was required to maintain very high gain in the wide low-power region, was forced to neglect the details of the spectrum in the signal band. In addition, these details were further blurred through inadequate computer precision while computing the coefficients of this highly tuned filter.

Since there was no spectral information above 0.092 Hz, the data were decimated by a factor of 4, increasing the sampling period to 5-1/3 seconds and reducing the folding frequency to 0.093 Hz. This effectively removed the zero-power regions. The resulting spectrum was still strongly non-white because of the narrow bandwidth of some of the modes and the shaping by the seismometer filter; even so, the decimation alone greatly reduced the scatter on the dispersion curves. The modal, composite, and composite-plus-noise seismograms of the filtered and decimated data are shown in Figure III-2.*

The ME spectra for these data were computed using gates of 25 points (133-1/3 seconds) and 6-point filters. Successive gates were shifted 12 time points.

The dispersion curves, derived experimentally by the ME technique, for the M_{11}, M_{21}, PL_{21}, PL_{22} and composite modal seismograms are shown in Figures III-3, III-4, III-6, III-8, and III-10 respectively.

*These may be compared to the unfiltered and undecimated traces shown in Figure 1 of Quarterly Report No. 3 (this contract).

A

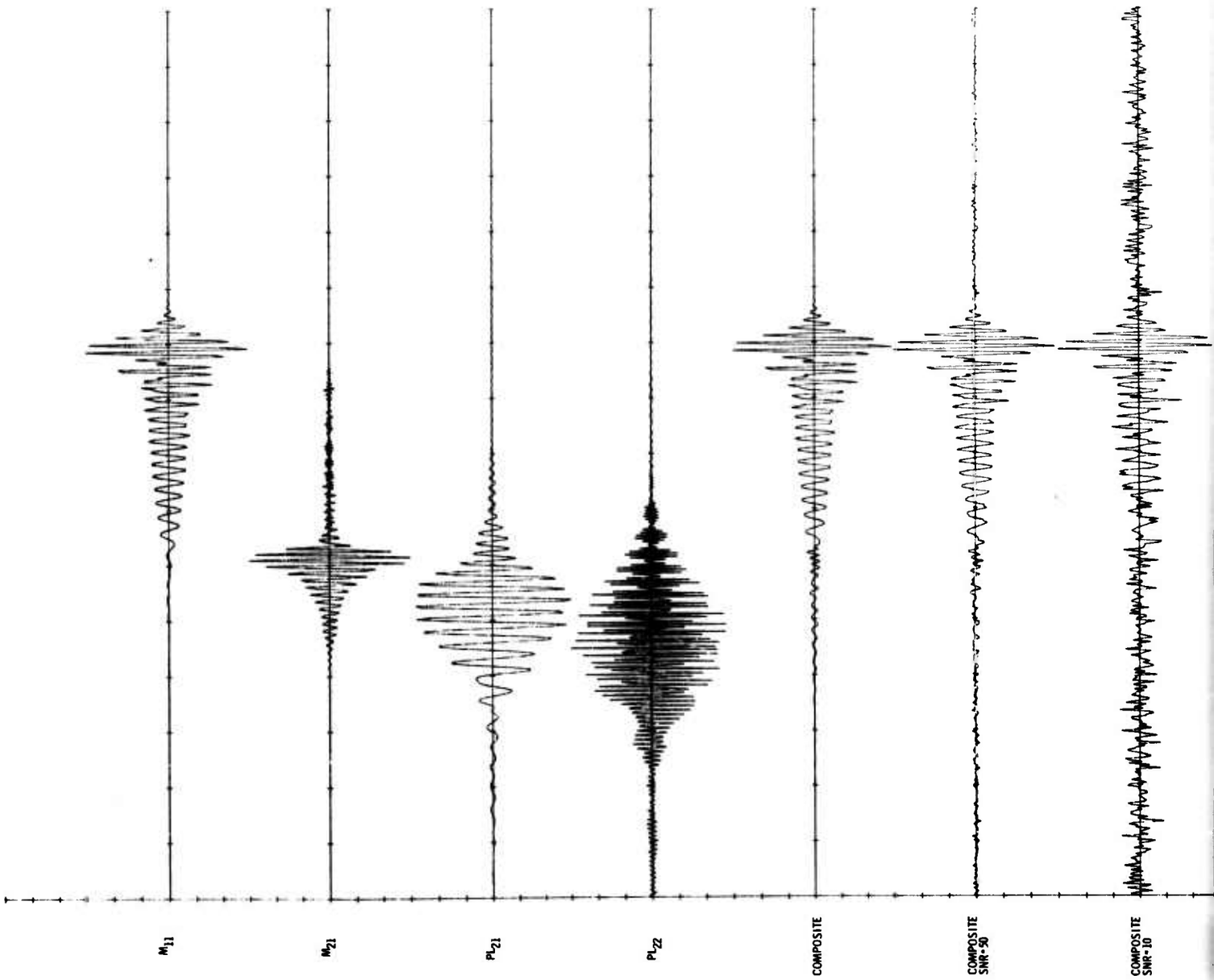

Figure III-2. Filtered and Decimated Individual Modes
Theoretical Seismogram at Four S/N Ra

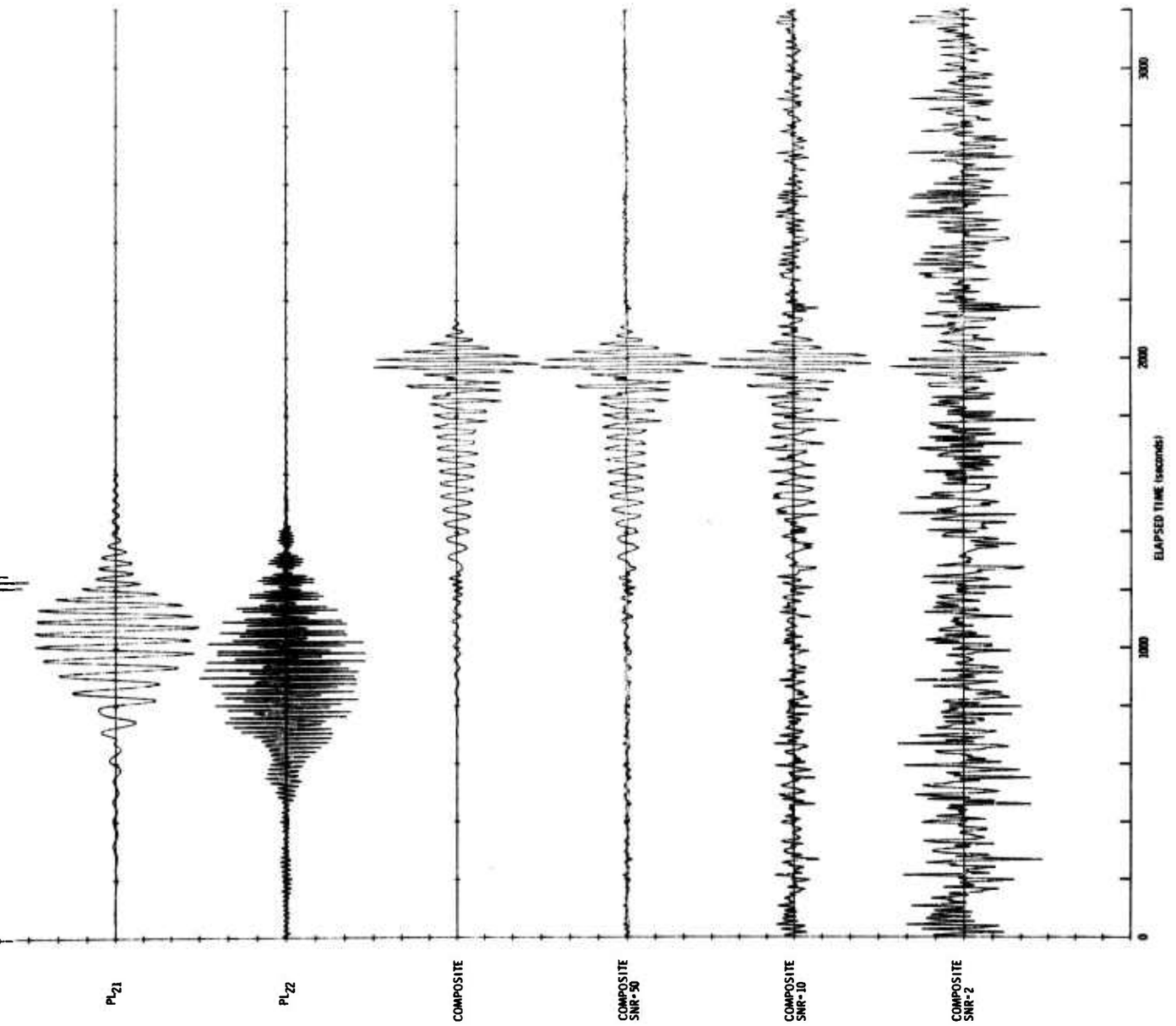

Figure III-2. Filtered and Decimated Individual Modes and Composite Theoretical Seismogram at Four S/N Ratios

The sets of spectra from which the peaks were selected are shown in Figures III-5, III-7, III-9, and III-11.* The group-velocity dispersion curves, in the form of travel-time plots, are linear in elapsed time (downward pointing tick-marks on horizontal axis) and nonlinear in group velocity (upward point tick-marks.) The theoretical group velocities computed from the model parameters are plotted for comparison.

The agreement of the experimental dispersions with theory is excellent for the M_{11}, M_{21}, and PL_{22} modes and the composite. The PL_{21} mode shows general agreement in frequency although the shapes of the two dispersions do not compare. Part of this lack of agreement is probably due to the same effects which led to decimation as discussed above.

With the exception of the M_{21} mode and the high-frequency end of the PL_{22} mode, the dispersions of the composite show the best agreement of all. The PL_{22} drops out approximately at the onset of M_{21}. With only 5 filter zeros to describe the spectrum, the stronger M_{21} and PL_{21} modes capture them.

The sparseness of the points on the M_{21} curve is due, in part, to the onset of the M_{11} mode which is much stronger. In addition, the nearly vertical dispersion curve for the M_{21} mode indicates a pulse-like waveform with most of the signal energy in a time gate about 200 seconds wide. Greater overlap between time gates would most likely fill in the curves.

The four sets of spectra from which the peaks were selected were all plotted with the same vertical scale. The tick marks on the vertical axis represent 10 dB of power. The horizontal axis is from 0.0 to 0.1 Hz. The first line of numbers under each plot is the starting and stopping times (relative to the event origin) of that time gate. The extreme sharpness of

* The spectra set of the M_{11} mode was not available for this report. It can be inferred from the composite spectra since it is the strongest component.

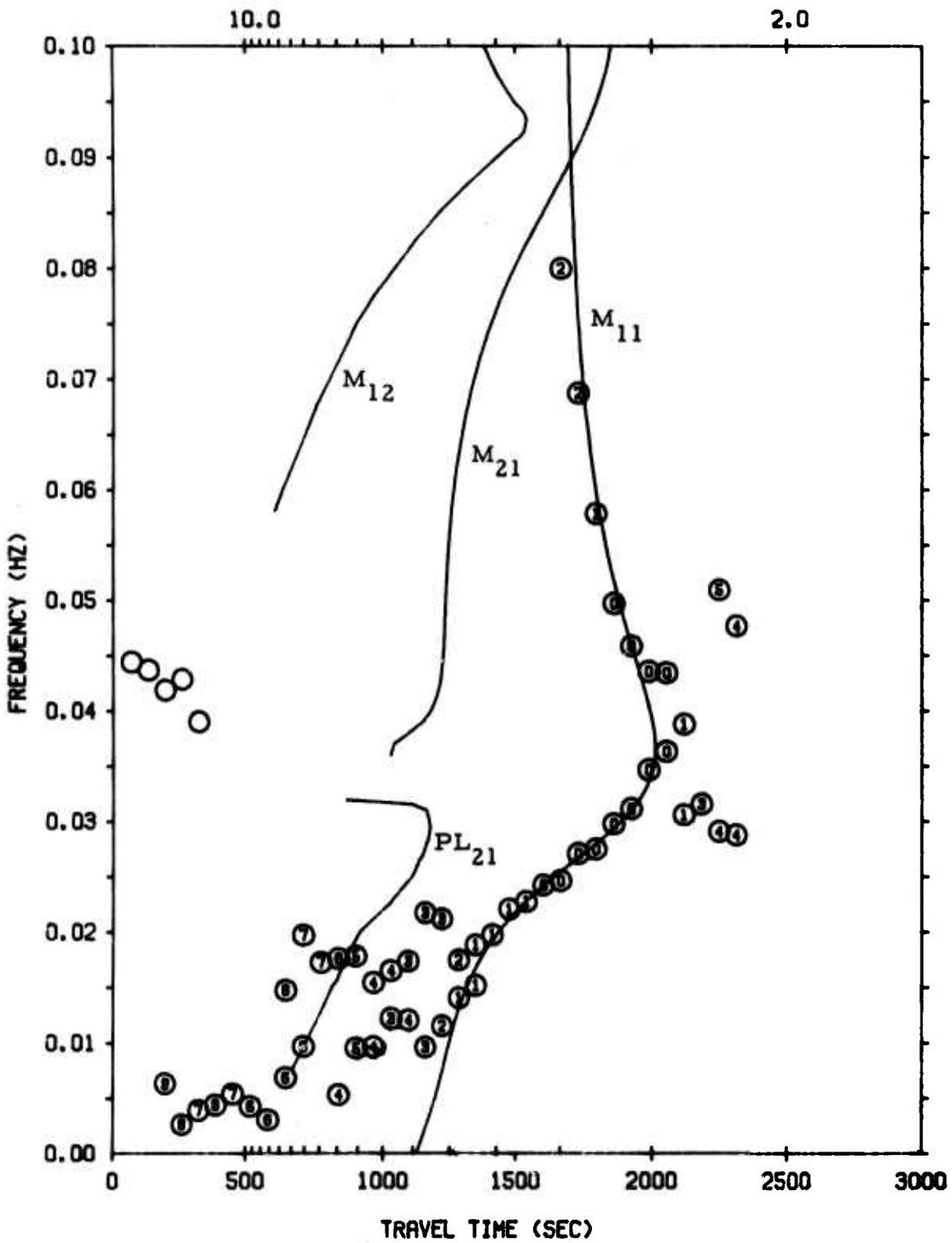

Figure III-3. Experimental Dispersion Curve for the M_{11} Mode. The Solid Lines are the Theoretical Group Velocities for Modes M_{11}, M_{21}, PL_{21} and PL_{22}.

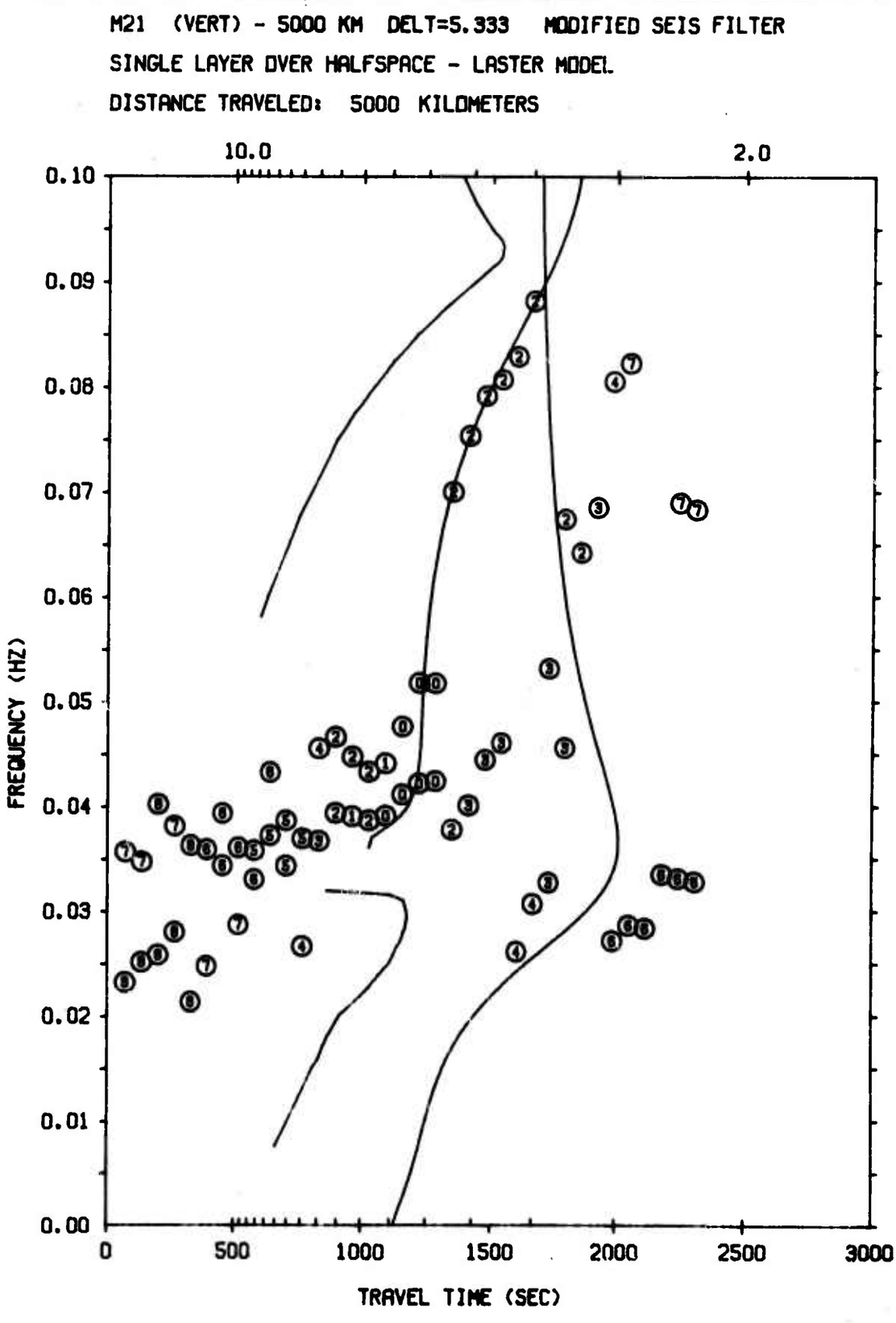

Figure III-4. Experimental Dispersion Curve for the M_{21} Mode

A

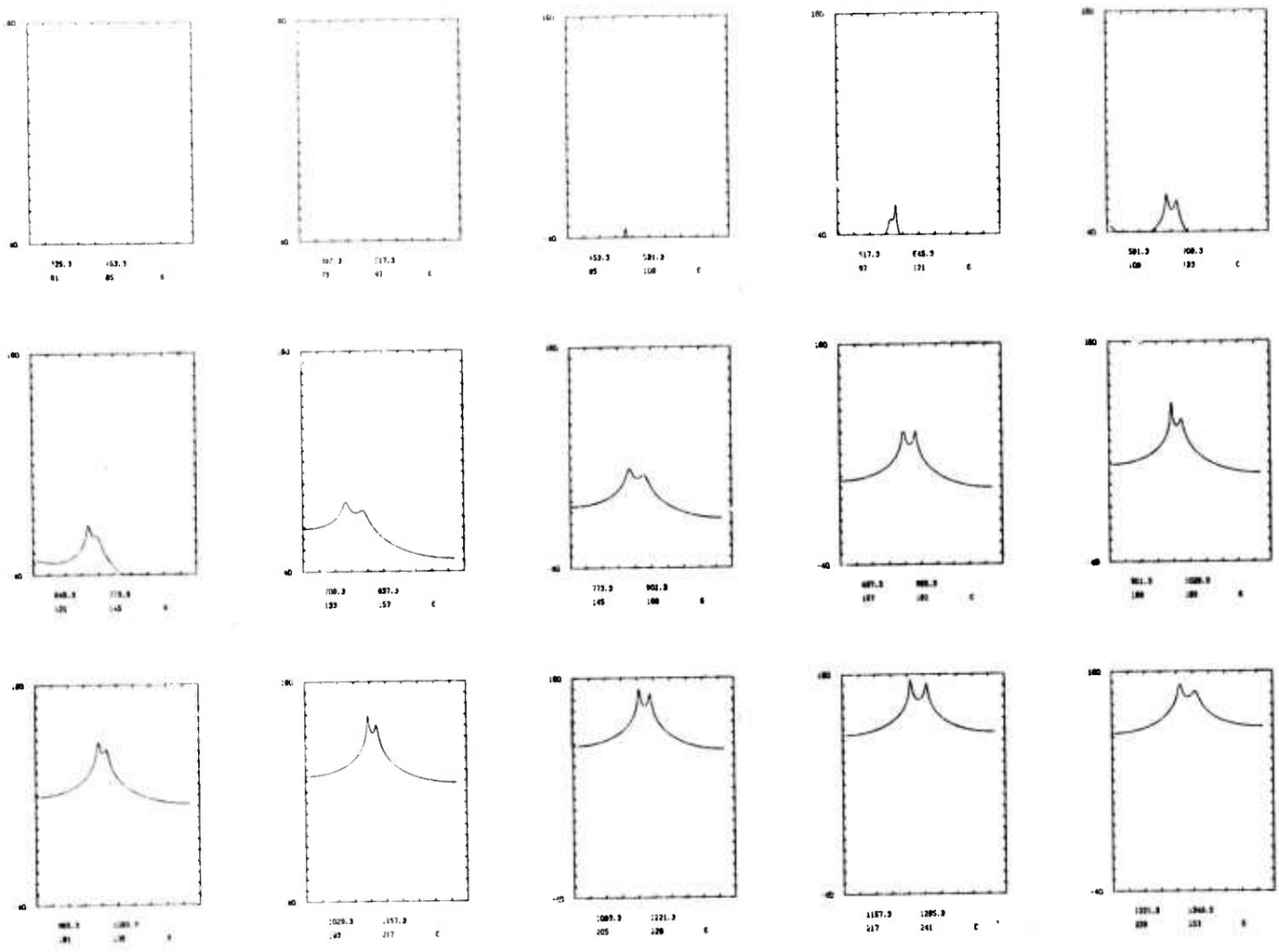

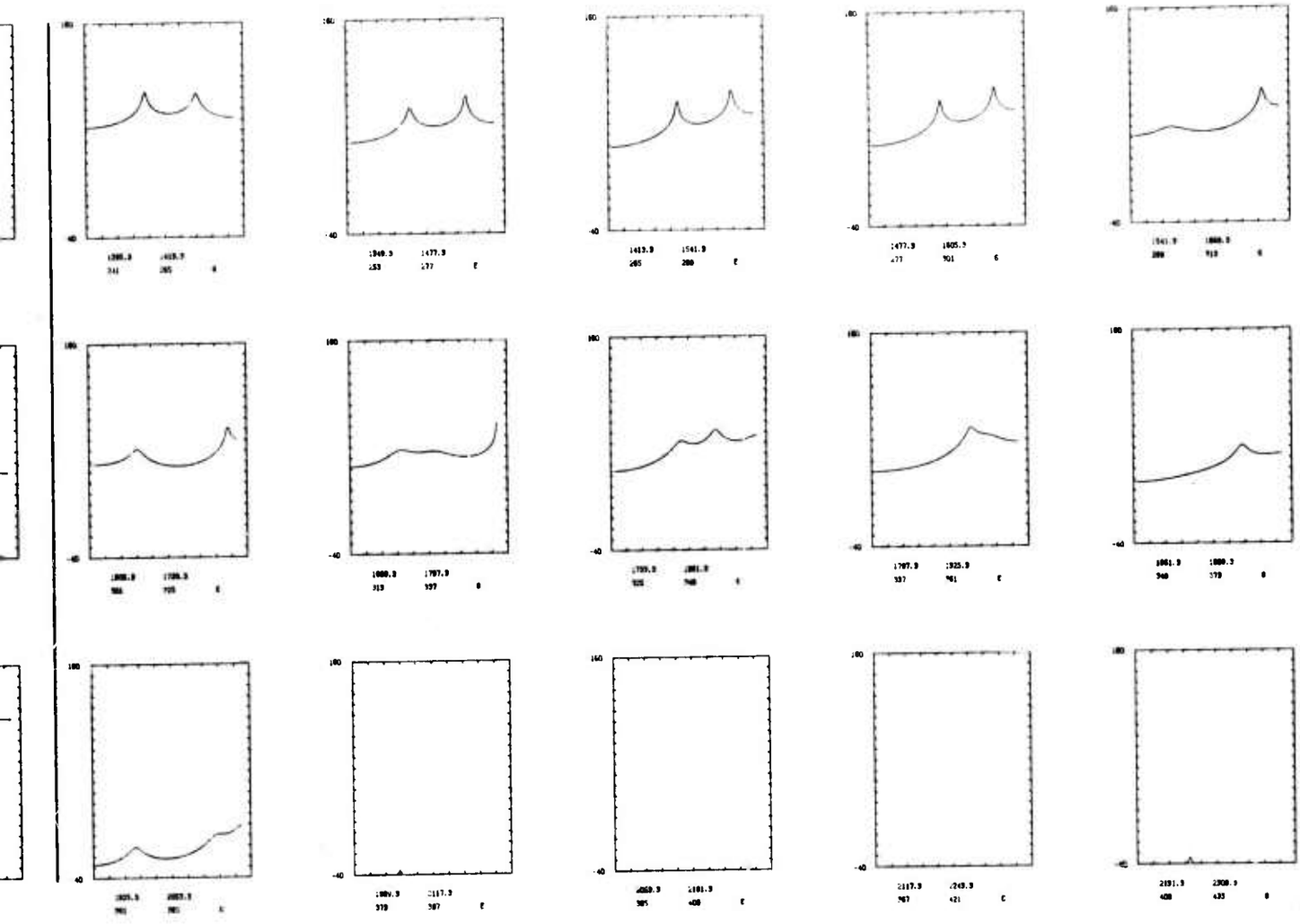

VERTICAL TICK MARKS REPRESENT 10 dB. HORIZONTAL AXIS IS FROM 0.0 TO 0.1 Hz. THE FIRST NUMBERS UNDER EACH PLOT ARE THE START AND STOP TIMES FOR THE DATA GATE (RELATIVE TO EVENT ORIGIN TIME). BELOW THIS ARE GIVEN THE SAMPLE NUMBER OF THE FIRST AND LAST DATA POINTS IN THE GATE AND FINALLY THE NUMBER OF CORRELATION LOGS USED IN COMPUTING THE ME SPECTRUM.

Figure III-5. ME Spectra for the M_{21} Mode

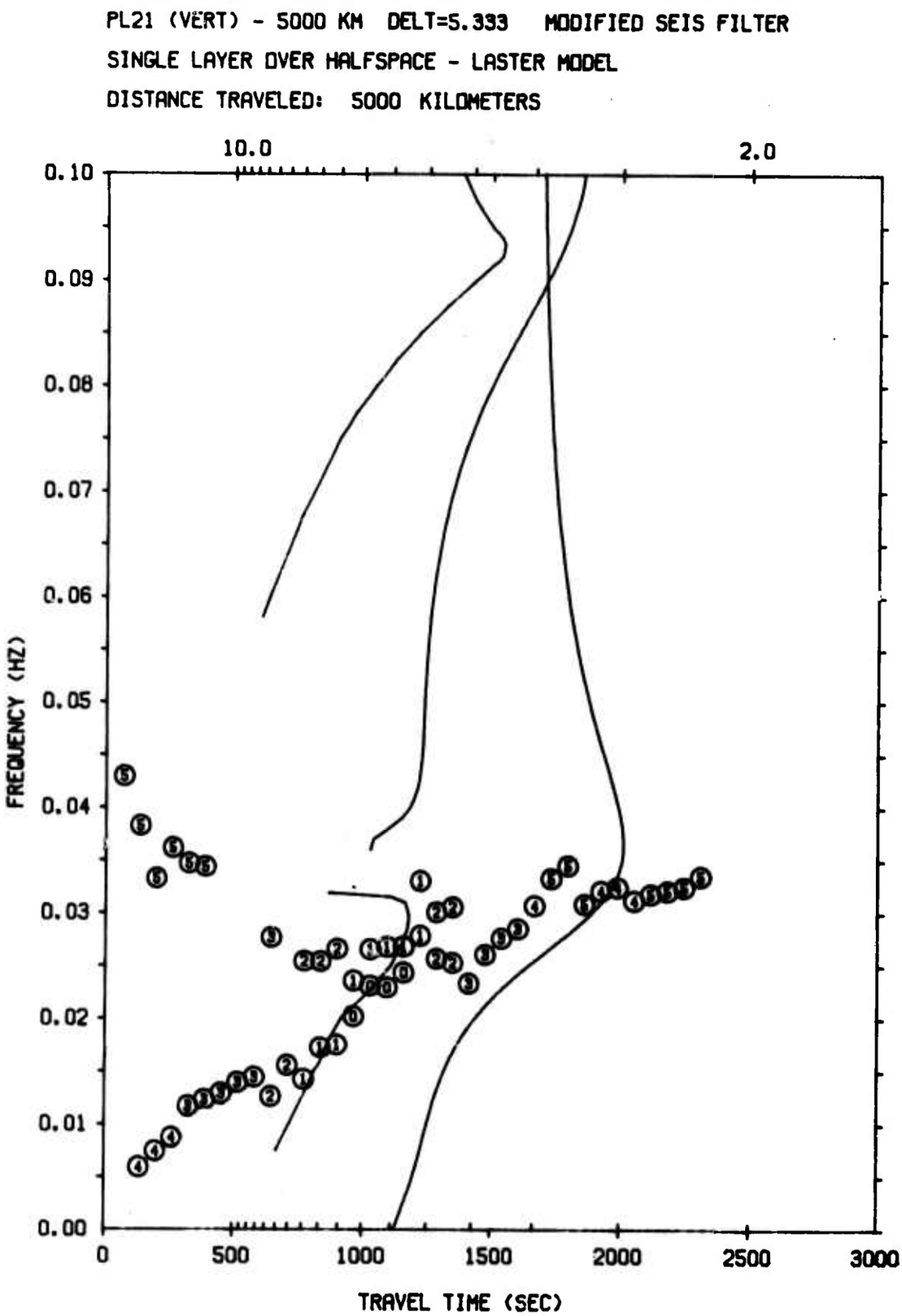

Figure III-6. Experimental Dispersion Curve for the PL_{21} Mode

A

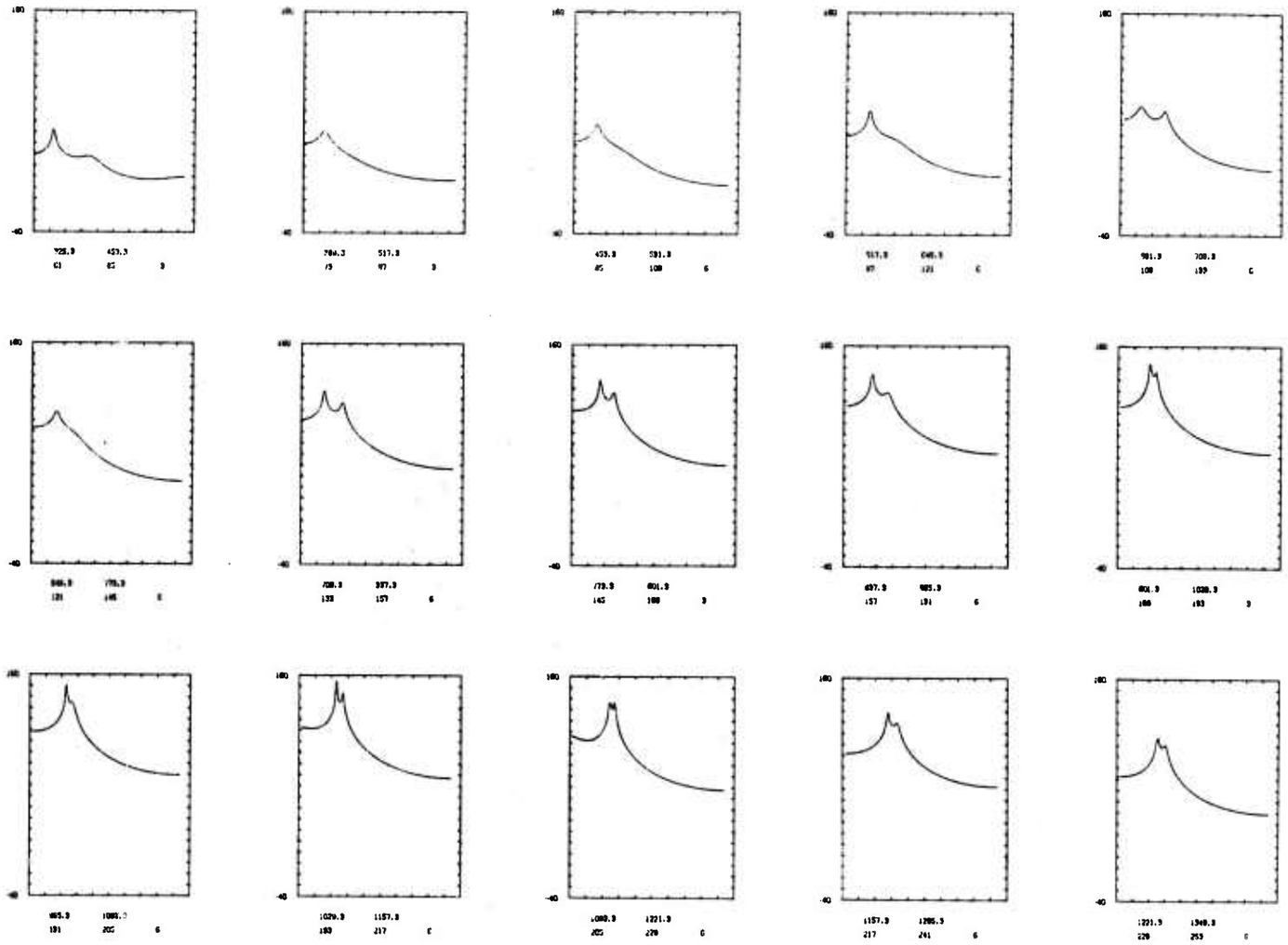

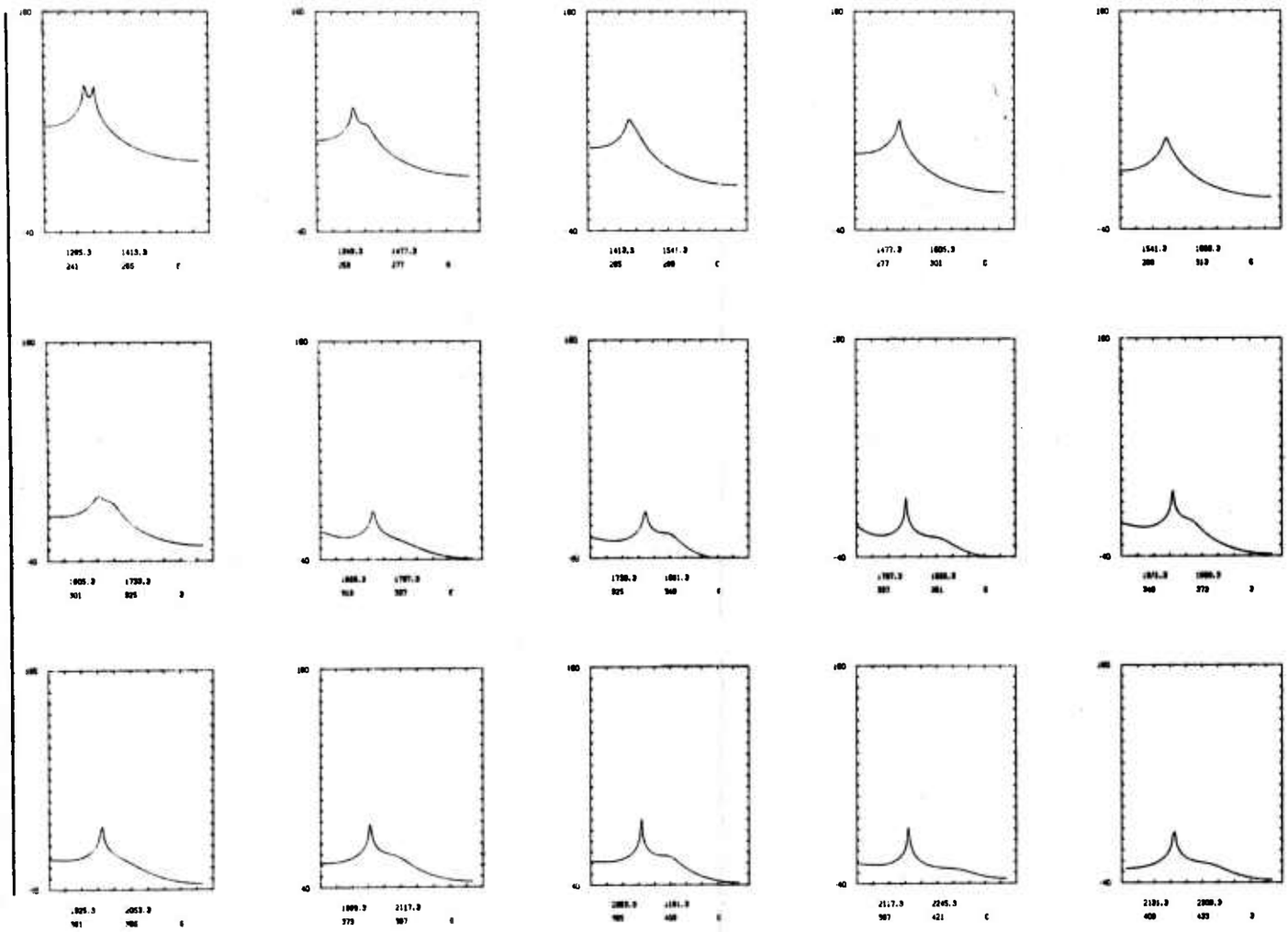

VERTICAL TICK MARKS REPRESENT 10dB. HORIZONTAL AXIS IS FROM 0.0 TO 0.1 Hz. THE FIRST NUMBERS UNDER EACH PLOT ARE THE START AND STOP TIMES FOR THE DATA GATE (RELATIVE TO EVENT ORIGIN TIME). BELOW THIS ARE GIVEN THE SAMPLE NUMBER OF THE FIRST AND LAST DATA POINTS IN THE GATE AND FINALLY THE NUMBER OF CORRELATION LOGS USED IN COMPUTING THE ME SPECTRUM.

Figure III-7. ME Spectra for the PL_{21} Mode

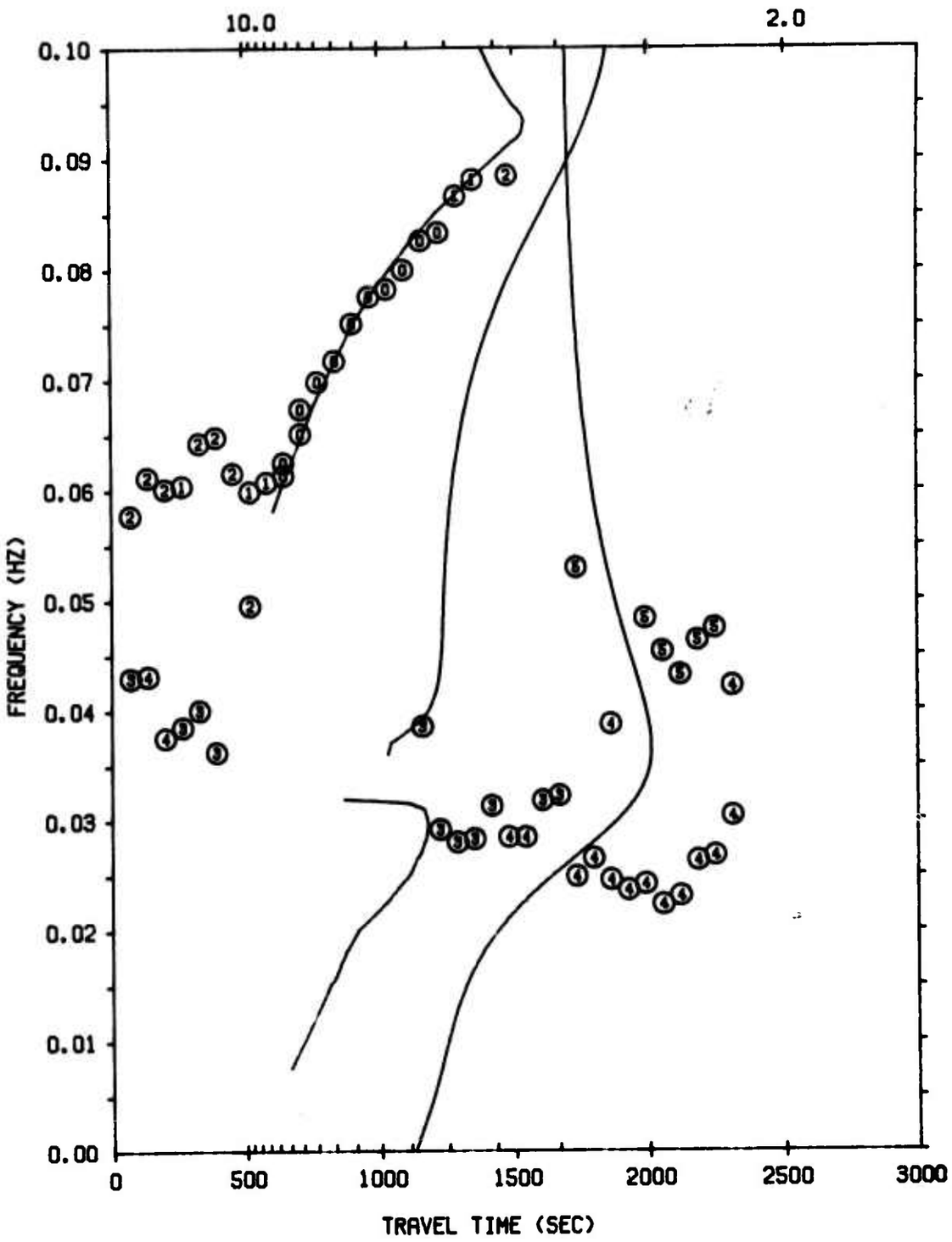

Figure III-8. Experimental Dispersion Curve for the PL_{22} Mode.

A

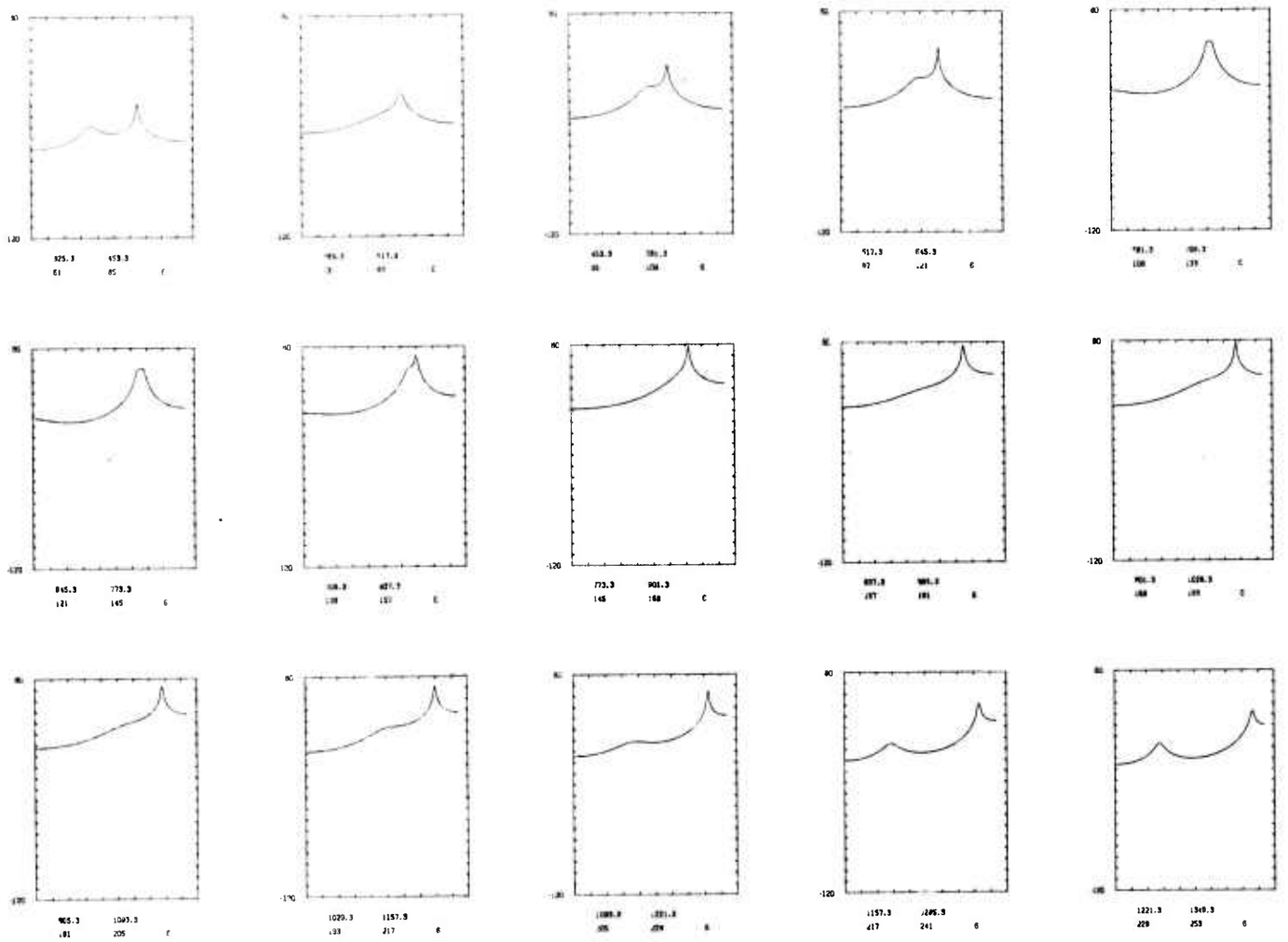

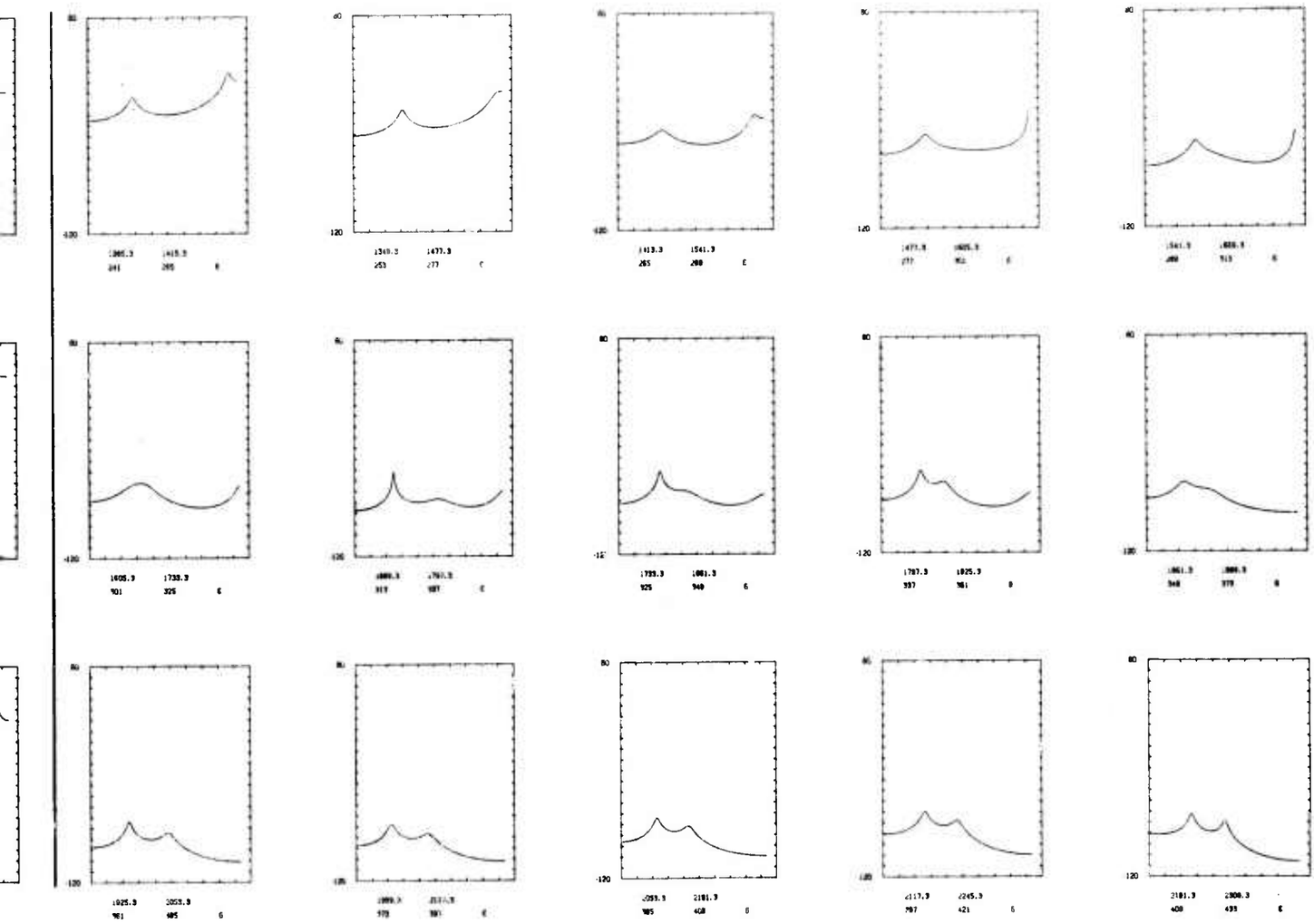

VERTICAL TICK MARKS REPRESENT 10dB. HORIZONTAL AXIS IS FROM 0.0 TO 0.1 Hz. THE FIRST NUMBERS UNDER EACH PLOT ARE THE START AND STOP TIMES FOR THE DATA GATE (RELATIVE TO EVENT ORIGIN TIME). BELOW THIS ARE GIVEN THE SAMPLE NUMBER OF THE FIRST AND LAST DATA POINTS IN THE GATE AND FINALLY THE NUMBER OF CORRELATION LOGS USED IN COMPUTING THE ME SPECTRUM.

Figure III-9. ME Spectra for the PL_{22} Mode

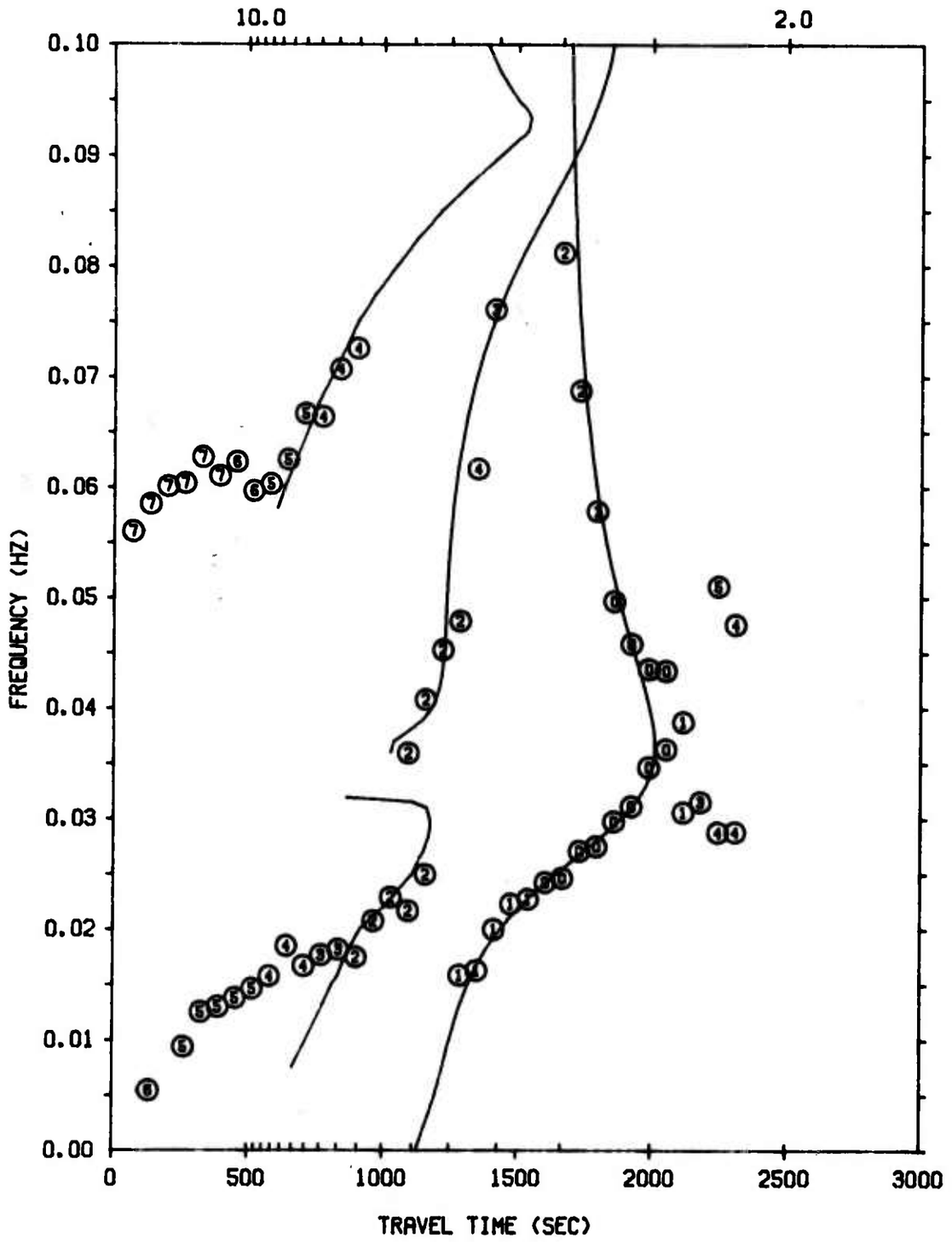

Figure III-10. Experimental Dispersion Curve for the Composite Seismogram

17

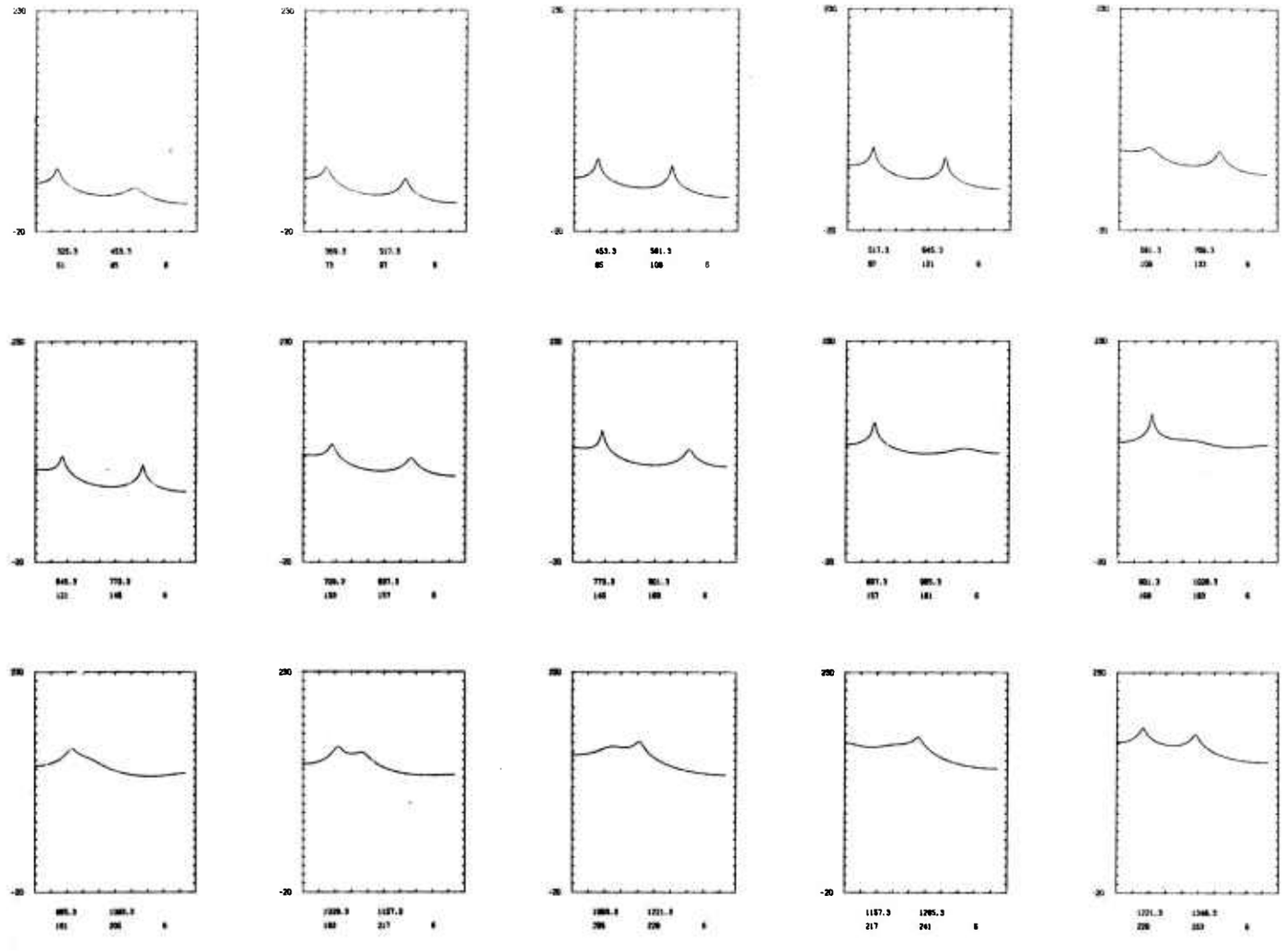

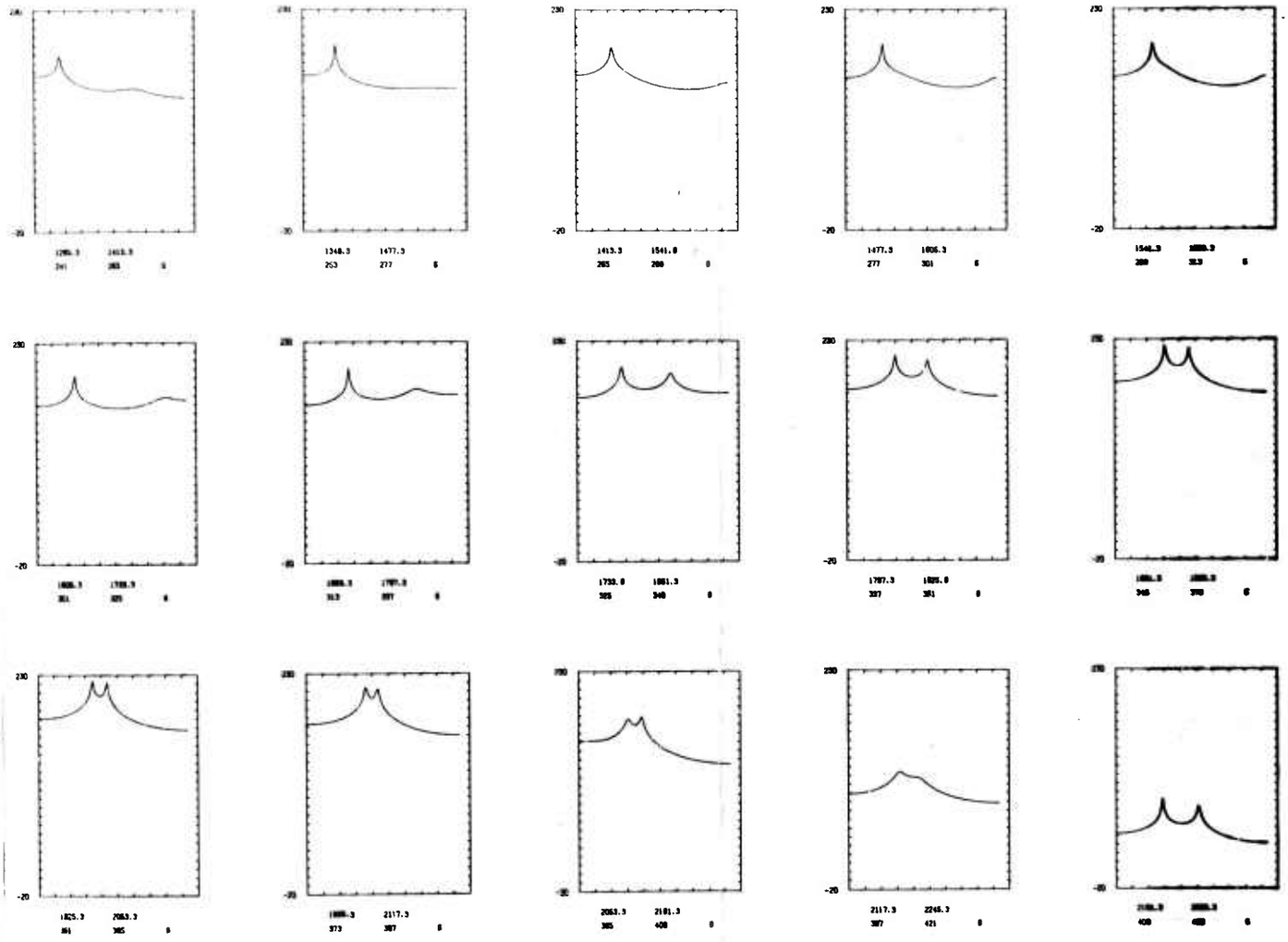

VERTICAL TICK MARKS REPRESENT 10 dB. HORIZONTAL AXIS IS FROM 0.0 TO 0.1 Hz. THE FIRST NUMBERS UNDER EACH PLOT ARE THE START AND STOP TIMES FOR THE DATA GATE (RELATIVE TO EVENT ORIGIN TIME). BELOW THIS ARE GIVEN THE SAMPLE NUMBER OF THE FIRST AND LAST DATA POINTS IN THE GATE AND FINALLY THE NUMBER OF CORRELATION LAGS USED IN COMPUTING THE ME SPECTRUM.

Figure III-11. ME Spectra for the Composite Seismogram

the ME spectra is evident. The dynamic range of the set of spectra of the individual noiseless modes exceeded 300 dB. To prevent a complete loss of detail on the spectra, the dynamic range for the individual modes was limited to 200 dB.

The dispersion curves produced from the signal-plus-noise seismograms are shown in Figures III-12, III-14, and III-16. The PL_{22} mode disappeared completely at SNR = 50; the PL_{21} and M_{21} modes are very weak, so weak in fact, that without the aid of the theoretical curves to guide the eye, it would be difficult to identify them. At a SNR=10, the PL_{21} mode has disappeared. The M_{21} mode is still visible; however, its peaks are about the same size as the noise peaks. The Raleigh mode is still strong. At SNR=2, all modes are washed out and there is no organized group velocity curve visible, even for the Rayleigh mode.

The spectra sets for the signal-plus-noise seismograms are shown in Figures III-13, III-15, and III-17. The greatly reduced dynamic range of these spectra due to the addition of noise is evident from the power density axes.

The approximate signal-to-noise ratios of the individual modes for the composite phase-noise traces are given in Table III-2. The M_{11} mode SNR is given as the same as the composite SNR.

Table III-2

APPROXIMATE S/N RATIOS FOR COMPOSITE PHASE-NOISE-TRACES

Composite SNR=	50	10	2
M_{11}	50	10	2
M_{21}	3.5	0.7	0.14
PL_{21}	2.0	0.4	0.08
PL_{22}	0.1	0.02	0.005

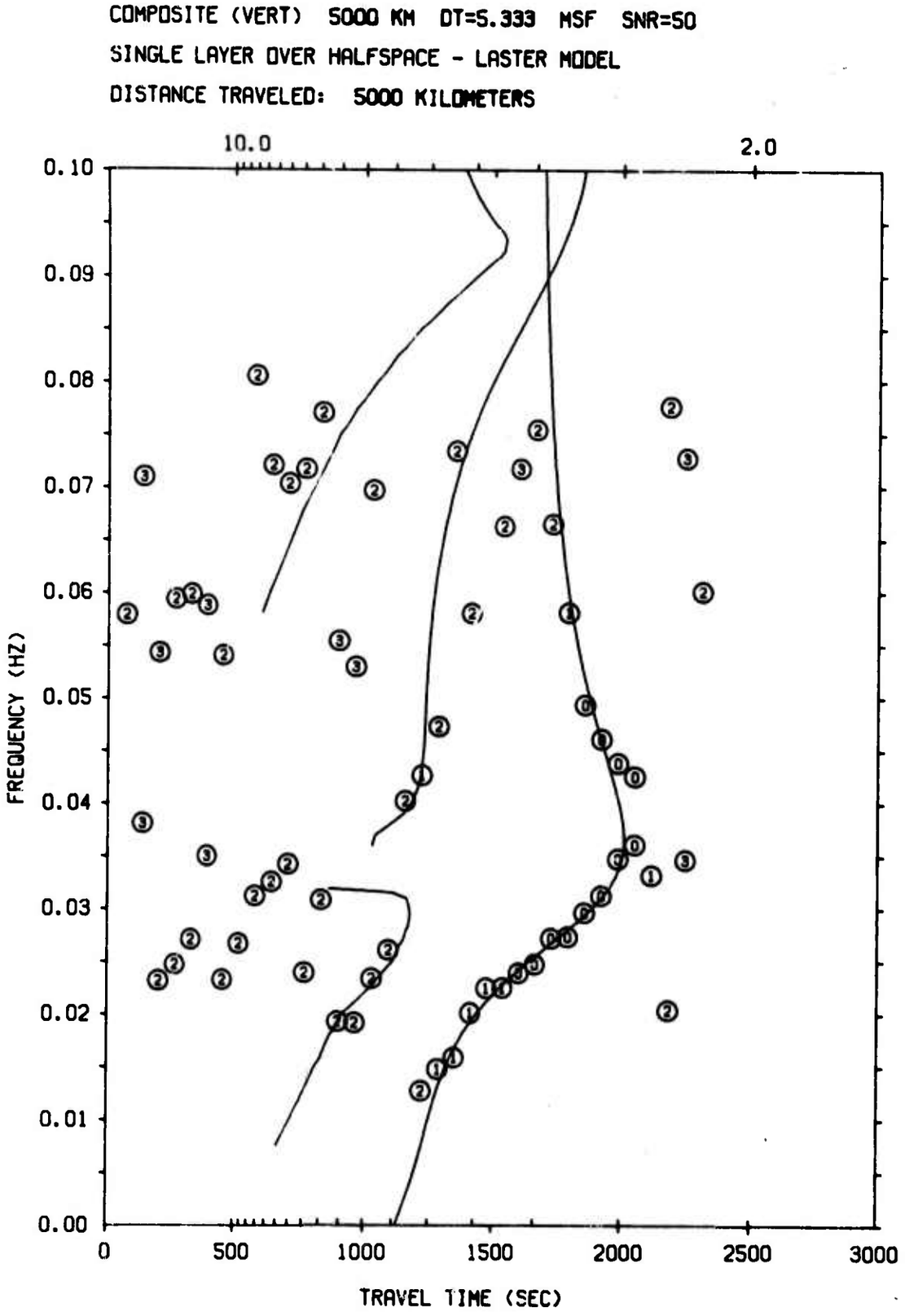

Figure III-12. Experimental Dispersion Curve for Composite + Noise (SNR=50) Seismogram

A

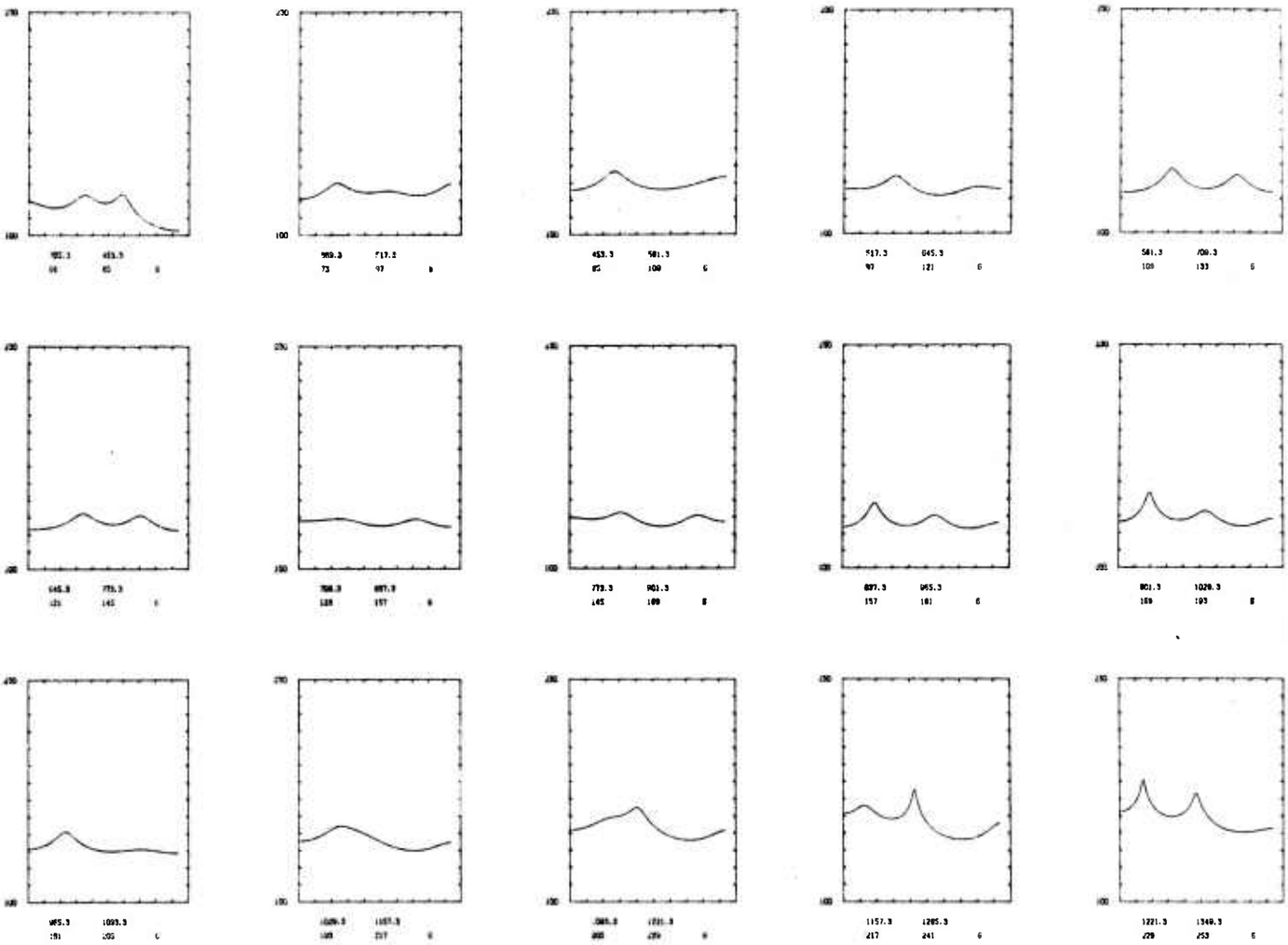

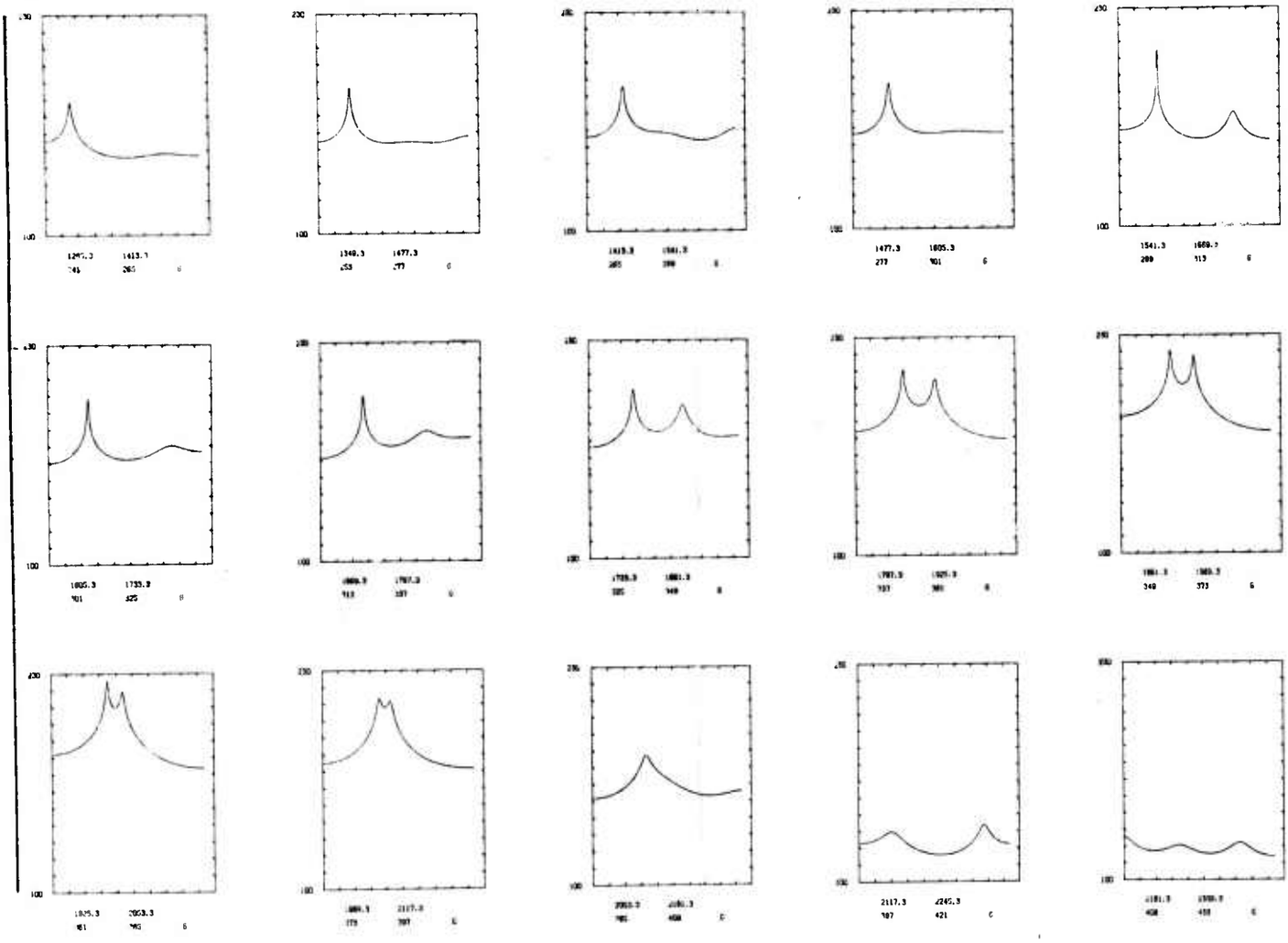

VERTICAL TICK MARKS REPRESENT 10 dB. HORIZONTAL AXIS IS FROM 0.0 TO 0.1 Hz. THE FIRST NUMBERS UNDER EACH PLOT ARE THE START AND STOP TIMES FOR THE DATA GATE (RELATIVE TO EVENT ORIGIN TIME). BELOW THIS ARE GIVEN THE SAMPLE NUMBER OF THE FIRST AND LAST DATA POINTS IN THE GATE AND FINALLY THE NUMBER OF CORRELATION LOGS USED IN COMPUTING THE ME SPECTRUM.

Figure III-13. ME Spectra for the Composite (SNR=50) Seismogram

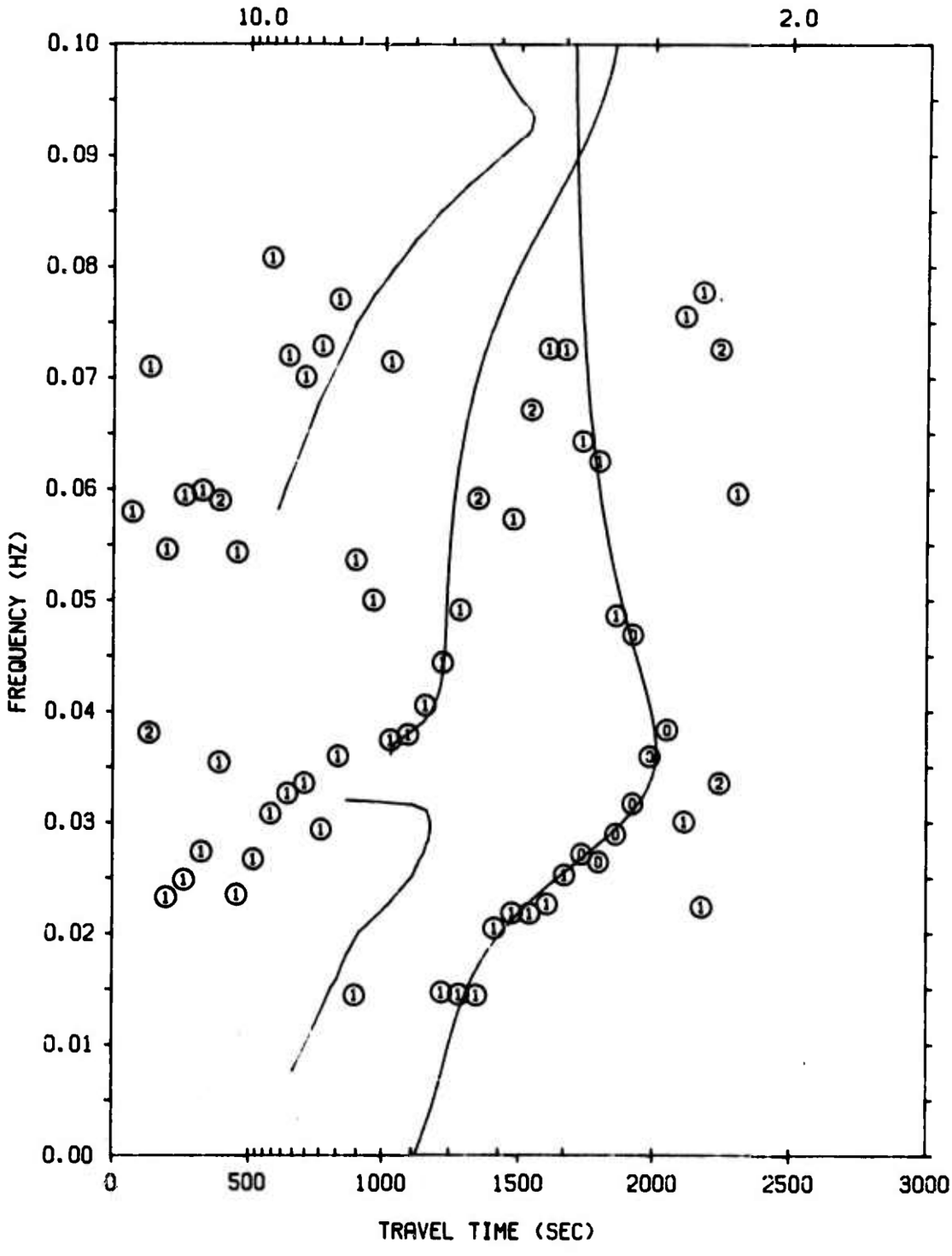

Figure III-14. Experimental Dispersion Curve for Composite + Noise (SNR=10) Seismogram

A

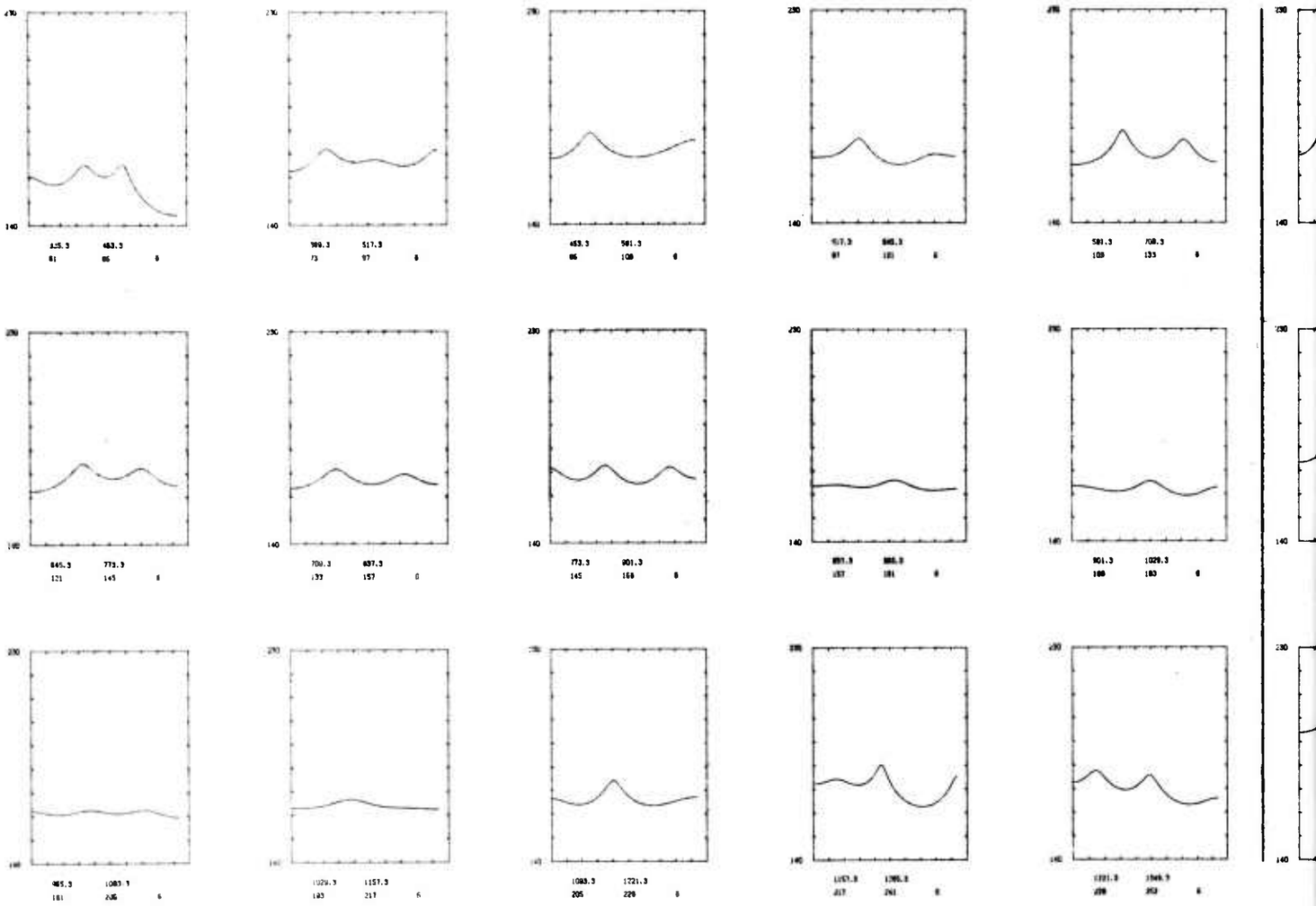

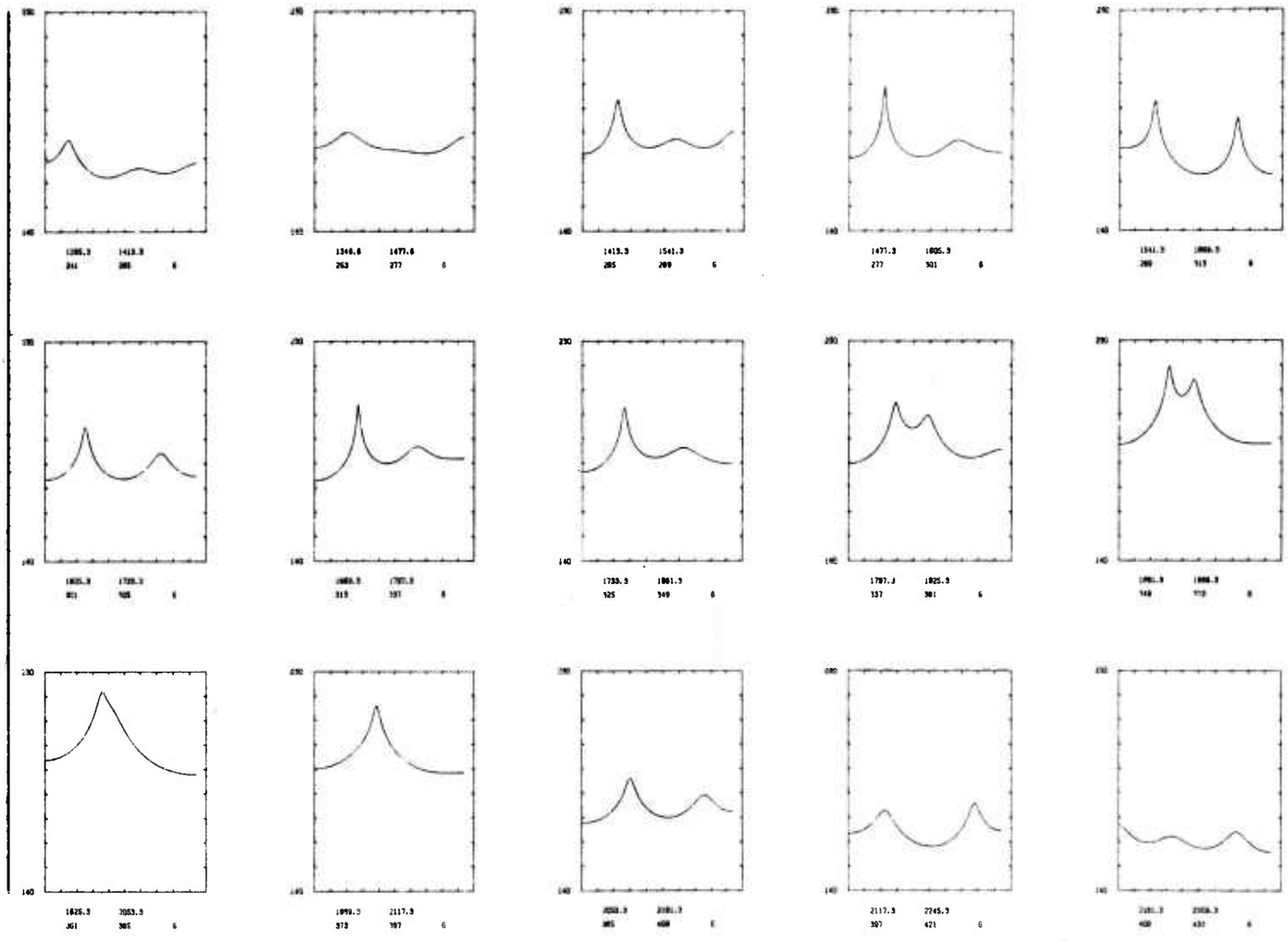

VERTICAL TICK MARKS REPRESENT 10dB. HORIZONTAL AXIS IS FROM 0.0 TO 0.1 Hz. THE FIRST NUMBERS UNDER EACH PLOT ARE THE START AND STOP TIMES FOR THE DATA GATE (RELATIVE TO EVENT ORIGIN TIME). BELOW THIS ARE GIVEN THE SAMPLE NUMBER OF THE FIRST AND LAST DATA POINTS IN THE GATE AND FINALLY THE NUMBER OF CORRELATION LOGS USED IN COMPUTING THE ME SPECTRUM.

Figure III-15. ME Spectra for the Composite (SNR=10) Seismogram

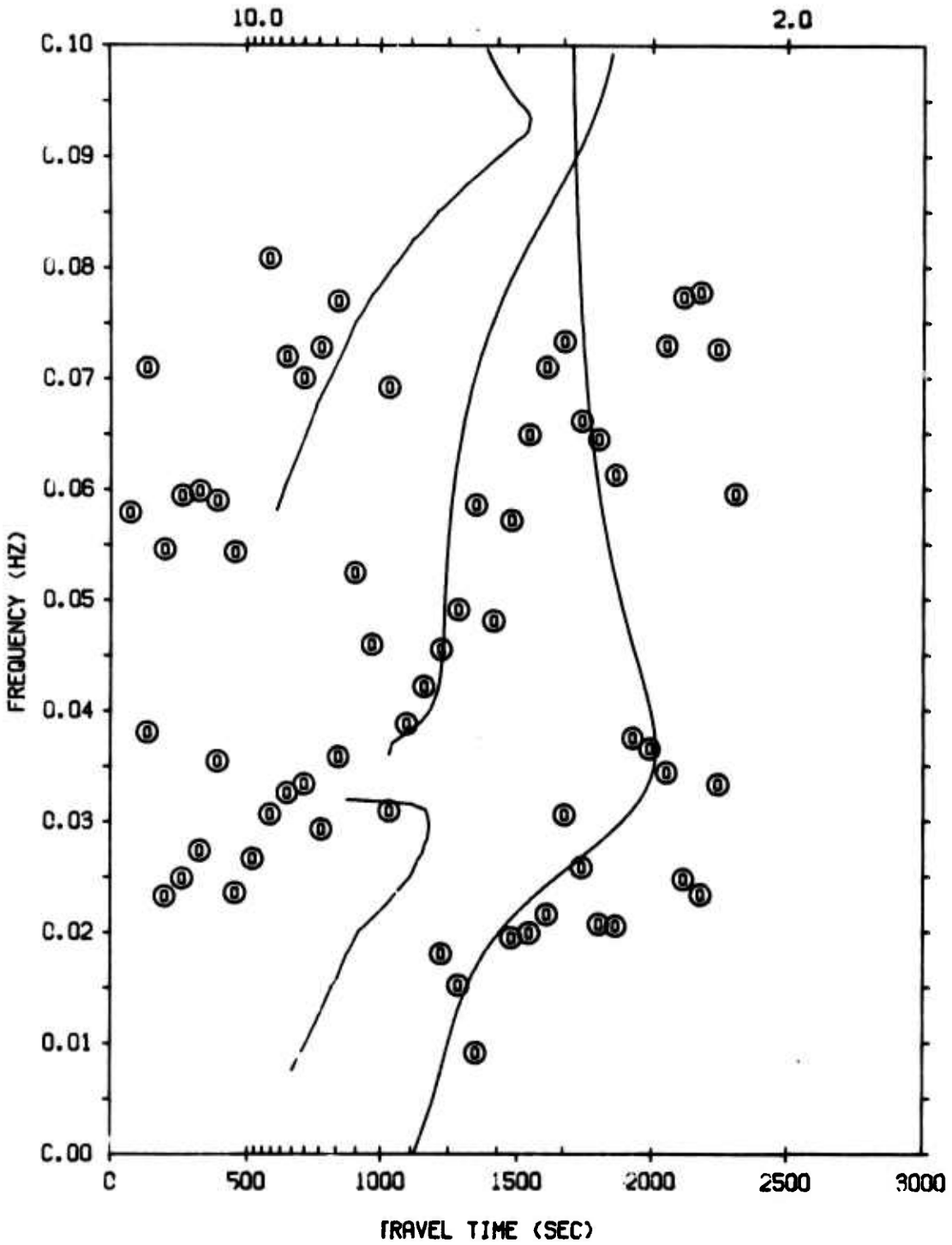

Figure III-16. Experimental Dispersion Curve for Composite + Noise (SNR=2) Seismogram

A

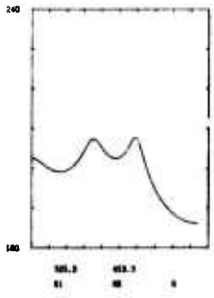

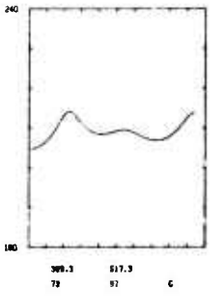

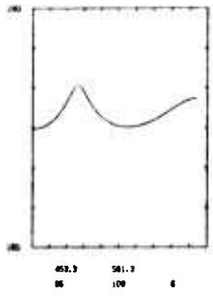

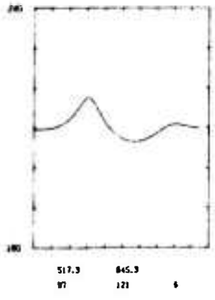

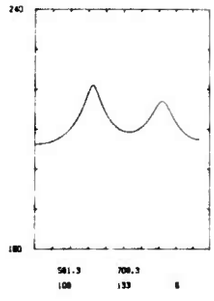

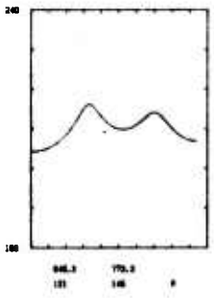

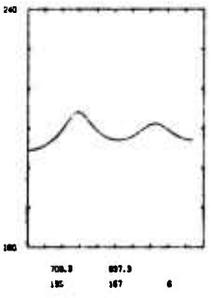

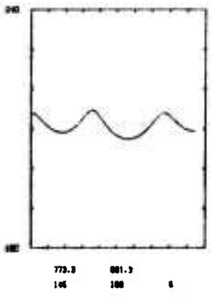

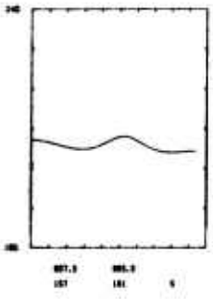

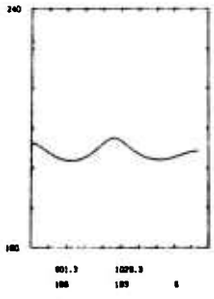

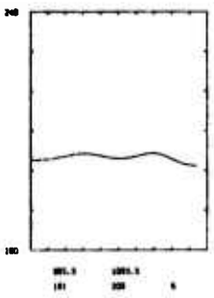

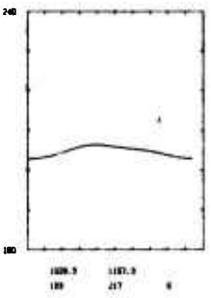

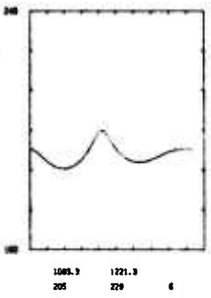

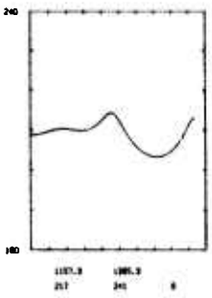

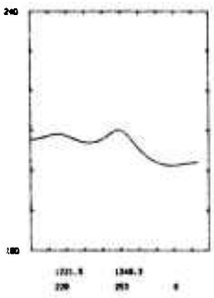

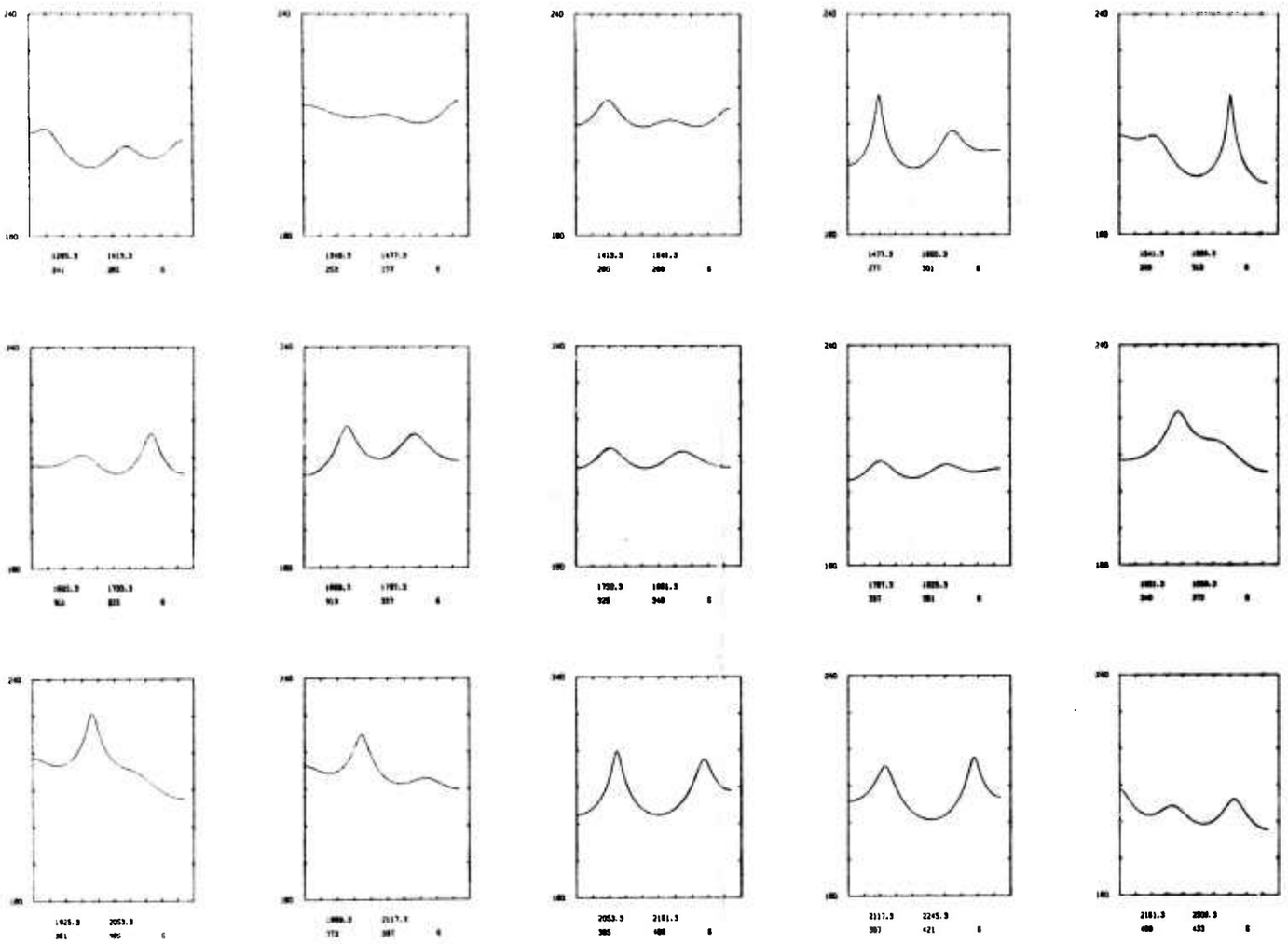

VERTICAL TICK MARKS REPRESENT 10 dB. HORIZONTAL AXIS IS FROM 0.0 TO 0.1 Hz. THE FIRST NUMBERS UNDER EACH PLOT ARE THE START AND STOP TIMES FOR THE DATA GATE (RELATIVE TO EVENT ORIGIN TIME). BELOW THIS ARE GIVEN THE SAMPLE NUMBER OF THE FIRST AND LAST DATA POINTS IN THE GATE AND FINALLY THE NUMBER OF CORRELATION LOGS USED IN COMPUTING THE ME SPECTRUM.

Figure III-17. ME Spectra for the Composite (SNR=2) Seismogram

From Table III-2 and the experimental dispersion plots, it seems that the various modes become indistinct or invisible at modal signal-to-noise ratios between 10 and 2, which is about when the Rayleigh mode also becomes indistinct to the eye.

The results of the application of maximum-entropy spectral analysis to theoretical seismograms for computing experimental group-velocity dispersion curves yield the following conclusions:

- Maximum-entropy spectral analysis on time-partioned seismograms can produce dispersion curves of high accuracy under conditions of large modal signal-to-noise ratio.
- At modal signal-to-noise somewhere between 10 and 2, the maximum entropy spectrum technique can no longer distinguish signals from noise when short time gates (25 data points) are used. The detection limit would be improved if more data (longer time gates) were used. This would be feasible only at longer distances where the wave-train is more dispersed.
- Even after various modes have been detected, proper identifications will be difficult without foreknowledge of the expected dispersion.
- The accuracy of the maximum entropy technique is strongly dependent on the precision of the calculations. Larger signal-to-noise events may introduce spurious peaks in the spectrum unless adequate machine precision is used.
- The data should be antialias filtered and decimated to the bandwidth of the spectral region of interest. Strongly non-white spectra should probably be pre-whittened. These measures will reduce machine precision requirement and the incidence of false spectral peaks.
- The present LASA long-period data is oversampled. The response of the LASA seismometers produces strong cutoff above 0.1 Hz, resulting in little power between 0.1 Hz and 0.5 Hz. Prior to application of maximum entropy spectral analysis on this data, the data should be antialias filtered and decimated.

SECTION IV

EXPERIMENTAL GROUP VELOCITY DISPERSION OF LASA LONG-PERIOD BEAMS

The group velocity dispersion curves of 29 events obtained from LASA long-period beams were computed by the maximum entropy technique. The events are listed in Table IV-1 along with their LASA magnitude, azimuth, and general location of epicenter.

For purposes of discussion and comparison, these events were loosely grouped on the basis of azimuth so that the propagation paths would be somewhat similar. These groups and the events assigned to them are:

California group: L-21 L-22, L-23, L-24, L-09

Kurile-Kamchatka group: L-04, L-19, L-60, L-61, L-67, EPX-70002

China-Kazakh group: L-30, L-31, L-32, L-33, L-34, L-35, L-36, L-37, L-38, L-39, L-40, L-41, L-63, EPX-14582, EPX-14646

European group: L-01, EPX-14649, EPX-18387

The data for these events were collected at various times over a period of two years. The events with EPX prefixes were recently obtained as beam outputs from the Seismic Array Analysis Center, and have been processed through the SAAC long-period event processor. The events with L prefixes were also obtained from SAAC, in early 1969. For the latter events, individual channels were obtained and the beams formed as part of this contract.

Table IV-1

LIST OF EVENTS FROM LASA LONG-PERIOD BEAMS

Name	m_b	Azimuth	Δ	Location
L-01	4.5	19.7	51.9	Greenland Sea
L-04	4.9	311.4	62.8	Kurile Trench
L-09	5.3	146.0	46.1	Panama
L-19	4.3	312.8	56.9	Kamchatka
L-21	3.8	209.2	17.2	Baja, California
L-22	4.8	205.1	16.7	Gulf of California
L-23	4.4	204.9	16.6	Gulf of California
L-24	3.9	203.8	17.0	Gulf of California
L-30	5.3	357.2	83.8	Eastern Kazakh
L-31	5.3	357.2	83.8	Eastern Kazakh
L-32	5.4	357.5	83.6	Eastern Kazakh
L-33	5.9	357.2	83.8	Eastern Kazakh
L-34	4.9	357.2	83.8	Eastern Kazakh
L-35	6.1	357.4	83.7	Eastern Kazakh
L-36	5.7	357.2	83.8	Eastern Kazakh
L-37	6.1	357.2	83.8	Eastern Kazakh
L-38	5.8	357.2	83.8	Eastern Kazakh
L-39	4.8	357.7	83.7	Eastern Kazakh
L-40	5.7	357.1	83.8	Eastern Kazakh
L-41	4.7	4.7	75.7	Central Russia
L-60	4.2	312.6	56.7	Kamchatka
L-61	4.9	314.8	53.0	Komandorsky Island
L-63	4.4	337.3	91.0	Kansu Province, China
L-67	4.4	328.3	88.0	Northeastern China
EPX-14582	5.3	358.9	94.5	Sinkiang Province, China
EPX-14646	4.7	358.3	91.1	Sinkiang Province, China
EPX-14649	4.5	27.8	58.4	Southern Norway
EPX-18387	5.8	22.4	89.0	Caucasus
EPX-70002	6.2	308.6	47.0	Amchitka

The results of the work on the theoretical seismograms indicated that the long-period LASA data were oversampled. The frequency response of the seismometers pass little energy above 0.1 Hz which is only 20 percent of the available bandwidth. Consequently all of the data were low-pass filtered to a maximum frequency of 0.12 Hz (-3dB) by a 51-point zero phase filter. The means were then removed, and the resulting traces were decimated by 4. This gave a new sampling period of 4 seconds and a folding frequency of 0.125 Hz. The decimated traces were then time-partioned and analyzed by the maximum entropy techniques. The ME spectra of the real data are not included since they are generally similar in appearance to the composite-plus-noise spectra in the previous section.

The filtered and decimated seismograms are shown in Figure IV-1. Prior to plotting, the beginning of each trace data record was adjusted to event origin time either by trimming or by adding sufficient leading zeroes. Thus the traces, as plotted, are in true elapsed time from event origin. This was done to facilitate comparisons between the seismograms and the dispersion plots.

The theoretical group-velocity dispersion curves for the M_{11} and M_{21} modes were computed from the TI-1 - perturbed LASA crustal Model.[10] These theoretical group-velocity dispersion curves are plotted on all of the real data group-velocity plots to serve as an aid in identifying their respective modes in the experimental data. Note, however, these curves imply that the LASA crustal model holds true for the entire propagation path from epicenter to LASA which is probably not the case for any of the events studied.

In the discussion below of the results of this study, we have generally given mainconsideration to the strongest peaks (those labelled with a zero). When these peaks show a smooth consistent trend, we consider the results good. The lower amplitude peaks, particularly the early arriving peaks, show significant scatter and only occasionally — when they show a consistent trend — are they discussed in detail.

A. THE CALIFORNIA GROUP

Events L-21 through L-24 occurred in the same vicinity at the northern end of the Gulf of California and have essentially a continental path. With distance of only 17°, they are not truly teleseismic. Event L-09, south of Panama, is teleseismic and is included in this group only because it is the solitary event in that direction. Its path includes the Pacific, Central America, the Gulf of Mexico, and the United States. The time-gate shift between spectra was 10 seconds for L-21, 16 seconds for L-22, L-23, and L-24, and 24 seconds for L-09.

The dispersions of the four Gulf of California events are seen in Figures IV-2, IV-3, IV-4, and IV-5. The travel times generally agree with the predicted times, but the actual dispersion is greater than that predicted by the LASA model. Two strong branches in the dispersion are visible. The higher frequency branch, which tends at any particular time to be twice the frequency of the lower branch, is higher mode energy, probably M_{21}.

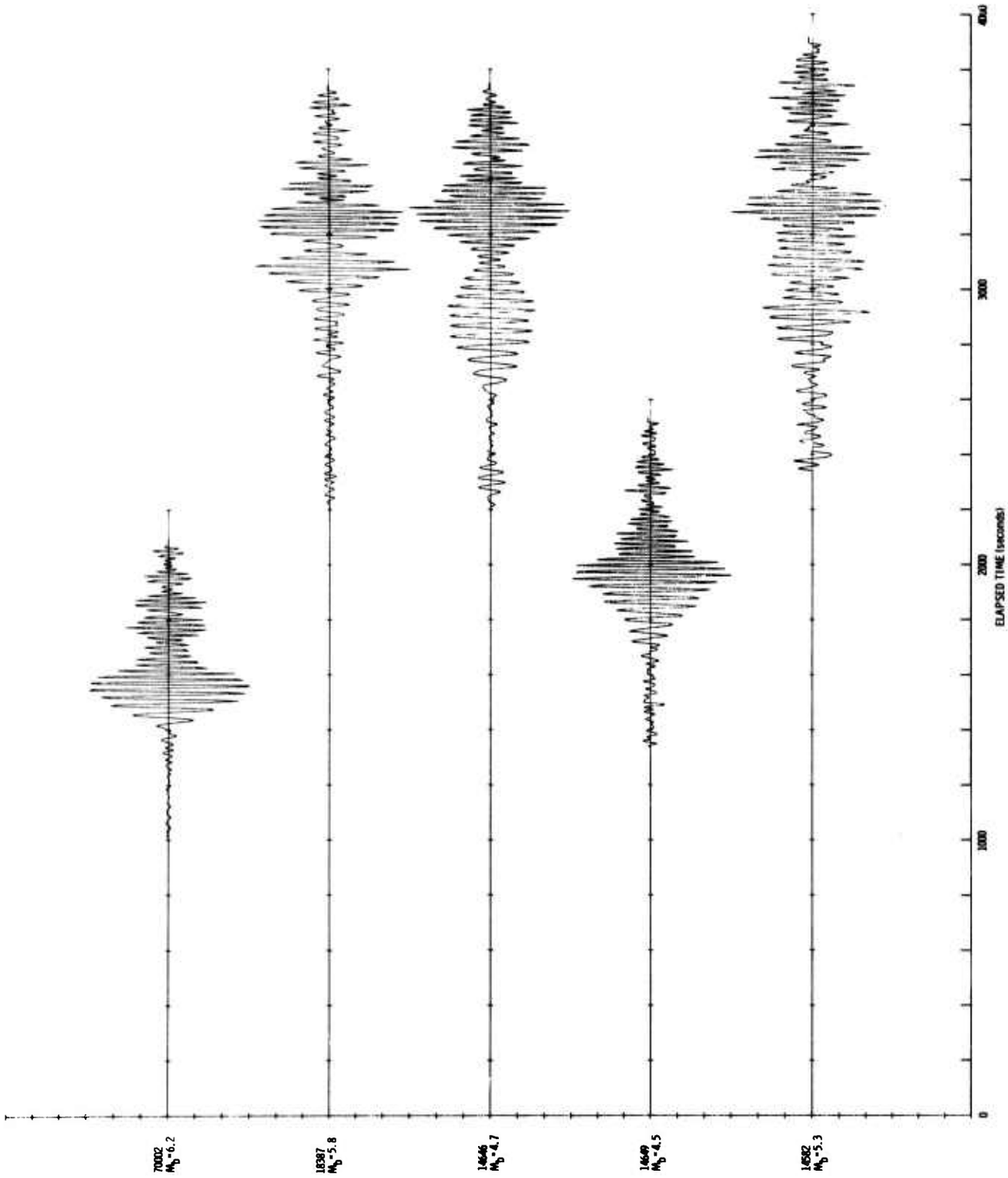

Figure IV-1. Event Seismograms (1 of 3)

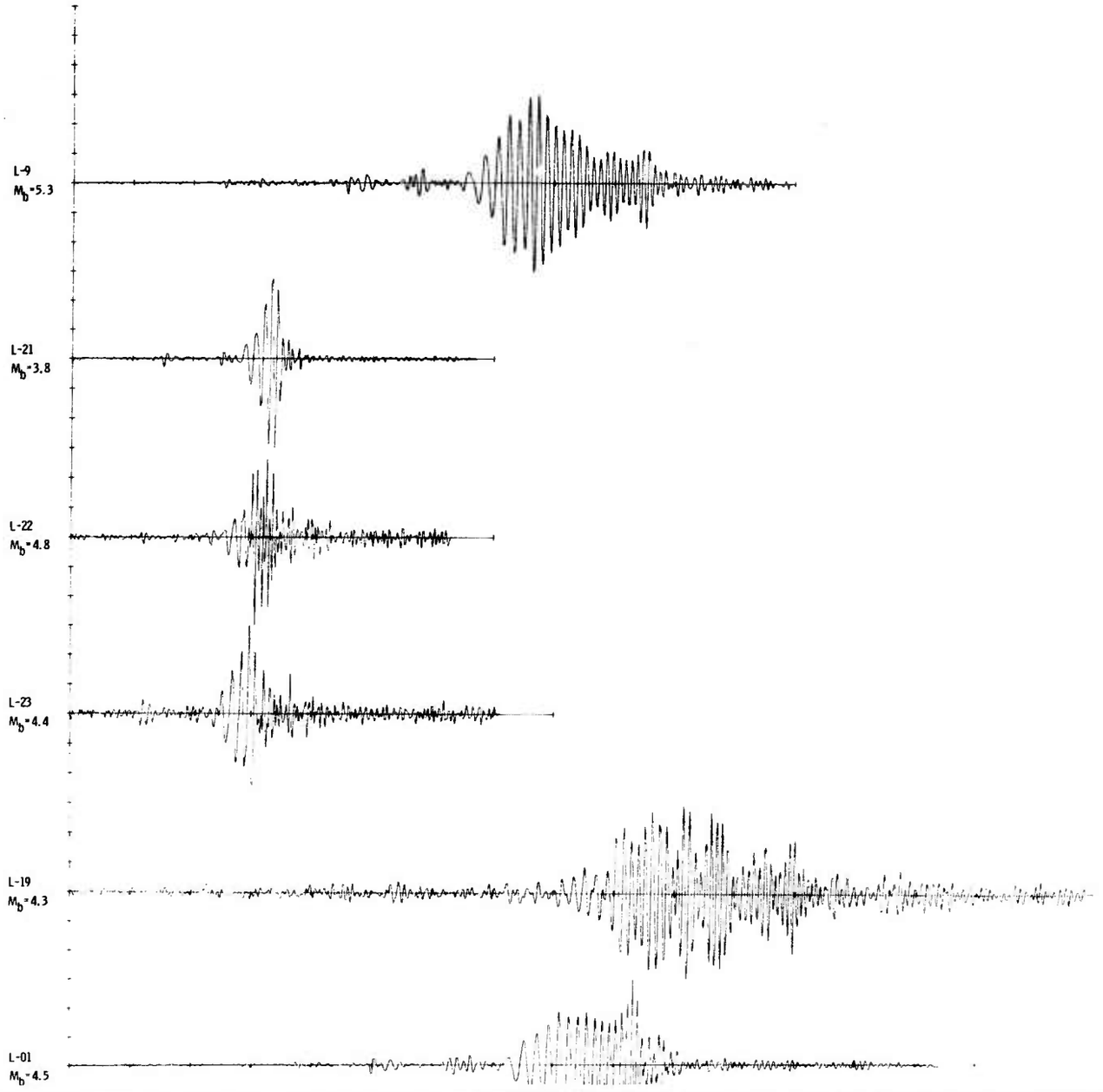
L-9
M_b=5.3
L-21
M_b=3.8
L-22
M_b=4.8
L-23
M_b=4.4
L-19
M_b=4.3
L-01
M_b=4.5

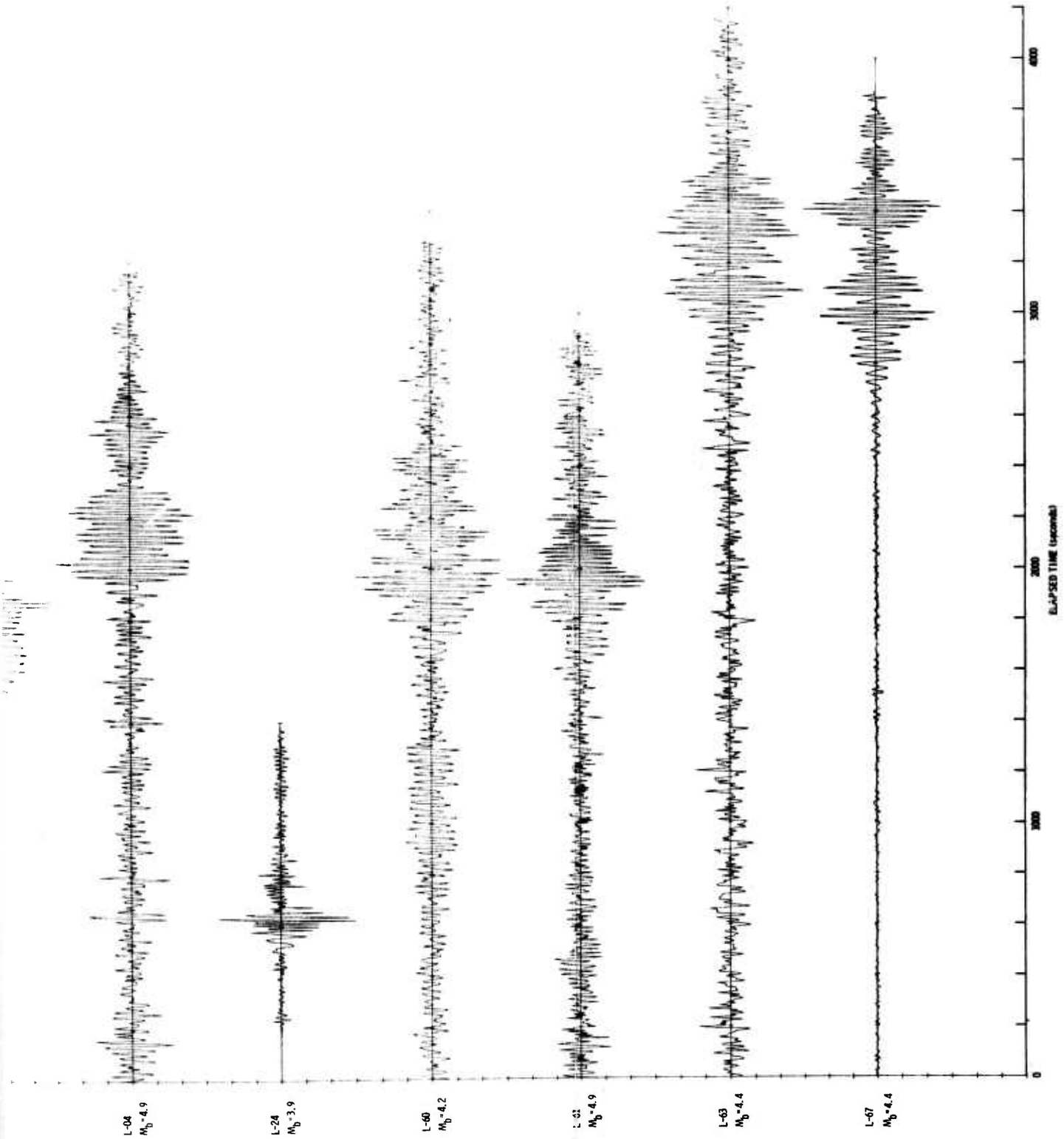

Figure IV-1. Event Seismograms (2 of 3)

17

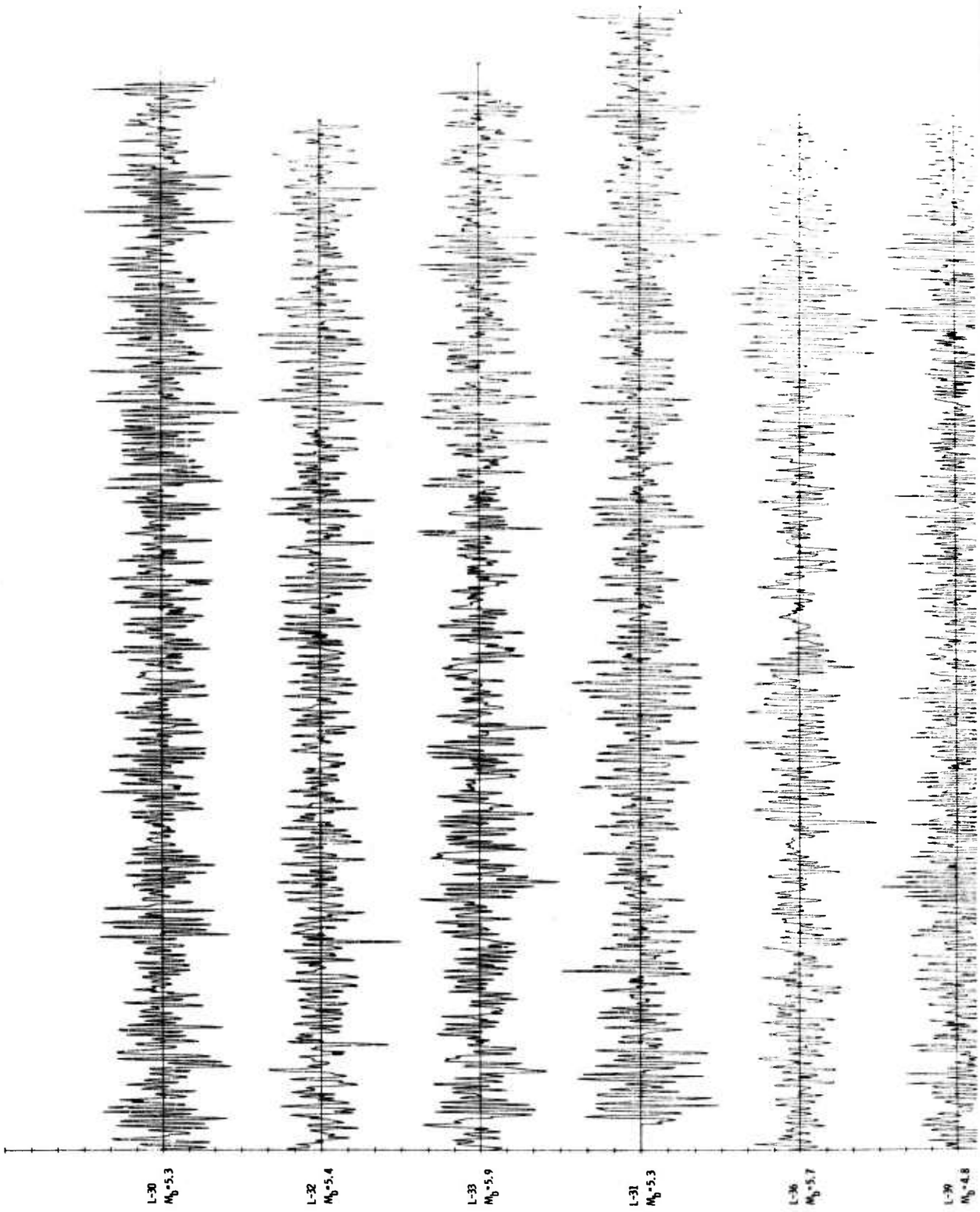

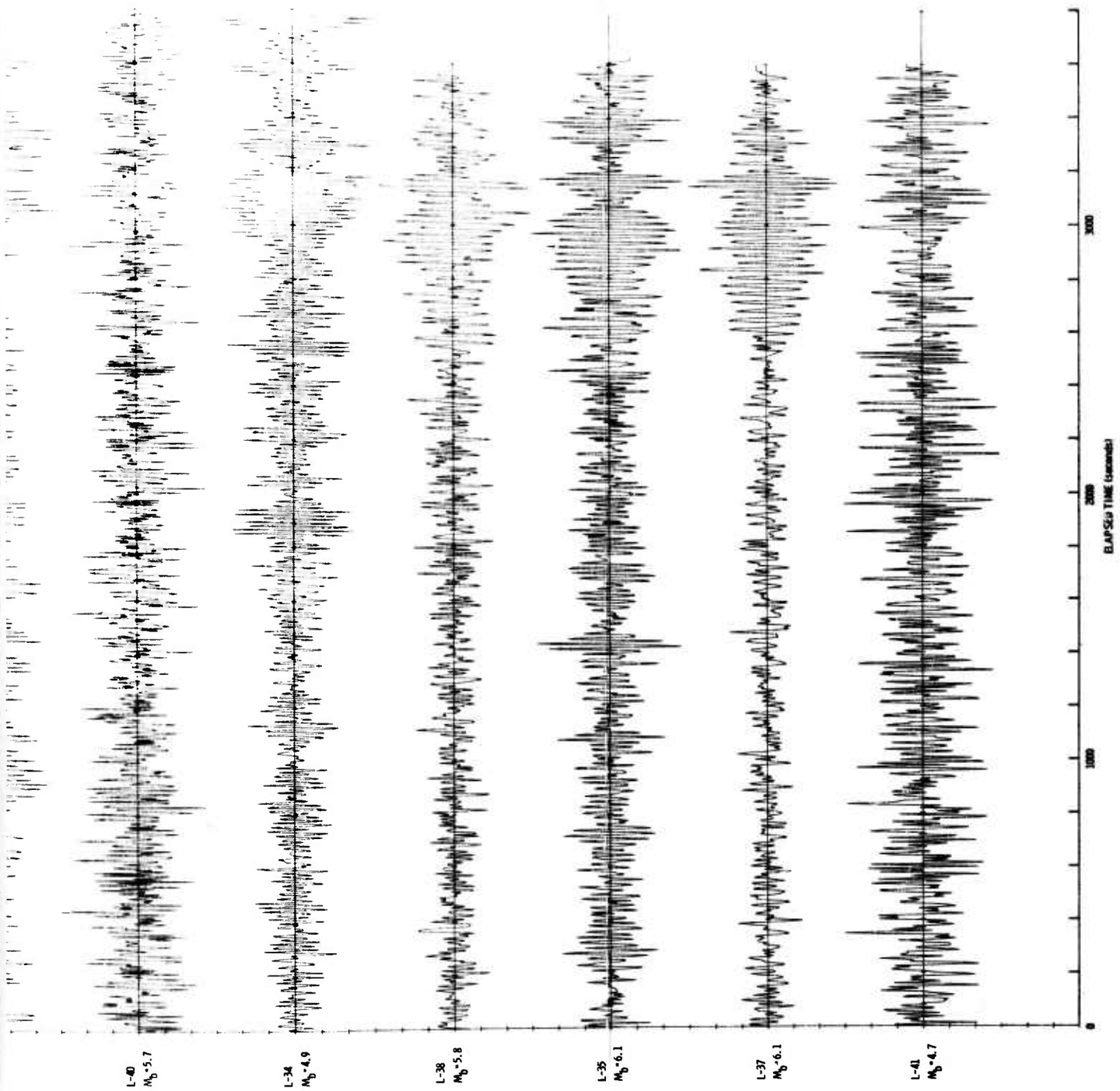

Figure IV-1. Event Seismograms (3 of 3)

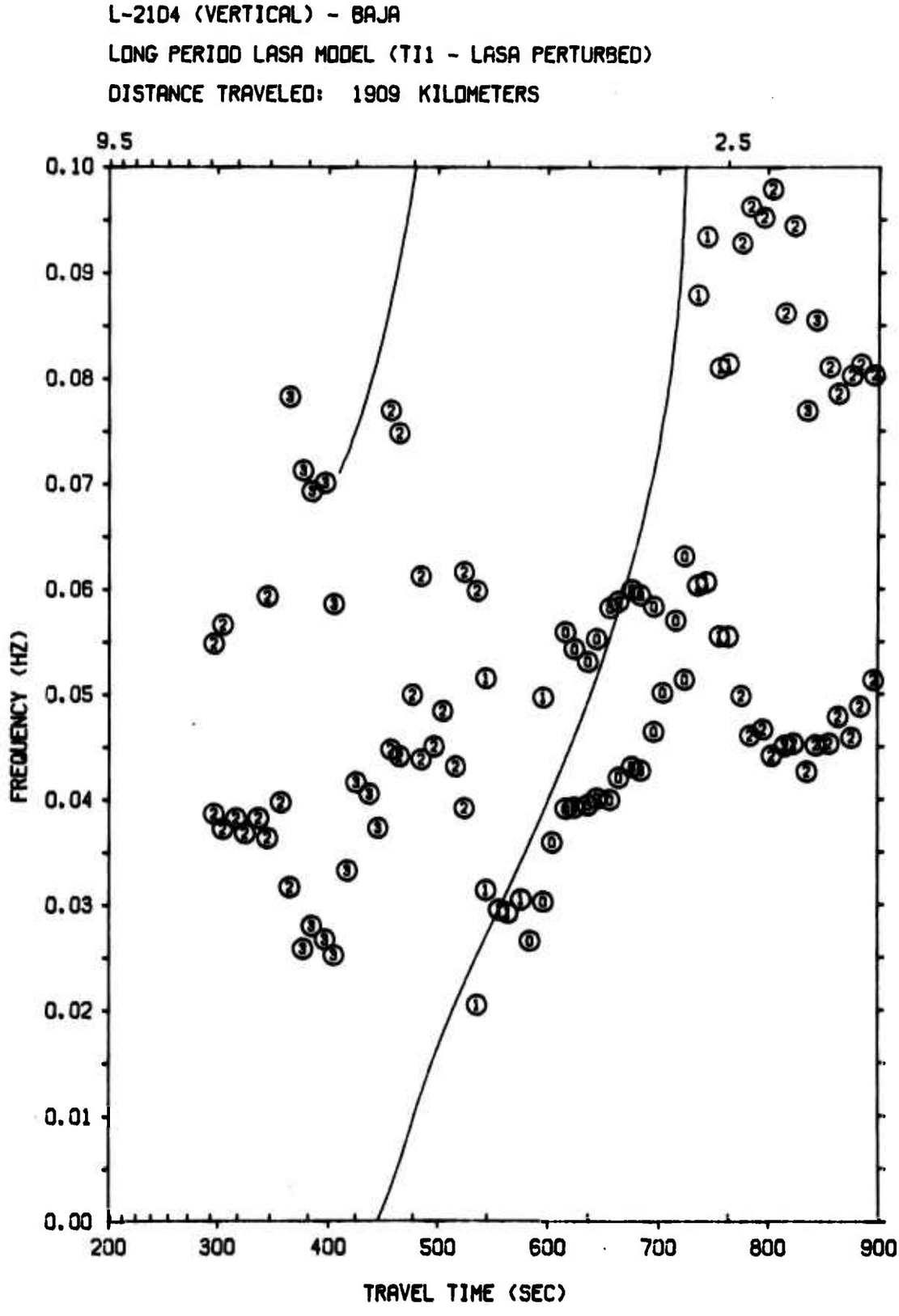

Figure IV-2. Experimental Dispersion Curve for L-21

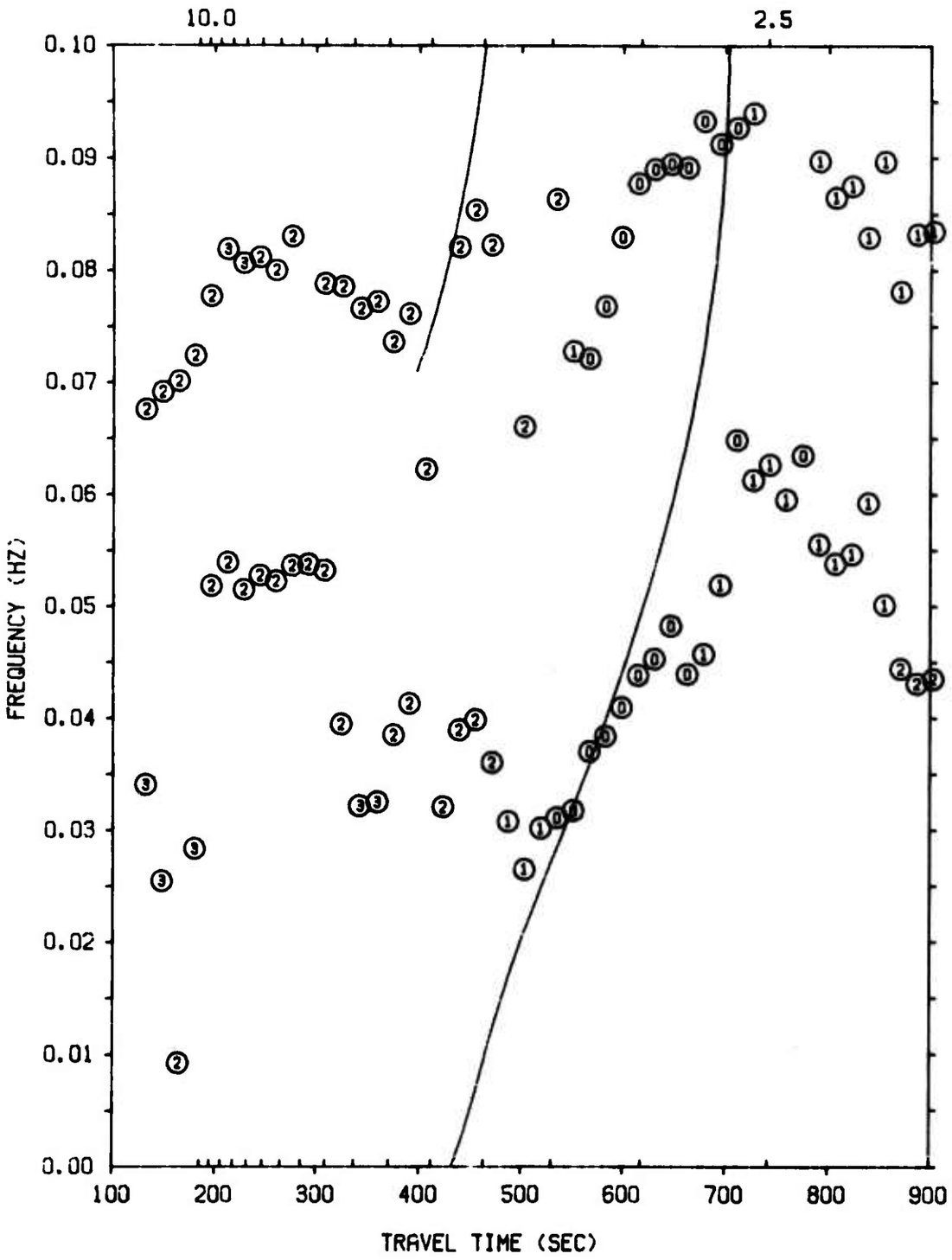

Figure IV-3. Experimental Dispersion Curve for L-22

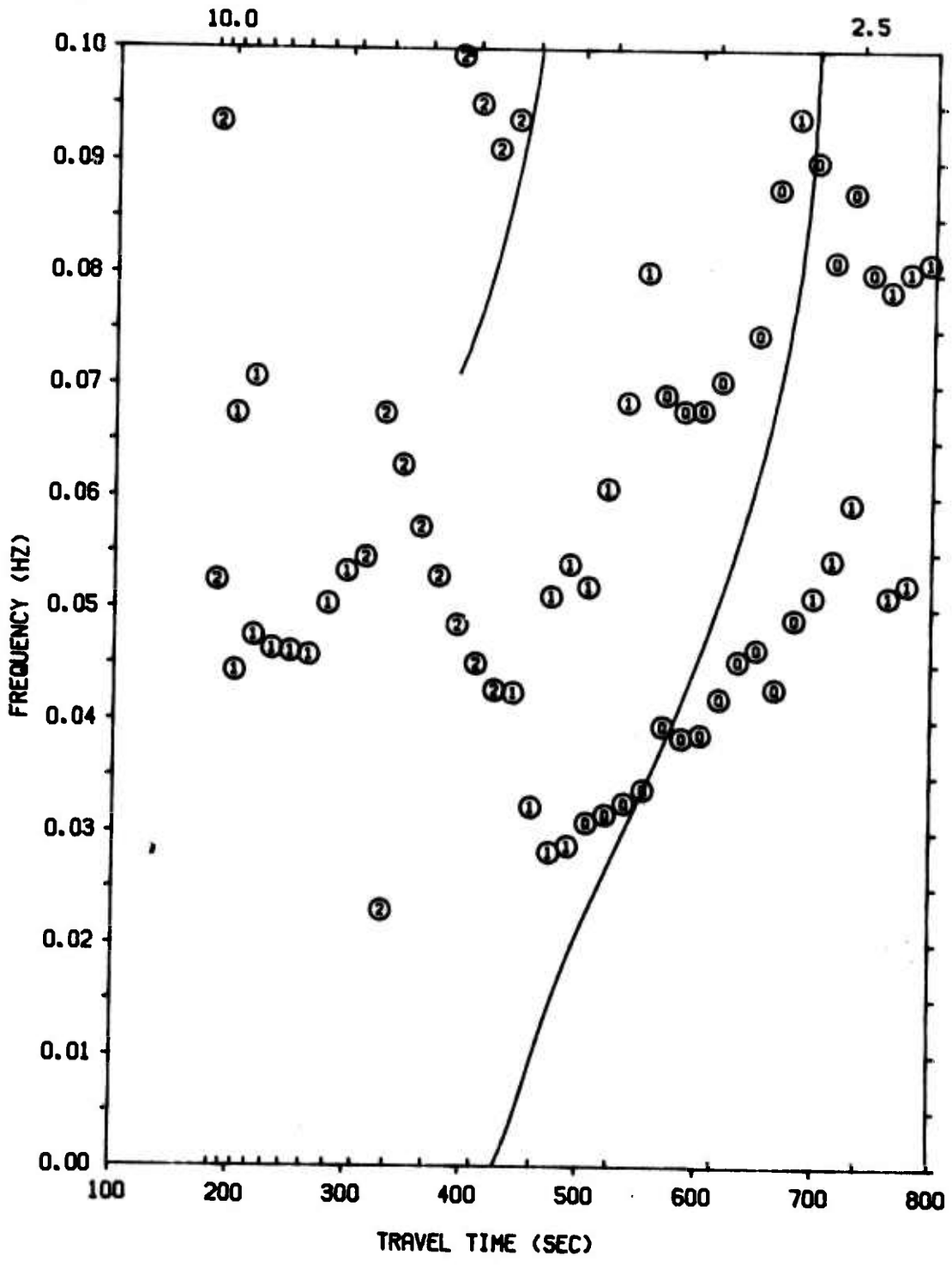

Figure IV-4. Experimental Dispersion Curve for L-23

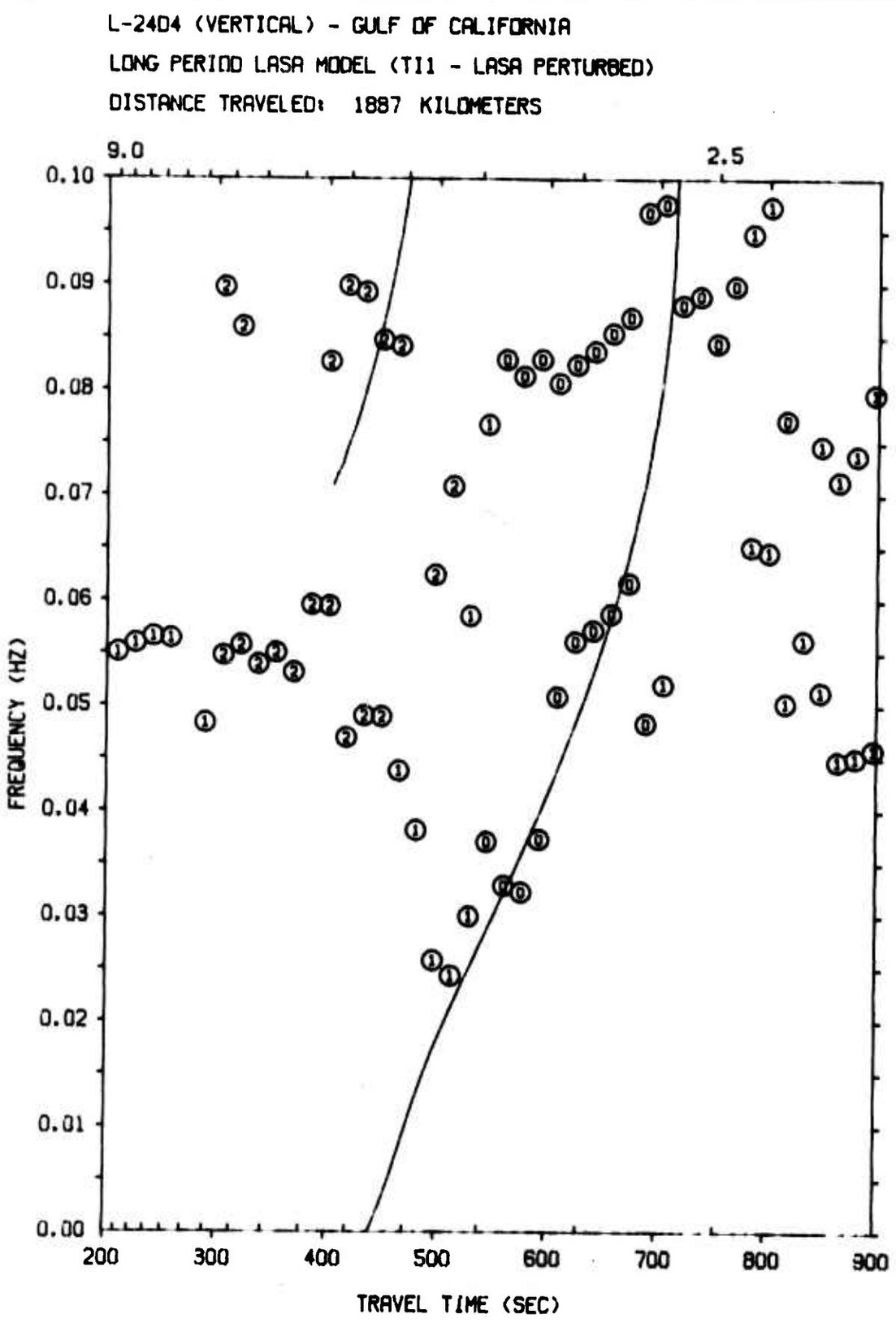

Figure IV-5. Experimental Dispersion Curve for L-24

Onset of the higher mode energy occurs at approximately the same time as the M_{11} onset. The presence of these two frequencies can be seen in the seismograms.

The P-wave arrivals can also be seen on the plots as a fairly compact bunch of points between 200- and 350-seconds, depending on the event. The smearing of the P-wave arrival in time is due to smoothing by the 100-second time window.

The dispersion of event L-09, Figure IV-6, is exceptionally clean and well-behaved and shows an almost straight-line frequency-travel-time characteristic. There is no apparent higher mode energy present. The computed dispersion is in reasonable agreement with the LASA dispersion and in some disagreement with the more oceanic type model for this path proposed by others.[11]

The analysis of the California group of events produced these conclusions:

- Strong higher mode energy was detected on four continental path events with epicenters in the northern part of the Gulf of California. These events are L-21, L-22, L-23, and L-24
- The LASA crustal model is only a fair approximation for the events in this group. M_{11} mode agreement is relatively good below 0.4 Hz, but M_{21} mode is extremely poor and inadequate for identification

B. THE KURILE-KAMCHATKA GROUP

The Kurile-Kamchatka group includes three events at or near the Kurile-Kamchatka Trench, L-04, L-19, and L-60; one event at Amchitka Island, EPX-70002; and one event in northeastern China, L-67. The propagation paths of L-04, L-19, L-60, and L-61 are very nearly identical

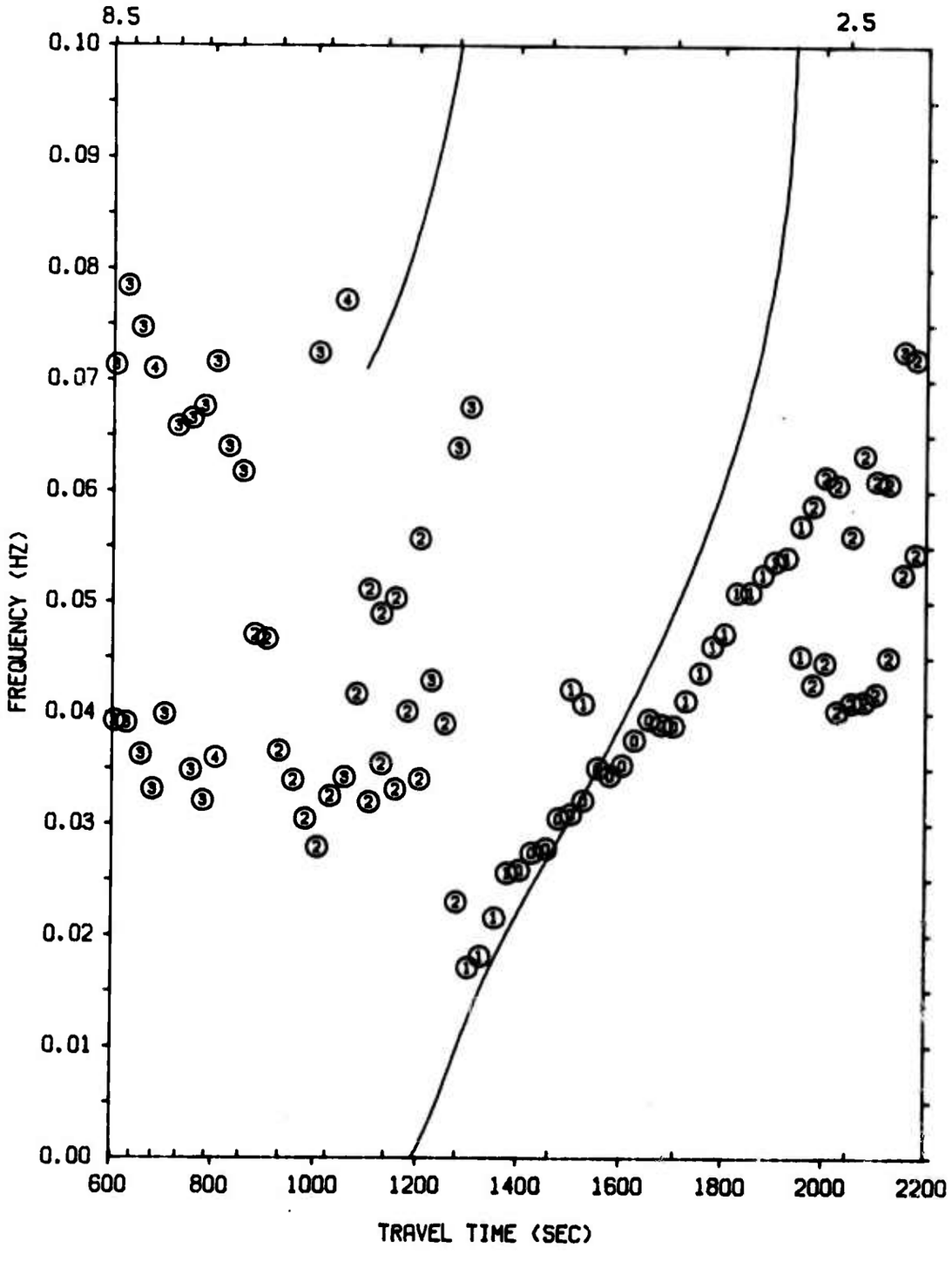

Figure IV-6. Experimental Dispersion Curve for L-09

with an azimuth range of only 3.4 degrees for the four. L-19 and L-60 are separated in azimuth by only 2.0 degrees, and their epicenters are separated by only about 22 km. The path for these four events crosses the Bering Sea and the southern coast of Alaska.

The path of event EPX-70002 follows the Aleutian Islands and crosses the Gulf of Alaska. The path of L-67 is almost entirely continental, crossing briefly the Chukchi Sea.

The group velocity dispersion found for L-04 is shown in Figure IV-7. Time-gate shift was 24 seconds. This event is characterized by a wave spectrum ranging only from 0.03 Hz to about 0.06 Hz. The main Rayleigh mode is only slightly dispersed and differs from the seismic noise only in power. No discernible higher mode was present.

The epicenters of L-19 and L-60 were very close together and occurred 8 days apart. Their dispersion plots, Figures IV-8 and IV-9, show well-dispersed Rayleigh modes which are remarkably similar to each other. Time shift between gates was 24 seconds for both. Onset occurs at about 1600 seconds and is signified by a small patch of low-power peaks around 0.028 Hz. The strongest peaks then arrive in two bunches at 0.04 HZ and at 0.05 Hz. At 2300 seconds, a single dispersed string of peaks rises to 0.07 Hz before dying out.

The plotting of the Rayleigh dispersion is a classic multipath phenomenon. (The cause could also be multiple sources.) The coherent mixing of the waves, one of which has been delayed about 100 seconds, produces an amplitude modulation resulting in the appearance of sum and difference frequencies. The modulation is evident in the seismograms. At about 2040 seconds, the frequency is about 0.045 Hz and the beat frequency of the wave envelope is about 0.008 Hz. The frequencies which must create these conditions are 0.045 ± 0.008 Hz which are approximately what appears in the dispersion.

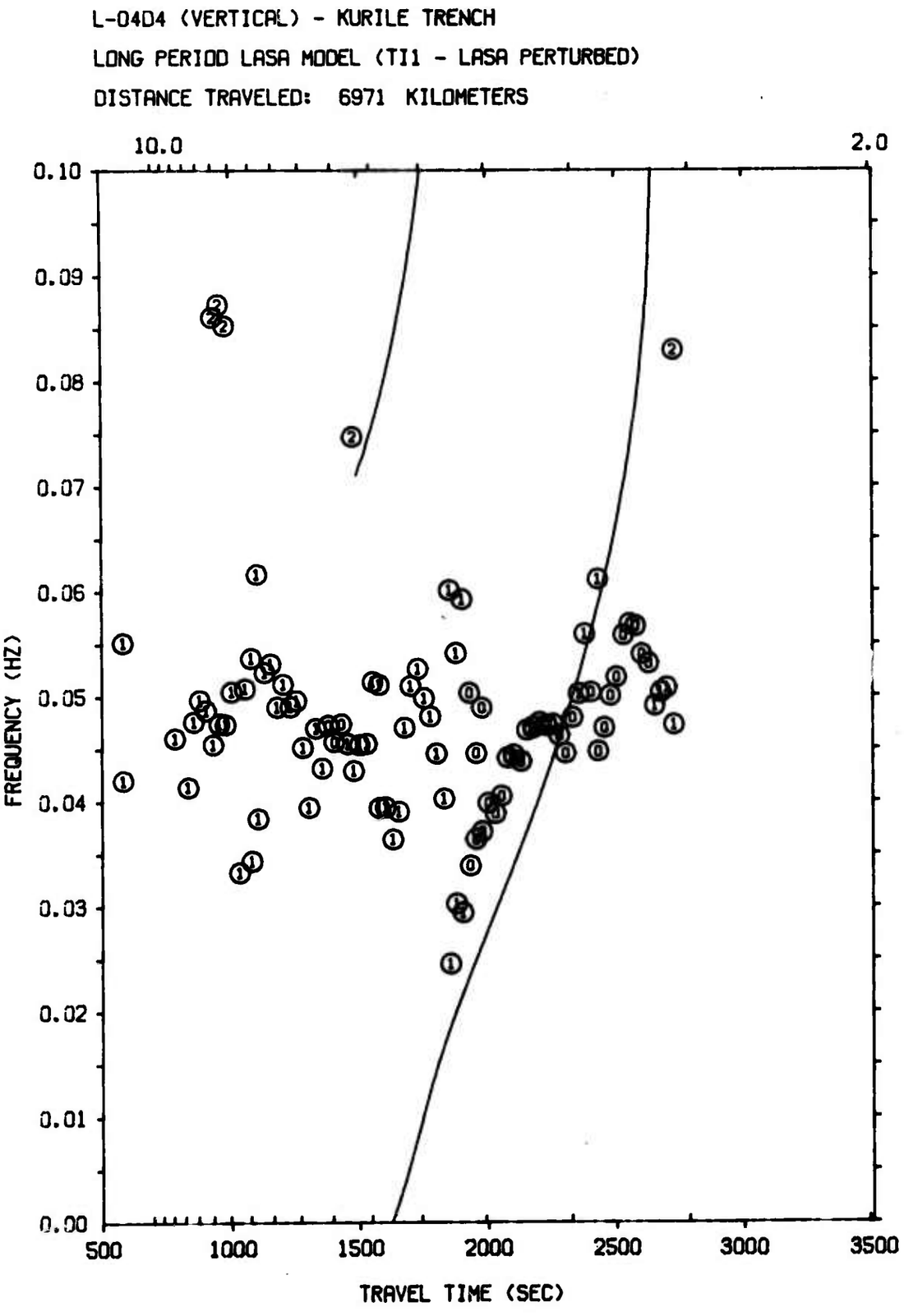

Figure IV-7. Experimental Dispersion Curve for L-04

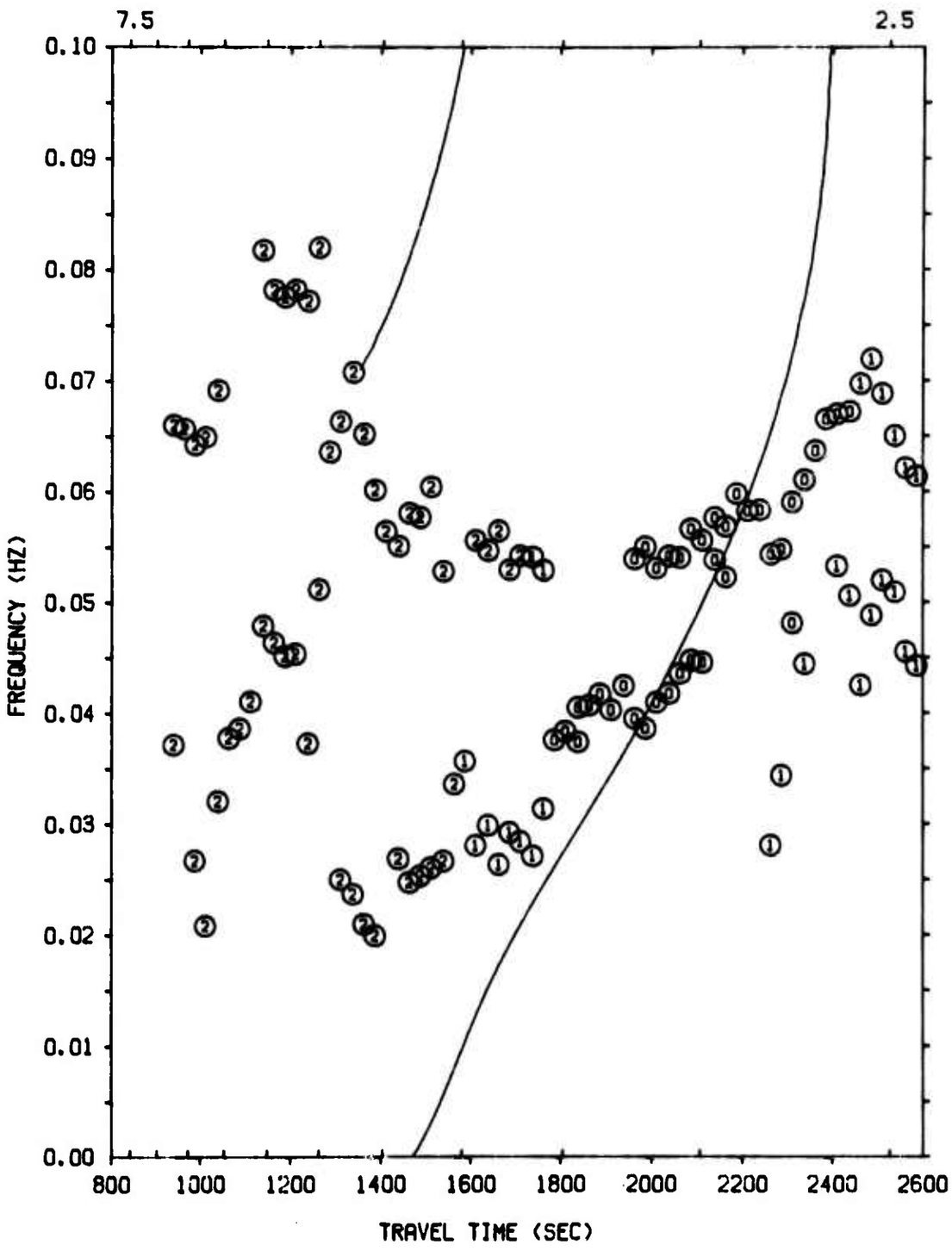

Figure IV-8. Experimental Dispersion Curve for L-19

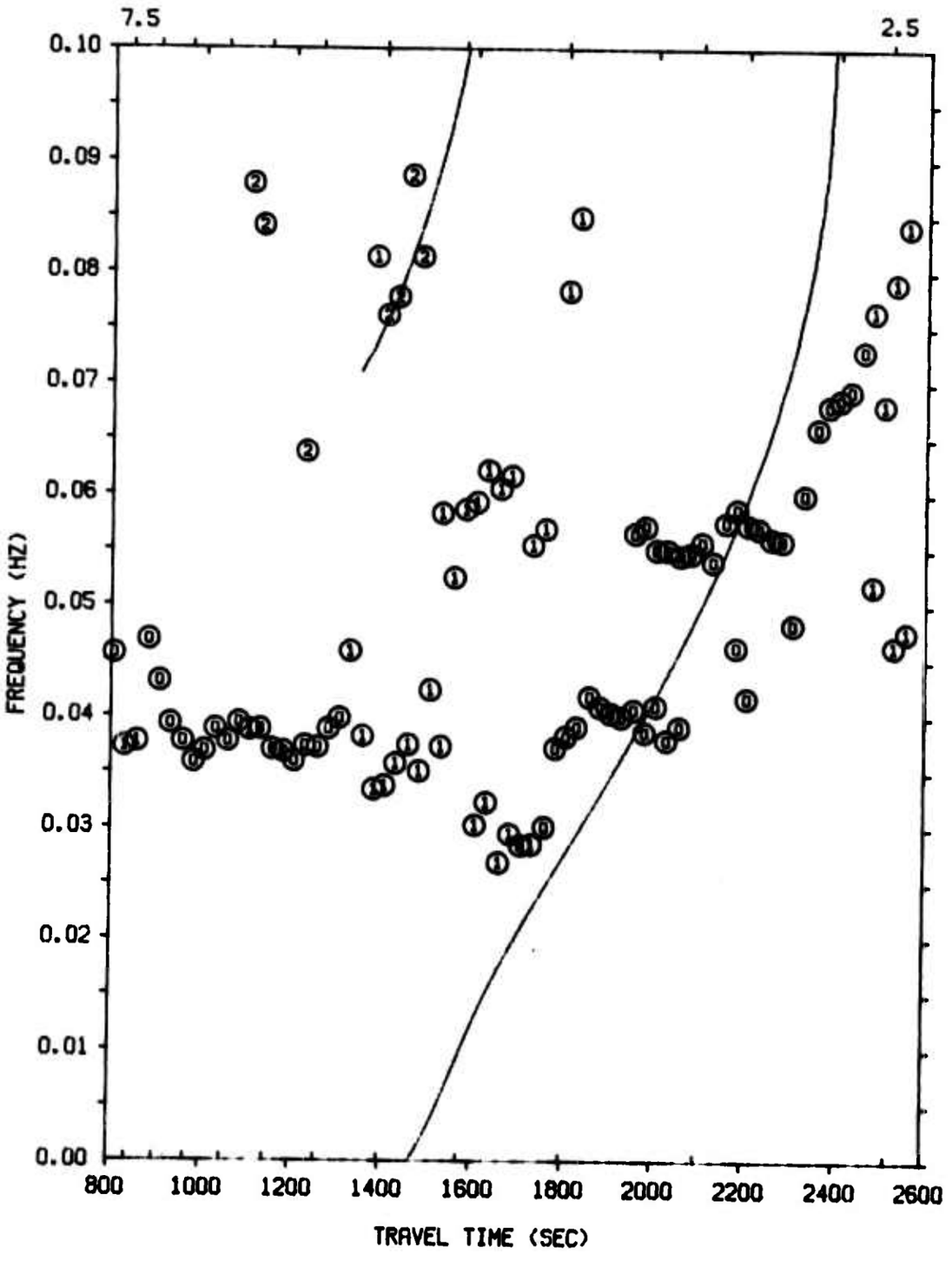

Figure IV-9. Experimental Dispersion Curve for L-60

What appears to be possible leaking mode energy, PL_{21}, can be seen in L-60 at 0.037 Hz between 900 and 1300 seconds travel time. These times correspond to a range of velocities between 7.0 to 4.8 km/sec. This identification is speculative since time velocity and particle motion of the waves are unknown.

Event L-61 displays a dispersion, Figure IV-10, which is in excellent agreement with the LASA model. No multipath effects or higher modes are visible.

L-67, Figure IV-11, also shows a dispersion which agrees closely with the LASA model. Time shift was 60 seconds. At onset, about 2400 seconds travel time, the wave maintains a single frequency at 0.03 Hz for about 300 seconds, after which normal dispersion begins. At 3000 seconds, higher frequency energy appears which is due to modulation of the envelope of the Rayleigh mode by multipath. The modulation becomes strong enough at 3300 seconds to split the dispersion curve in a manner similar to L-19 and L-60. No true higher mode is apparent either on the seismogram or travel-time plot.

The experimental dispersion of event EPX-70002 is shown in Figure IV-12. The length of this seismogram was such that little pre-arrival noise was available for analysis. No higher modes are present, but there is splitting of the M_{11} dispersion due to multipath interference. The multipath can also be seen in the amplitude modulation of the M_{11} envelope.

The results of the analysis of the Kurile-Kamchatka group produced the following conclusions:

- What is identified as possible PL_{21} "leaking" mode energy was detected in event L-60. This identification is unsupported since actual velocity and particle motion is unknown.
- No normal higher shear modes were observed.

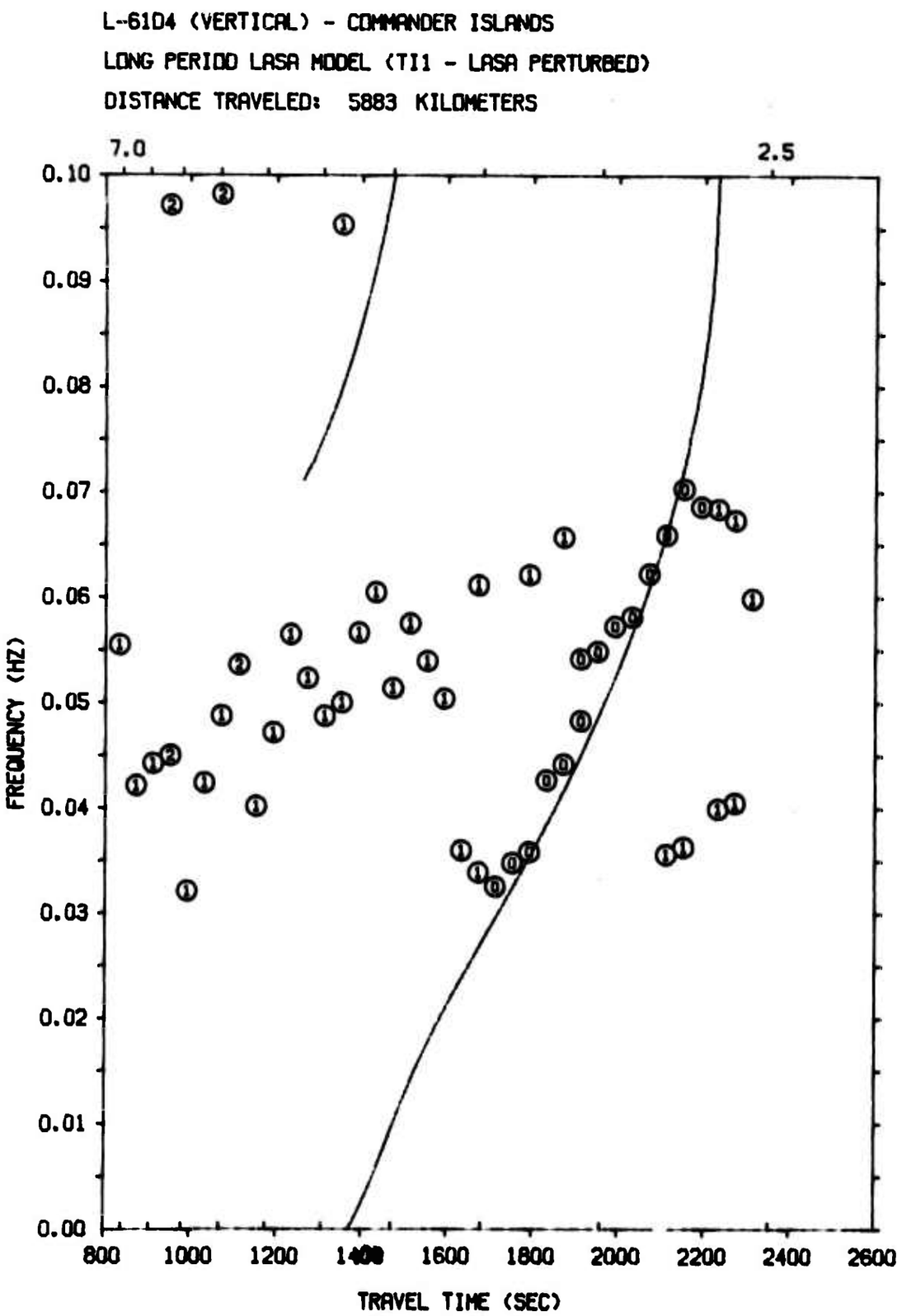

Figure IV-10. Experimental Dispersion Curve for L-61

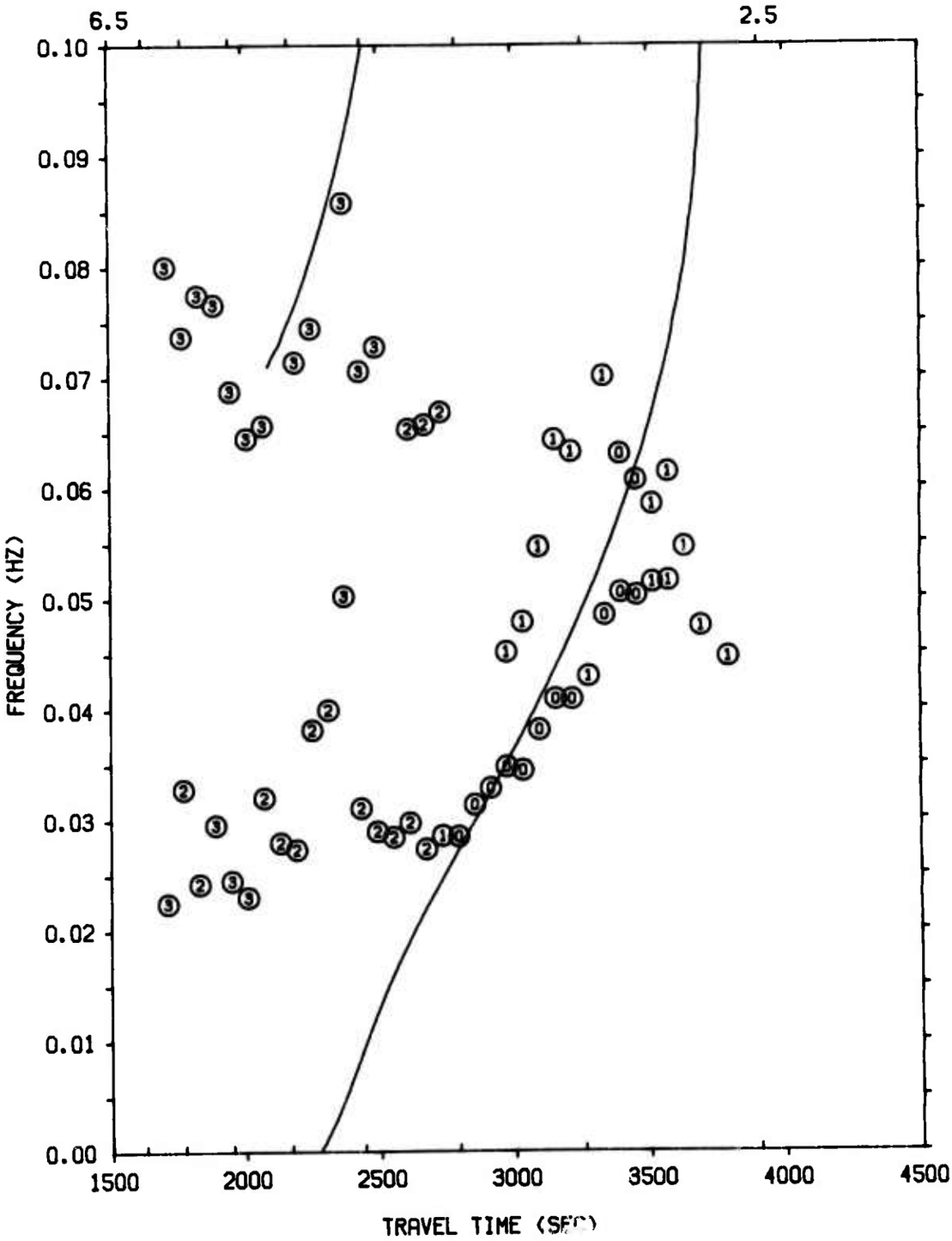

Figure IV-11. Experimental Dispersion Curve for L-67

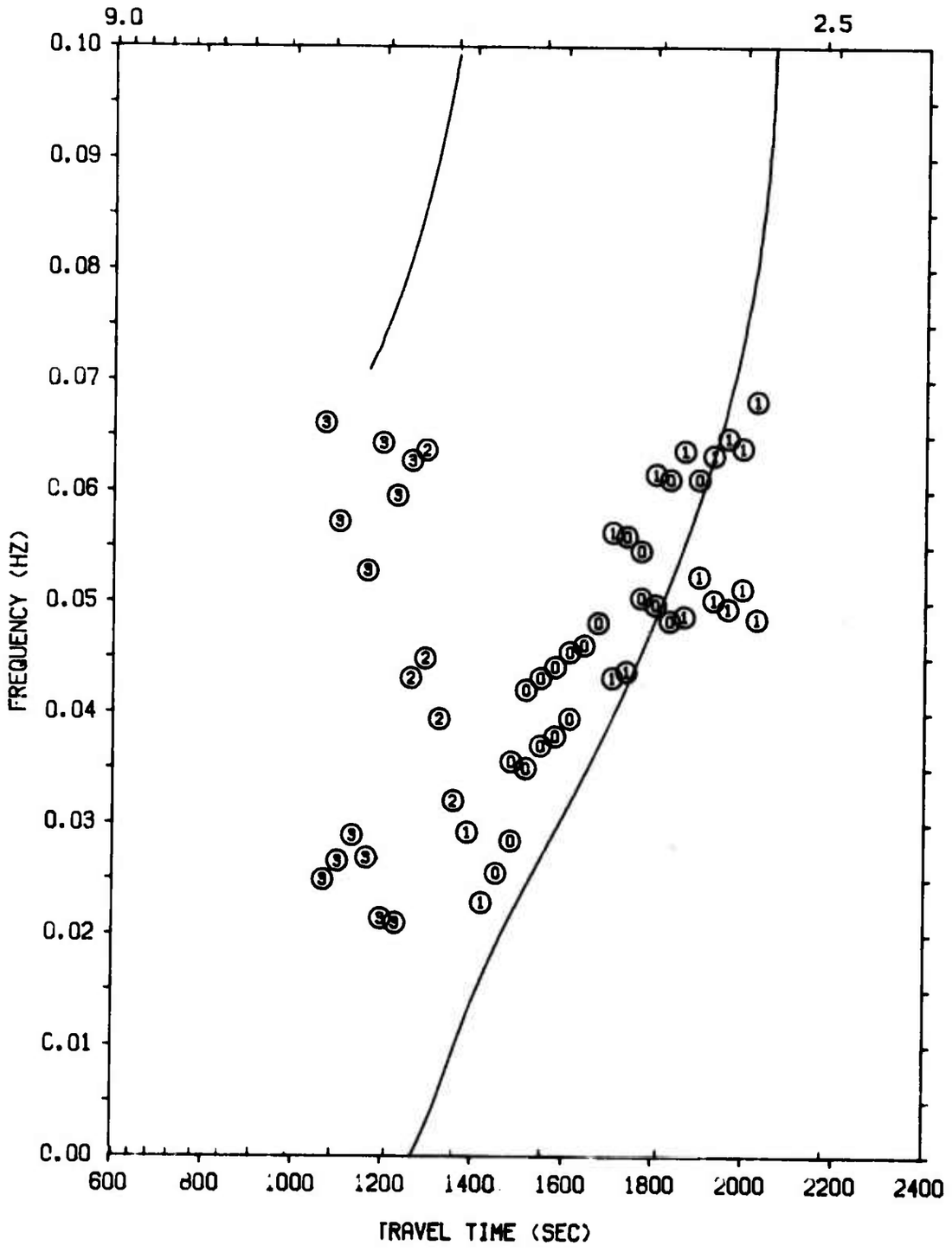

Figure IV-12. Experimental Dispersion Curve for EPX-70002

- Presumed multipath interference is common in events from this area. This is characterized by a well-developed amplitude modulation of the Rayleigh wave envelope and splitting of the experimental group velocity dispersion curve. This splitting may cause systematic errors in conventionally measured dispersion.
- The measured group velocities of the Rayleigh modes are in good agreement with those predicted by the LASA crustal model; however, the variation with frequency is somewhat greater than that predicted by the model.

C. THE CHINA-KAZAKH GROUP

The China-Kazakh group is made up of events which have propagation paths across the Arctic Ocean. The minimum oceanic path length is larger than 2500 km. Events L-30 through L-41, with the exception of L-35 and L-37, are generally of very low signal-to-noise ratio. Events L-63, EPX-14582, and EPX-14646 have much larger signal-to-noise ratios. It was expected that no higher modes would be detected because of the poor signal-to-noise ratio; however, for at least one event, L-35, strong high-frequency energy was found.

The group velocity dispersion of L-30 is shown in Figure IV-13. Despite no visible event on the seismogram, a definite indication of a dispersed wave is shown on the travel-time plot. It is possible that this line of peaks is a random occurrence, but the good agreement with the arrival times predicted with the LASA crustal model argues against it. The narrowband noise centered about 0.059 Hz is not event related.

The dispersion plots of L-31, L-32, L-33, and L-34 are shown in Figures IV-14, IV-15, IV-16, and IV-17 respectively. None of these plots show any evidence of event-related surface wave energy. L-34 also has narrowband energy centered at 0.065 Hz. This energy increased in strength during the time of arrival expected from the LASA model; however, this is probably only a chance occurrence.

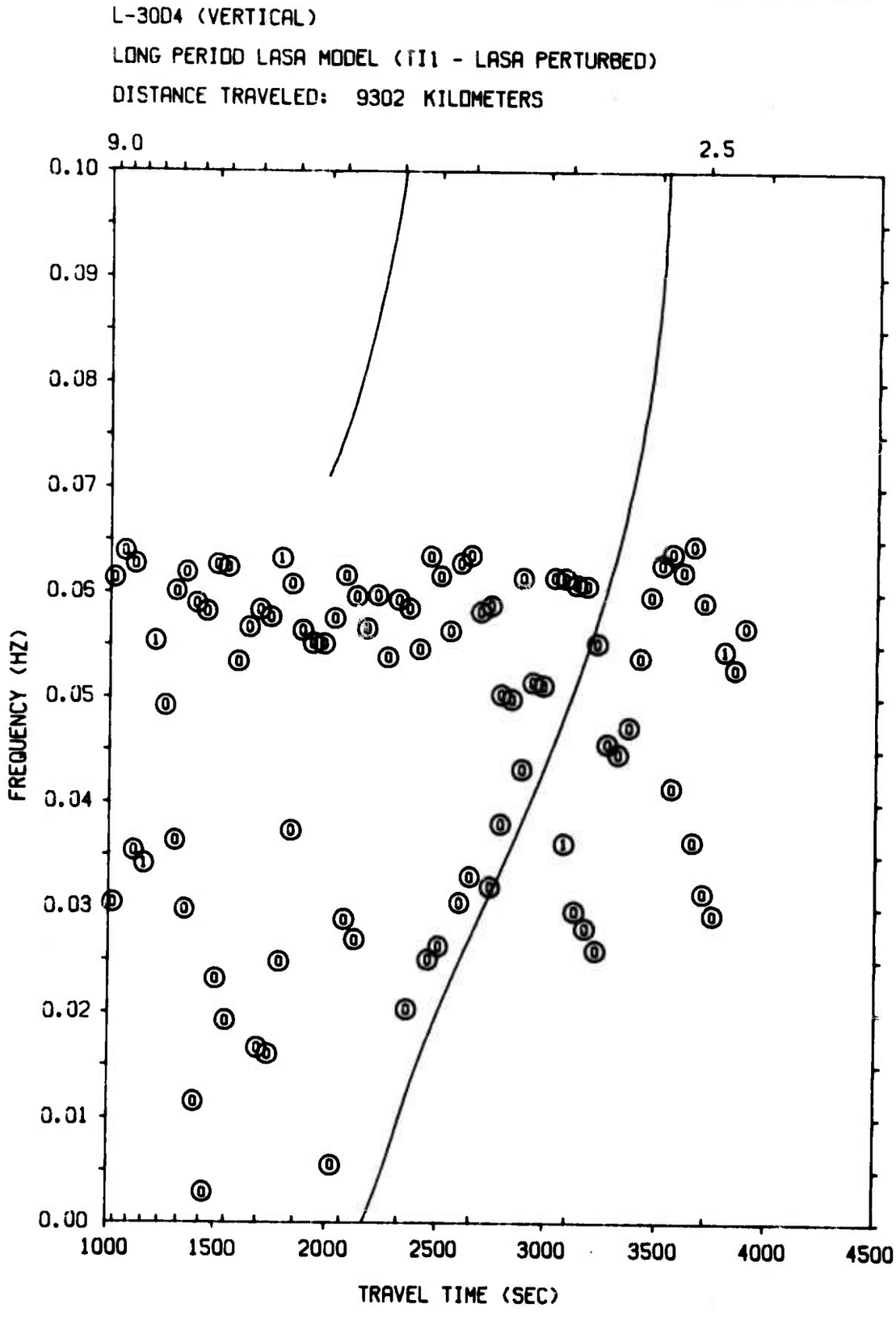

Figure IV-13. Experimental Dispersion Curve for L-30

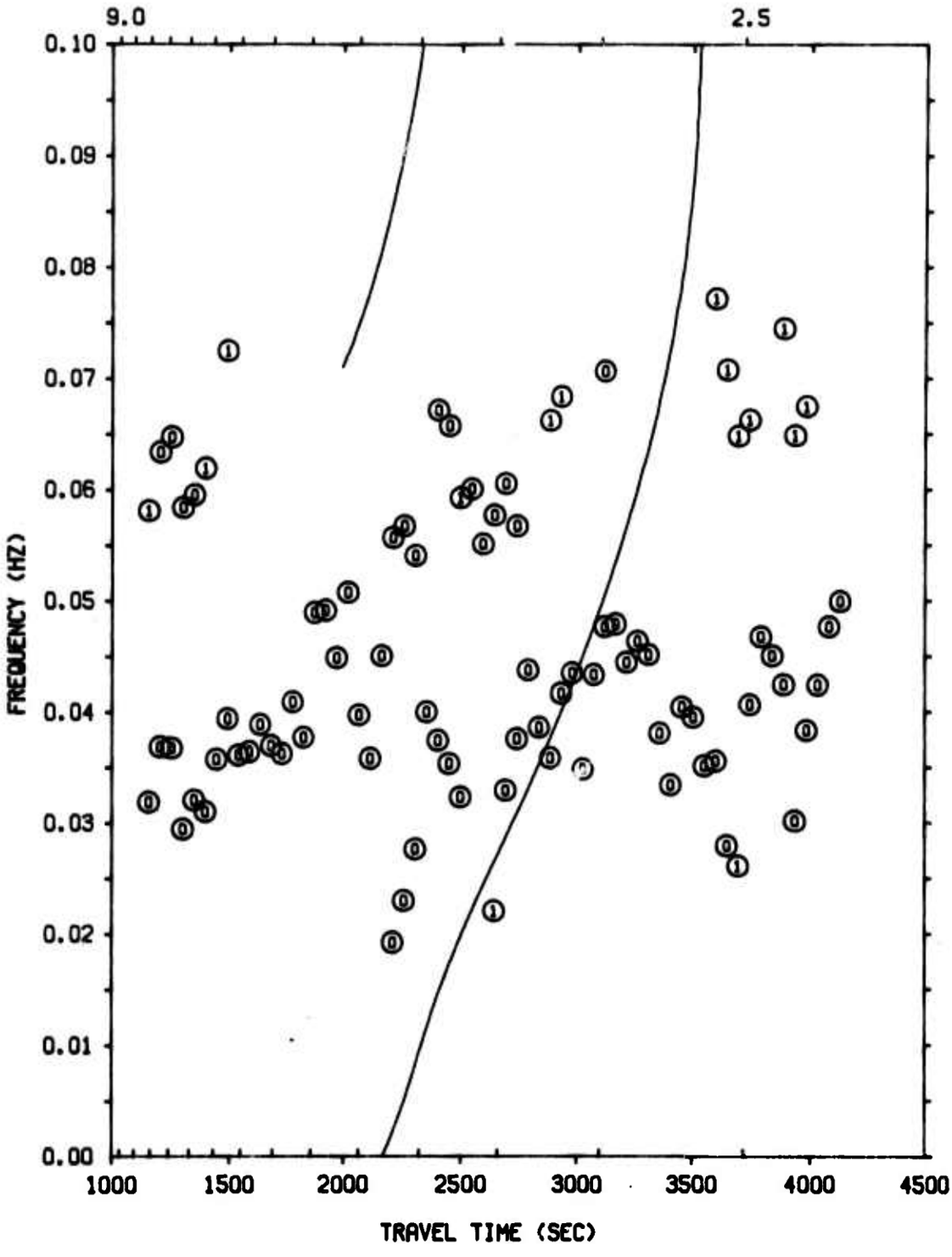

Figure IV-14. Experimental Dispersion Curve for L-31

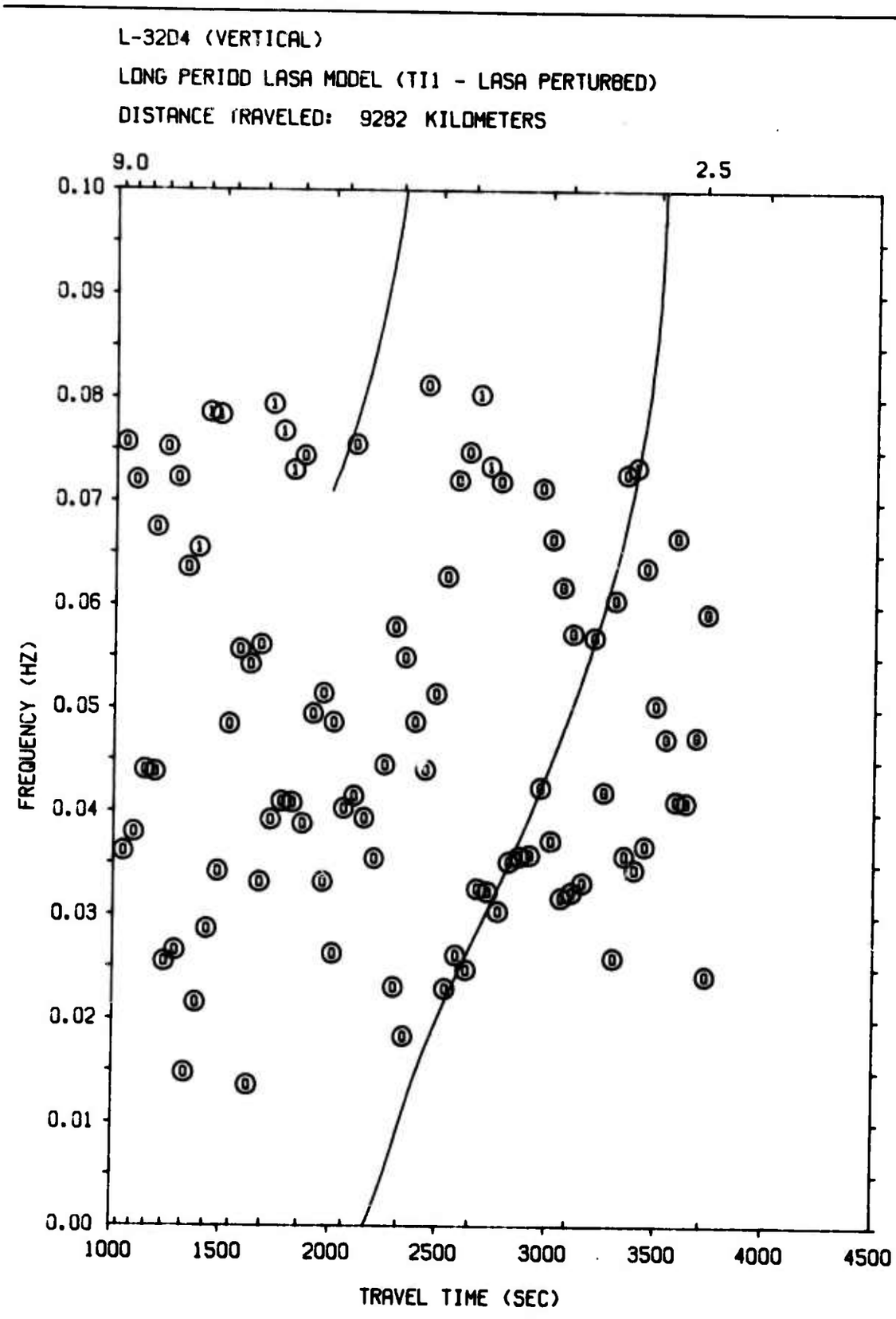

Figure IV-15. Experimental Dispersion Curve for L-32

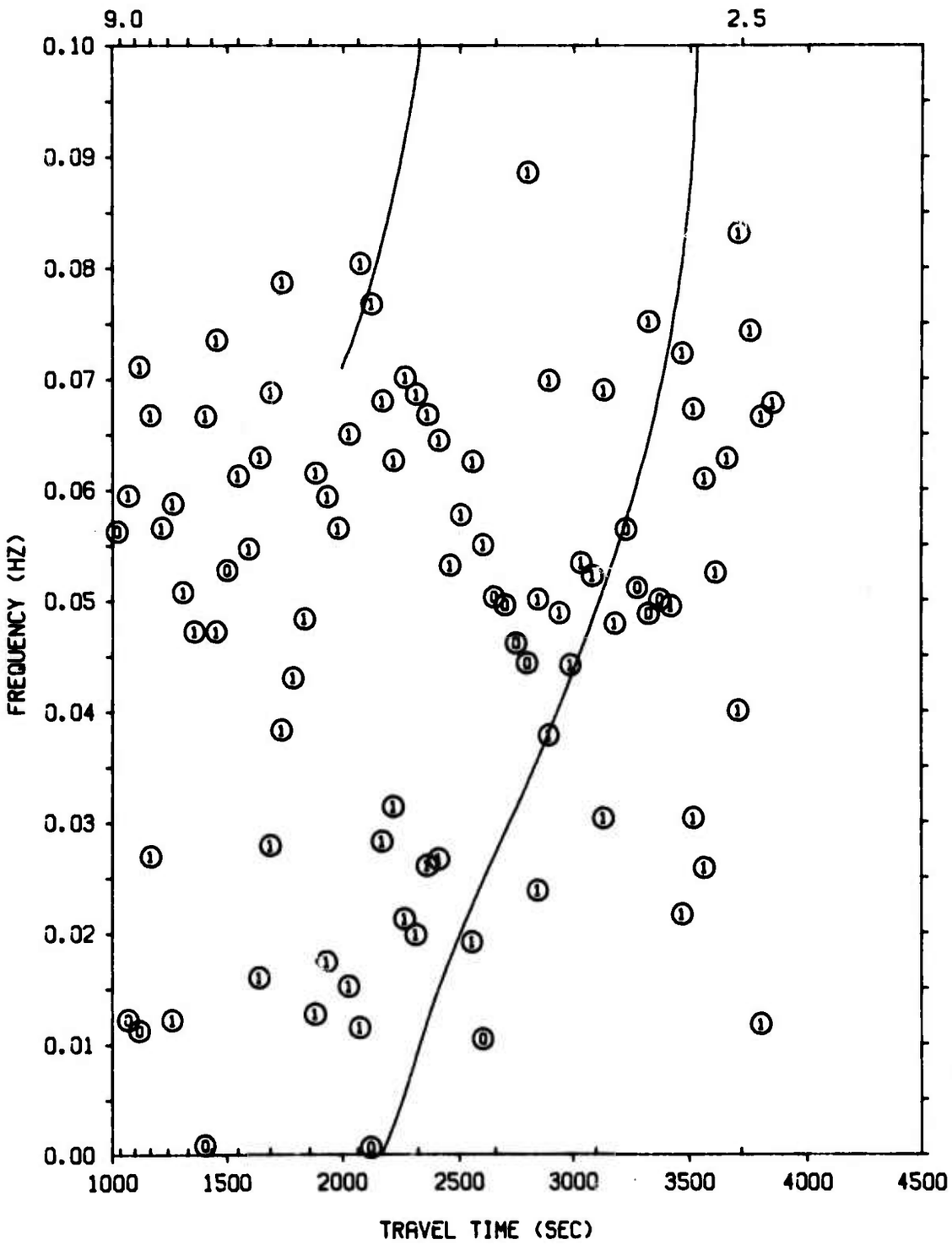

Figure IV-16. Experimental Dispersion Curve for L-30

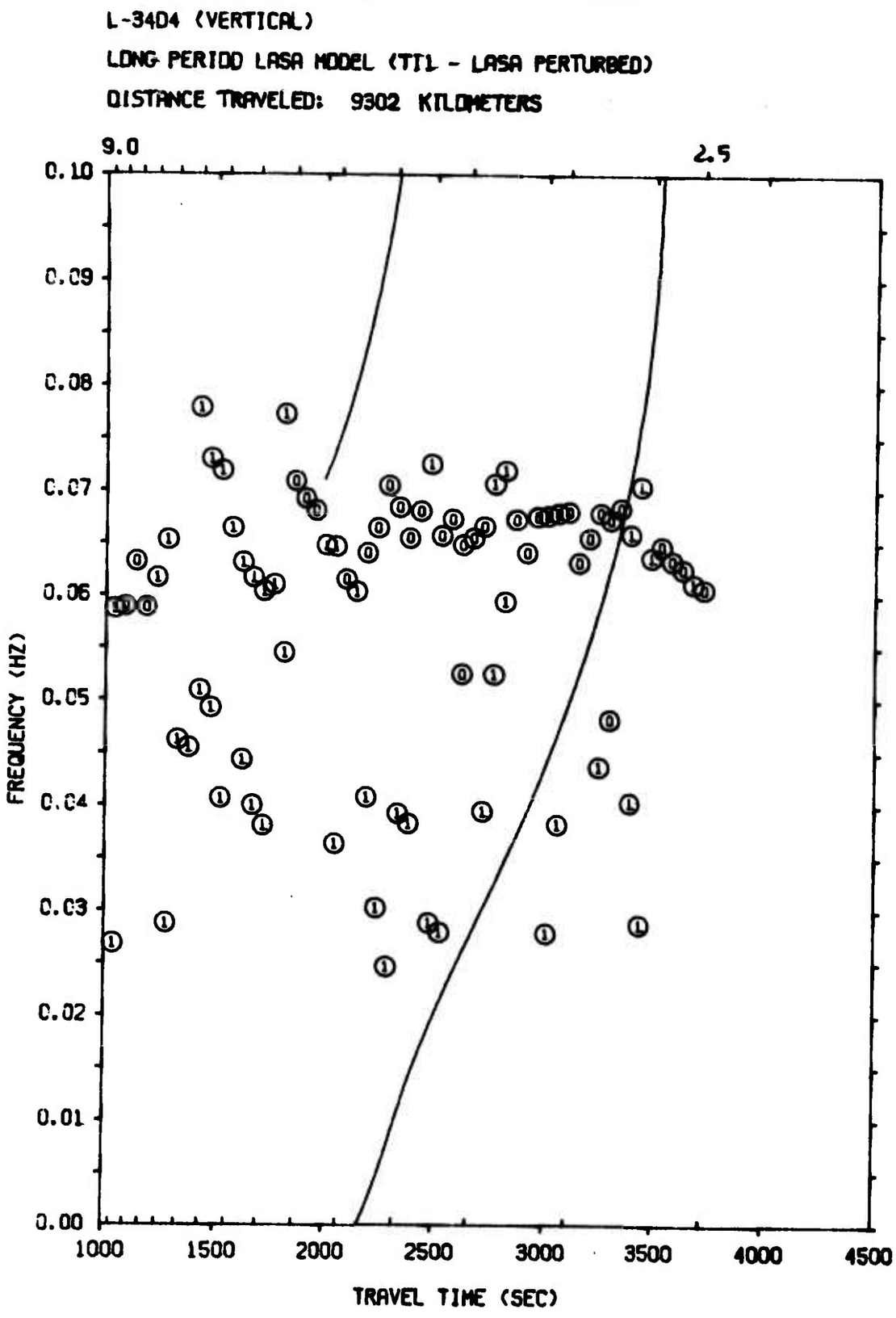

Figure IV-17. Experimental Dispersion Curve for L-34

Event L-35 has a larger signal-to-noise ratio than most of the events in this group. Its group velocity dispersion, Figure IV-18, shows excellent agreement with the model. Time-gate shift was about 25 seconds. In addition to the well-defined M_{11} mode, there are indications of two different higher modes. The first appears as a set of peaks between 0.08 Hz and 0.095 Hz at a travel time of around 2300 seconds. This corresponds to a group velocity of about 4 km/sec. This set also occurs very close to the predicted M_{21} mode for the LASA model.

The other higher mode energy is evidenced by a dispersed line of points beginning at 0.055 Hz at a travel line of 2400 seconds (4 km/sec) and running up to 0.095 Hz at 3100 seconds (3 km/sec). Since the seismogram is well modulated, the latter line of peaks may be multipath. This event is one of the few that produced energy of significance above 0.08 Hz.

Event L-36 has a recognizable wavetrain on its seismogram. However, its groups velocity dispersion (Figure IV-19) is rather weak. It follows the LASA model prediction very well, but if the curve were not there, it would be difficult to pick the event dispersion by eye. The failure of the ME technique to "detect" the Rayleigh wave can only be explained by saying that the wave was not particularly dispersed and that only the amplitude of the earth motion increased.

The dispersion found for event L-37 is shown in Figure IV-20. Agreement between the experimental M_{11} dispersion and predicted dispersion is almost exact. Gate shift was 48 seconds. When this event was examined initially during preliminary testing,[12] a string of points between 2000 and 2500 seconds and 0.05 Hz to 0.075 Hz seemed to indicate higher mode energy. This first test used very little overlap and it is probably only by chance that those peaks were in a line. This test with more overlap and an improved filter design algorithm[4] shows no indication of higher modes. The set of peaks between

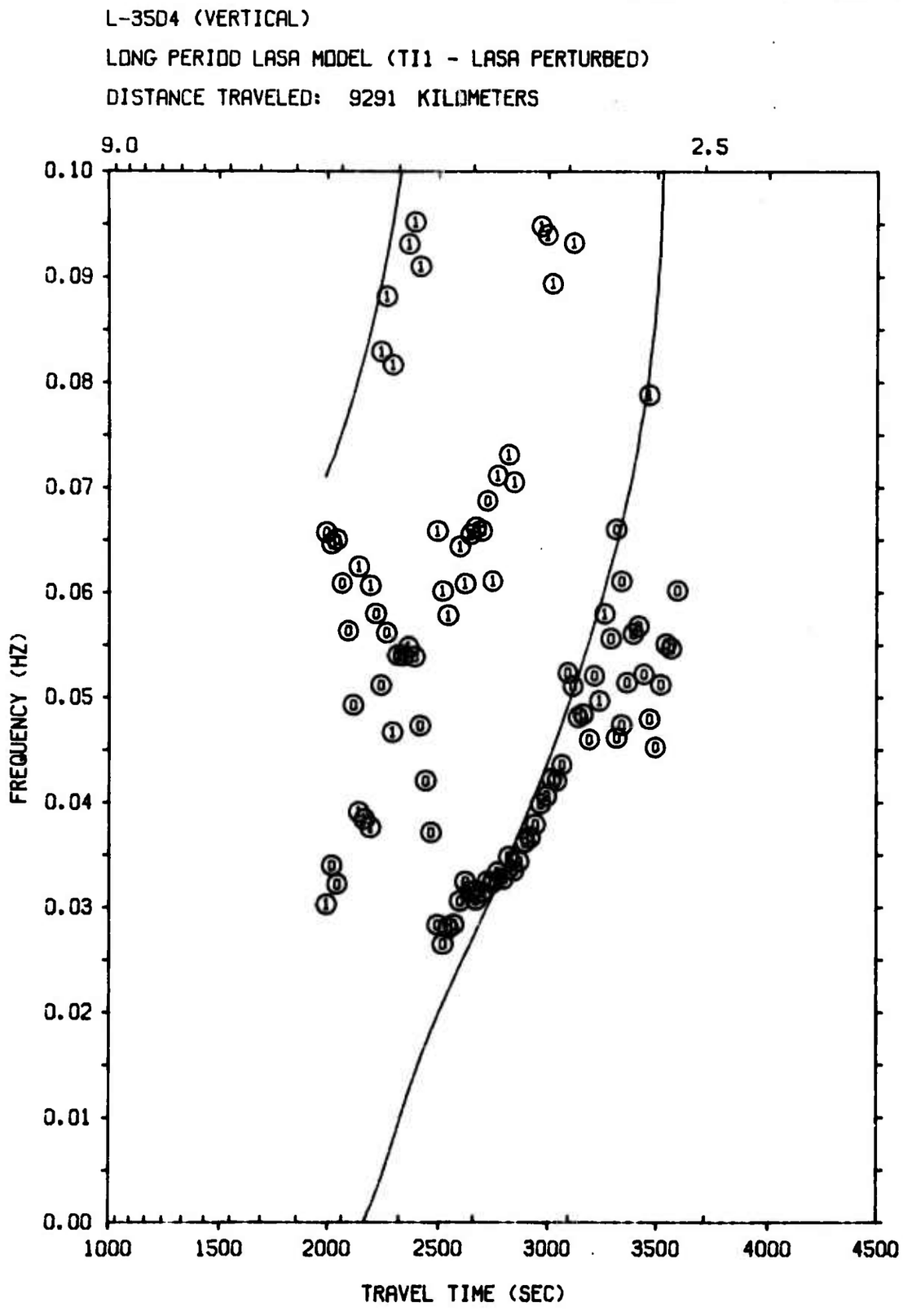

Figure IV-18. Experimental Dispersion Curve for L-35

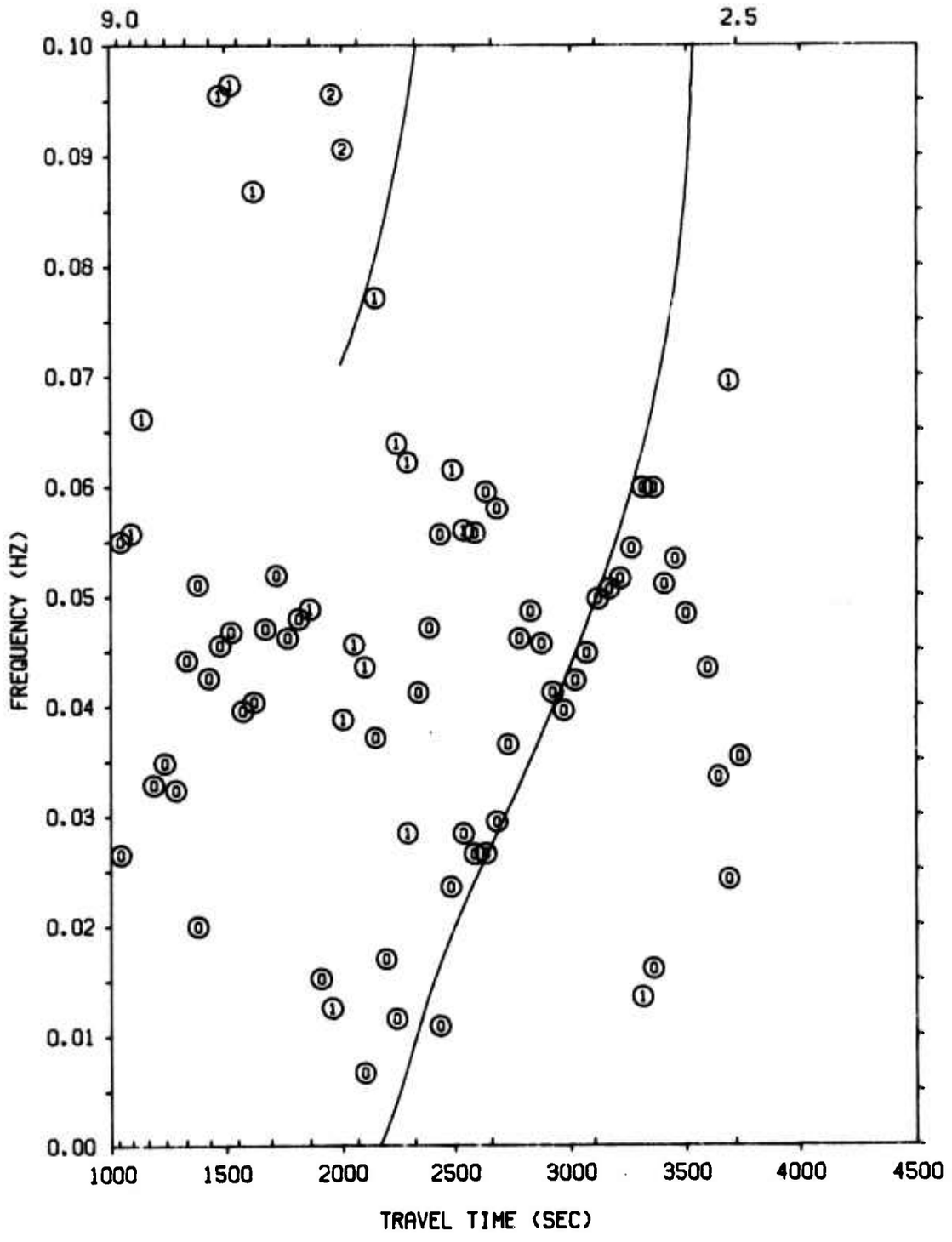

Figure IV-19. Experimental Dispersion Curve for L-36

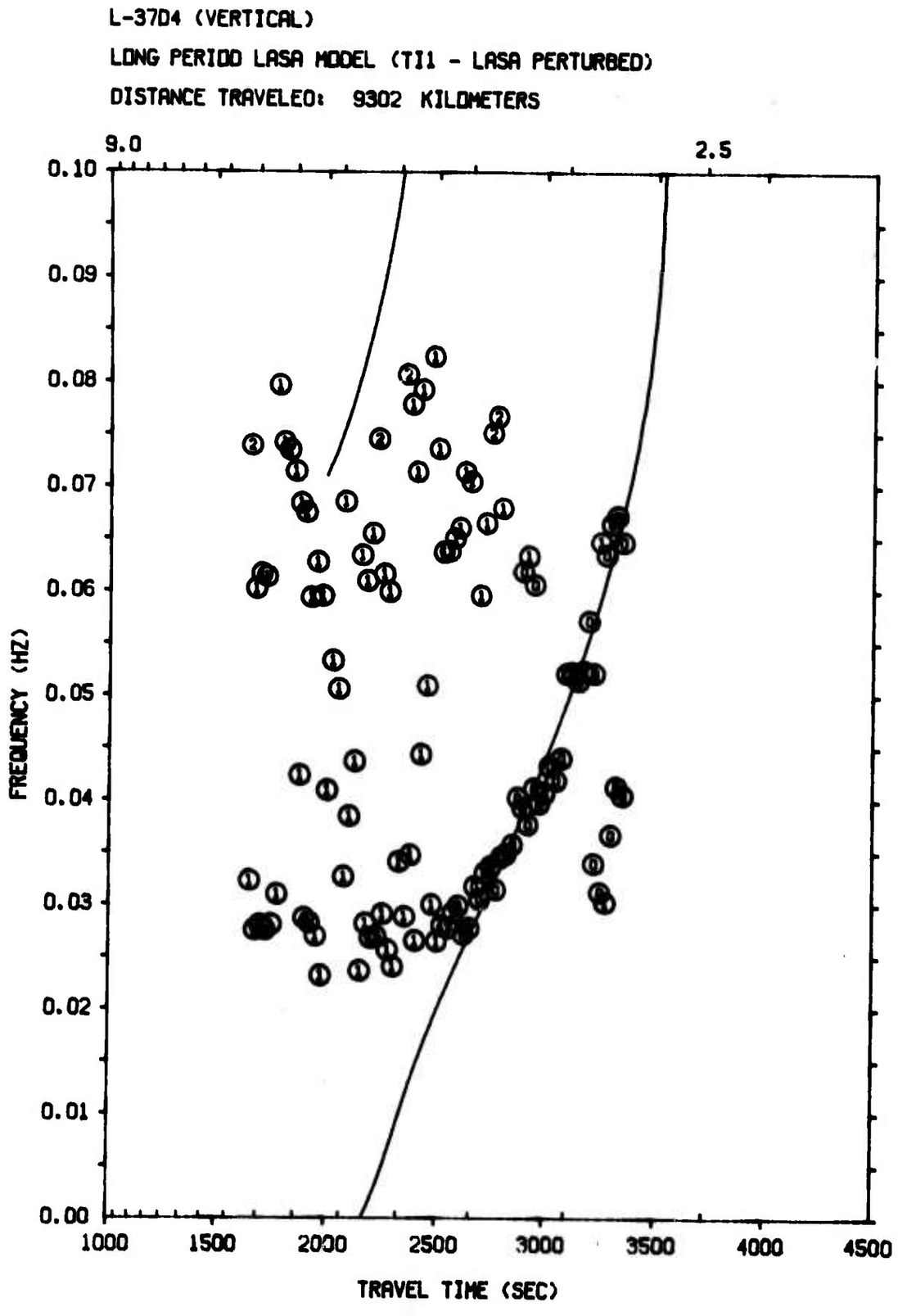

Figure IV-20. Experimental Dispersion Curve for L-37

0.03 Hz and 0.04 Hz at 3300 seconds, which were also present on the first test, remain unexplained but are most likely noise. The seismogram record ends at this point so additional processing is not possible.

The dispersion of L-38, Figure IV-21, shows a moderately persistent dispersion which agrees with the model although it is visible mainly by power rather than shape. This event also contains low-frequency peaks at 3400 seconds, similar to L-37. For this event, they appear to be noise. There is no apparent higher mode energy present.

Event L-39 has two features of note on its dispersion plot, Figure IV-22. First, there is narrowband noise at 0.06 Hz similar to L-30. Second, there appears to be perhaps four separate Rayleigh wave arrivals present. These begin roughly at 1600, 2100, 2600, and 3200 seconds on the plot. The third curve at 2600 seconds lies closest to the LASA predicted curve but arrives later than predicted by 100-300 seconds. Events in this region usually show close agreement with the LASA curve.

The curve beginning around 3200 seconds is from the surface waves of another event in the Andreanof Island whose origin time was 33-1/2 minutes after that of L-30. These waves can be seen in Figure IV-1 (sheet 2). The earlier two curves are most likely artifacts. A check of the LASA bulletins did not reveal any events which could account for them.

Events L-40 and L-41, Figures IV-23 and IV-24, show no indication of any dispersive wavetrains. Event L-41 has narrowband noise at two frequencies, at 0.03 Hz and at 0.07 Hz.

Event L-63, Figure IV-25, has a group-velocity dispersion in good agreement with the predicted dispersion. A few larger peaks appear around 2900 and 3500 seconds; however, it is most likely that these peaks are multipath or are related to the two relatively wide bands of noise at 0.02 Hz and 0.065 Hz.

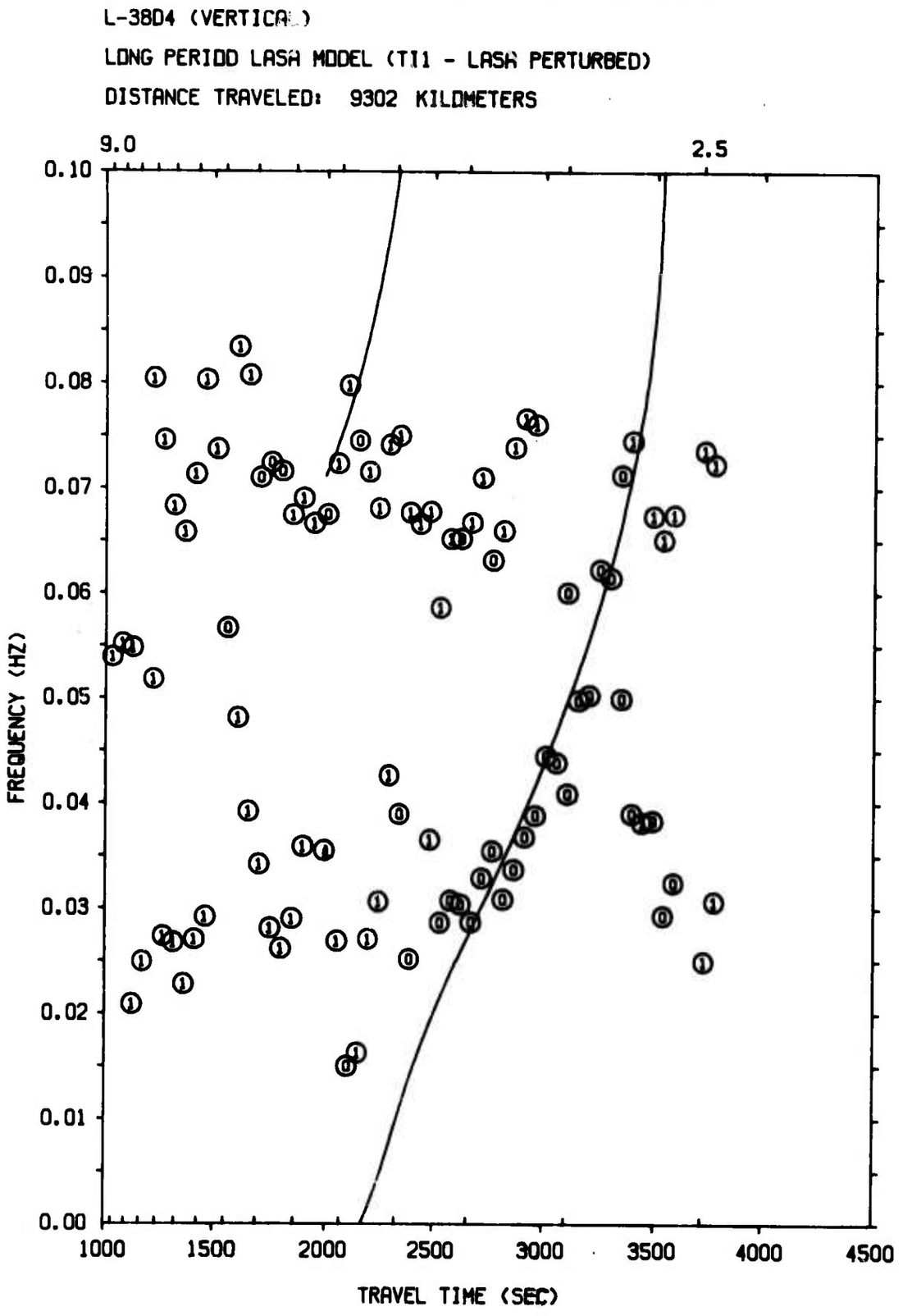

Figure IV-21. Experimental Dispersion Curve for L-38

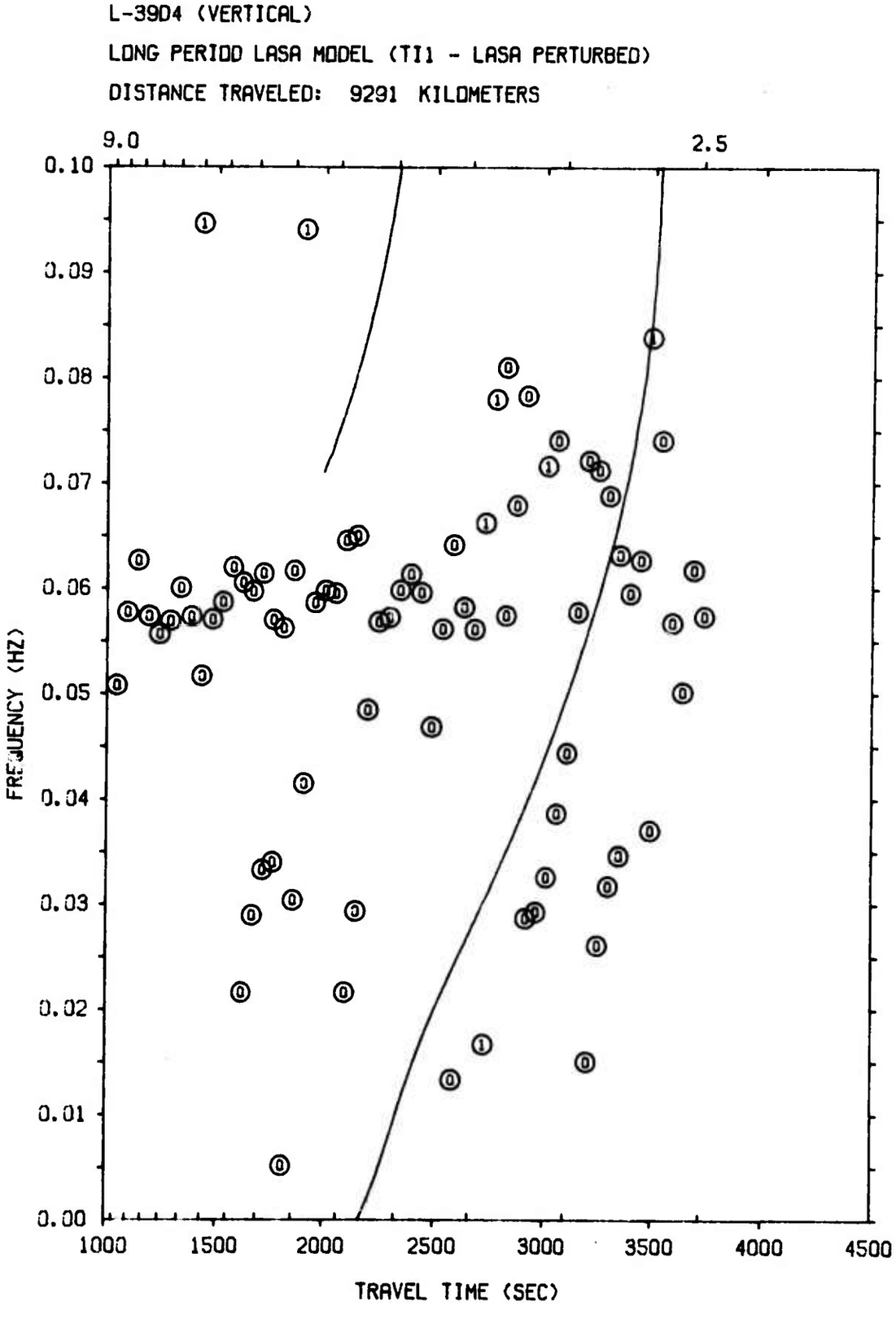

Figure IV-22. Experimental Dispersion Curve for L-39

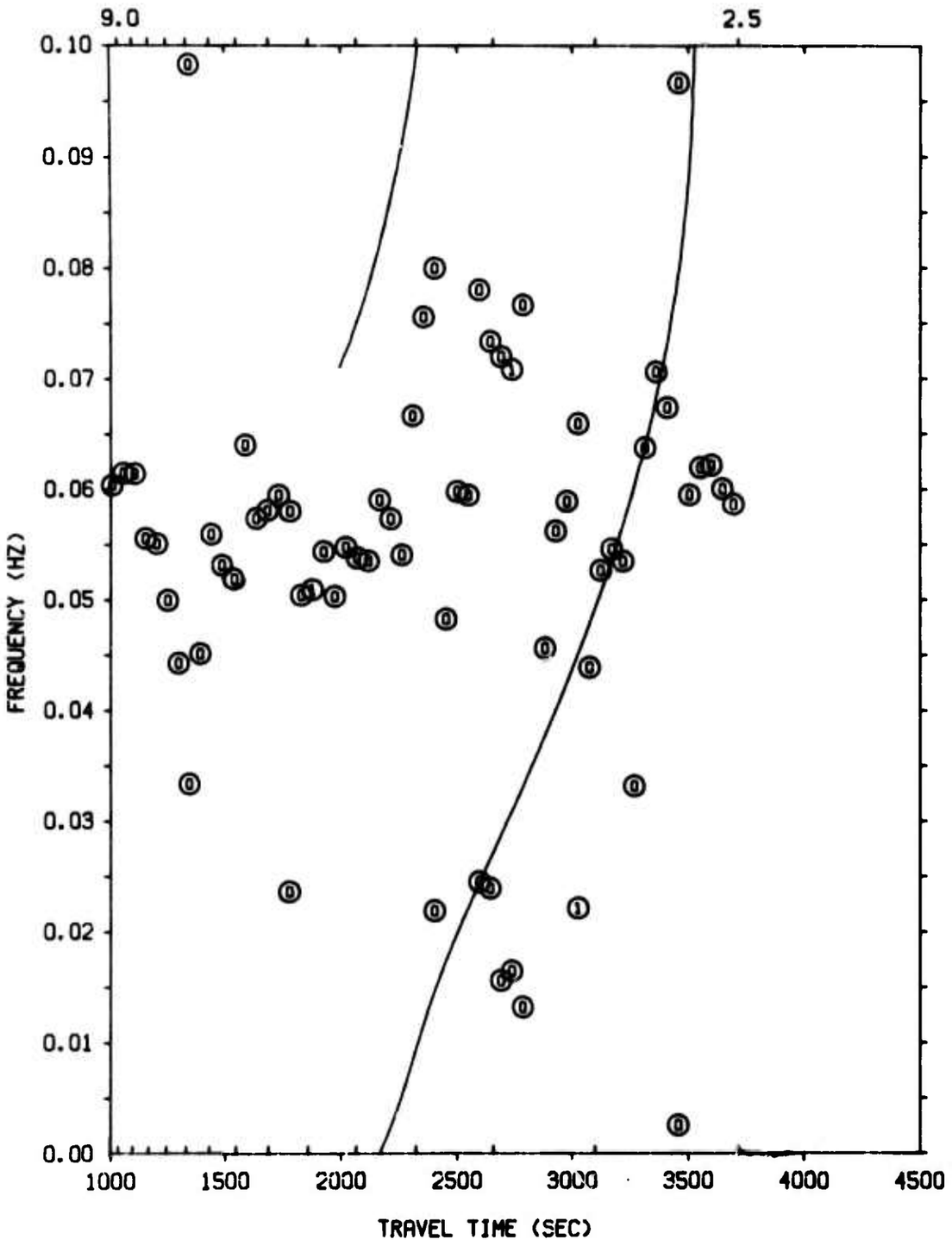

Figure IV-23. Experimental Dispersion Curve for L-40

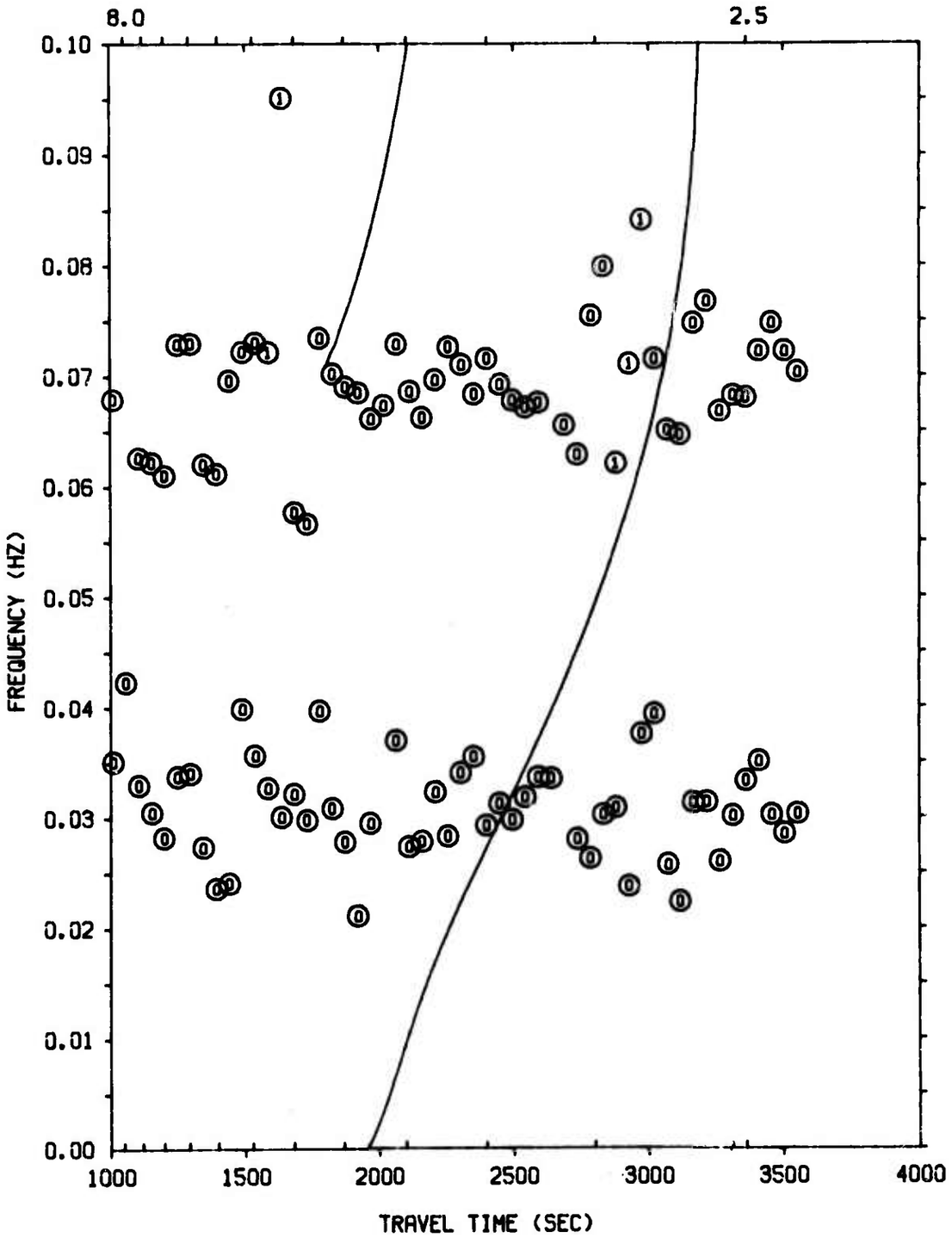

Figure IV-24. Experimental Dispersion Curve for L-41

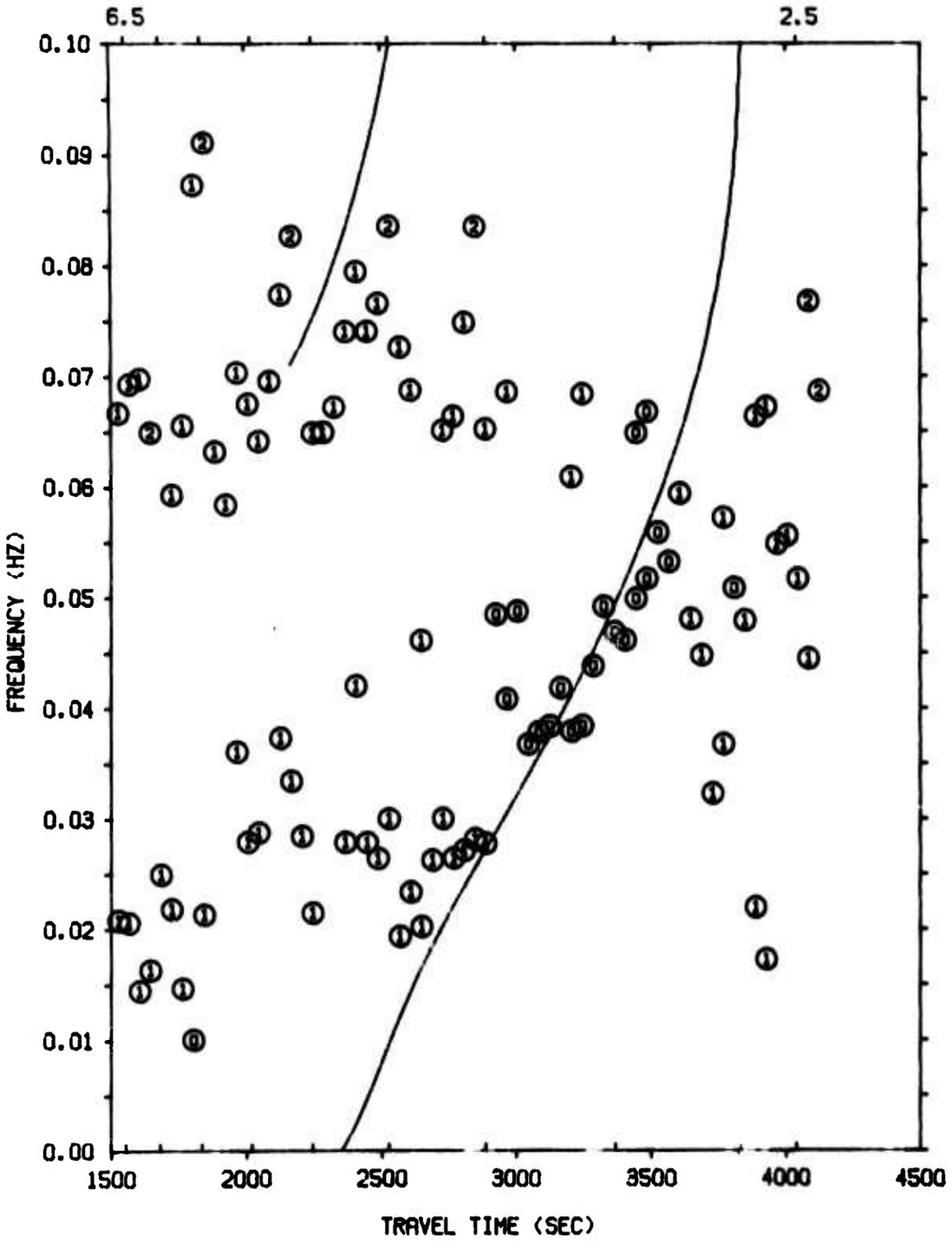

Figure IV-25. Experimental Dispersion Curve for L-63

Events EPX-14582 and EPX-14646 are Sinkiang events received from SAAC. Their dispersions are shown in Figures IV-26 and IV-27. Both events have very good agreement with the predicted group velocities. The seismograms were edited according to a group velocity range of 2.7 km/sec to 4.5 km/sec. This does not leave sufficient time record to analyze for higher modes through visual comparison of the pre-arrival noise. For this reason, the line of peaks from 0.03 Hz to 0.055 Hz beginning at 2400 seconds in Figure IV-26 cannot be categorized. For the same reason, the bunches of points at 0.03 Hz and 0.065 Hz in Figure IV-27 are not interpretable.

The major results and conclusions of the interpretation of the results for the China-Kazakh group are:

- The TI-1 LASA crustal model yields group velocity dispersion curve for the Rayleigh mode which agrees closely with the measured group velocities for events in the China-Kazahk group. This agreement is only coincidental however.
- Event L-35 exhibits two indications of possible higher mode energy. One of these is probably multipath; the other cannot be definitely identified without additional evidence.
- Some events contain substantial amounts of narrow-band noise in one or two bands which precedes the arrival of the Rayleigh mode. These events are L-30, L-31, L-34, L-39, L-41, and L-63. These bands are usually at a frequency of about 0.06 Hz and occasionally at 0.03 Hz.
- The five events processed which were obtained from SAAC had insufficient pre-arrival noise data to ascertain noise behavior which prevented possible higher mode detection.
- The ability of the maximum entropy technique to detect and measure surface-wave energy is limited generally to events whose signal-to-noise ratio is large enough to also allow their detection by eye. This corresponds to a signal-to-noise ratio between approximately 3 and 4.

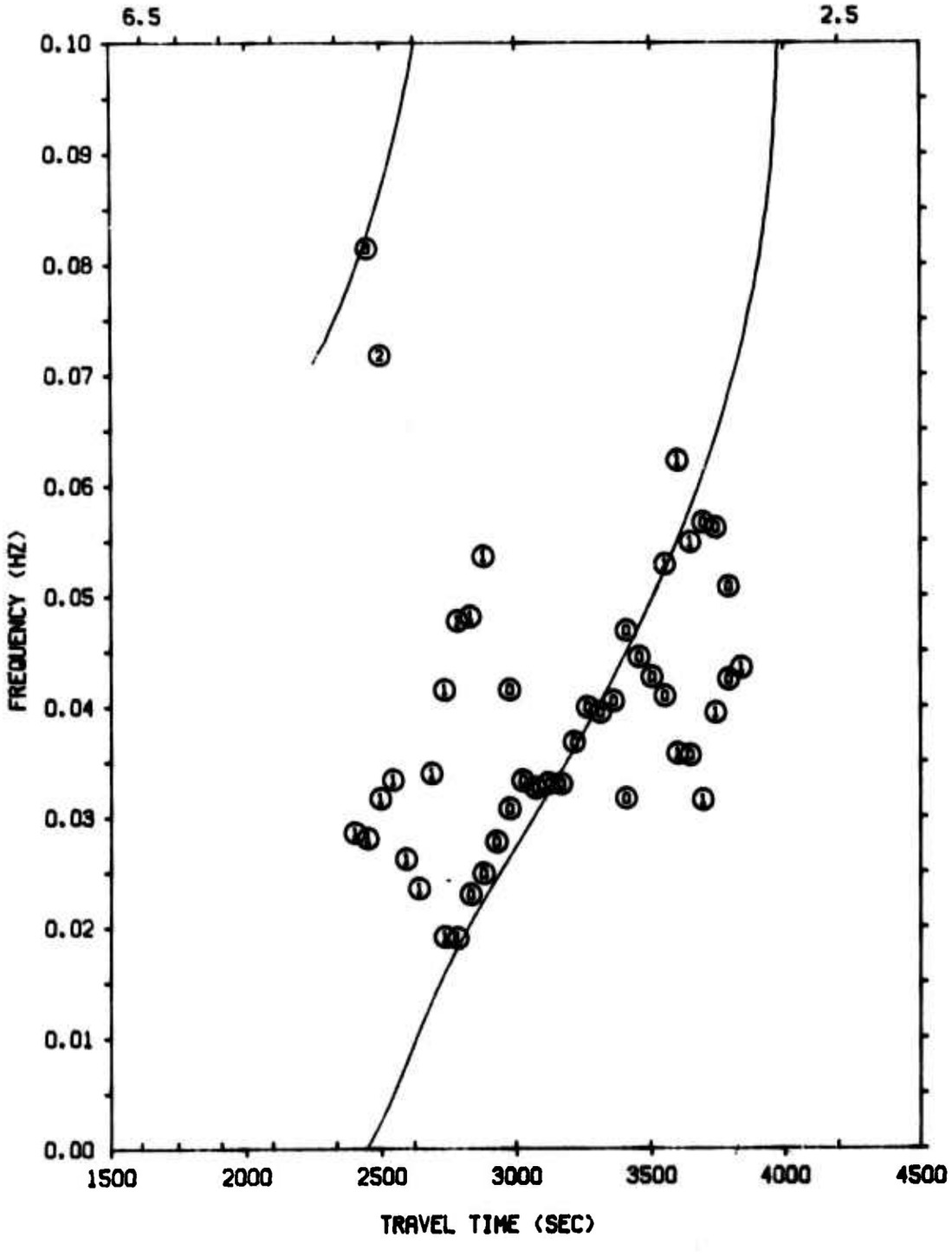

Figure IV-26. Experimental Dispersion Curve for EPX=14582

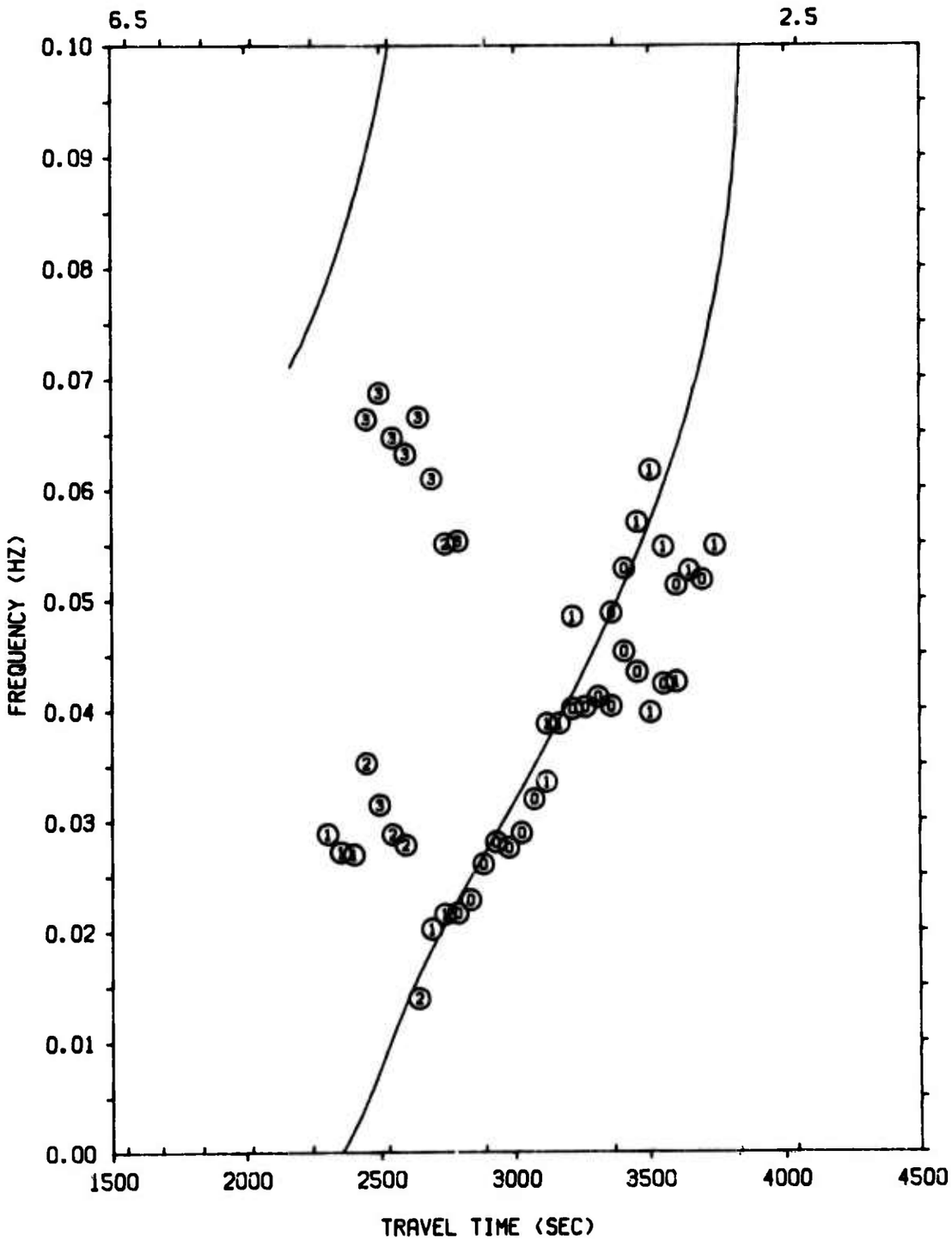

Figure IV-27. Experimental Dispersion Curve for EPX-14646

D. THE EUROPEAN GROUP

The European group consists of only three events: L-01, in the Greenland Sea, EPX-14649 in southern Norway, and EPX-18387 in the southern Caucasus. The range of azimuths is about 8 degrees. Except for crossing the Greenland Sea, a distance of approximately 1600 km, the paths are principally continental.

Event L-01 is a particularly "clean" event with high signal-to-noise ratio. Its group velocity dispersion, shown in Figure IV-28, agrees well with the LASA model prediction with the event group velocity slightly faster (0.1 km/sec) than predicted. Onset of the Rayleigh wave begins at a 0.015 Hz which is lower than that observed for most of the events analyzed. The smoothness of the dispersion curve is interrupted by a splitting at 0.055 Hz. This splitting is caused by the very sudden amplitude decrease occurring around 1900 seconds, which is reminiscent of the theoretical M_{11} mode behavior seen in Figure III-2.

S-waves arrival at about 1000 seconds appears as the "1" and "2" labeled peaks at 0.03 Hz.

Higher mode energy, probably M_{21}, appears at 0.04 Hz and 1250 seconds and sweeps rapidly to 0.075 Hz by 1450 seconds. Not shown in Figure IV-28 but visible in Figure IV-1 (sheet 1) is an indication of probably PL mode at 600 seconds. The presumed M_{21} energy does not agree with the model prediction but seems to have more of an oceanic character. Again, correct identification of PL-mode energy would require additional information not available here.

Event EPX-14649 produced a dispersion curve, Figure IV-29, similar to that of L-01. The break in the dispersion of L-01 at 0.055 Hz also occurs for this event indicating a crustal mechanism for the rapid drop in amplitude. The record is too short to tell if any modes other than Rayleigh mode are present.

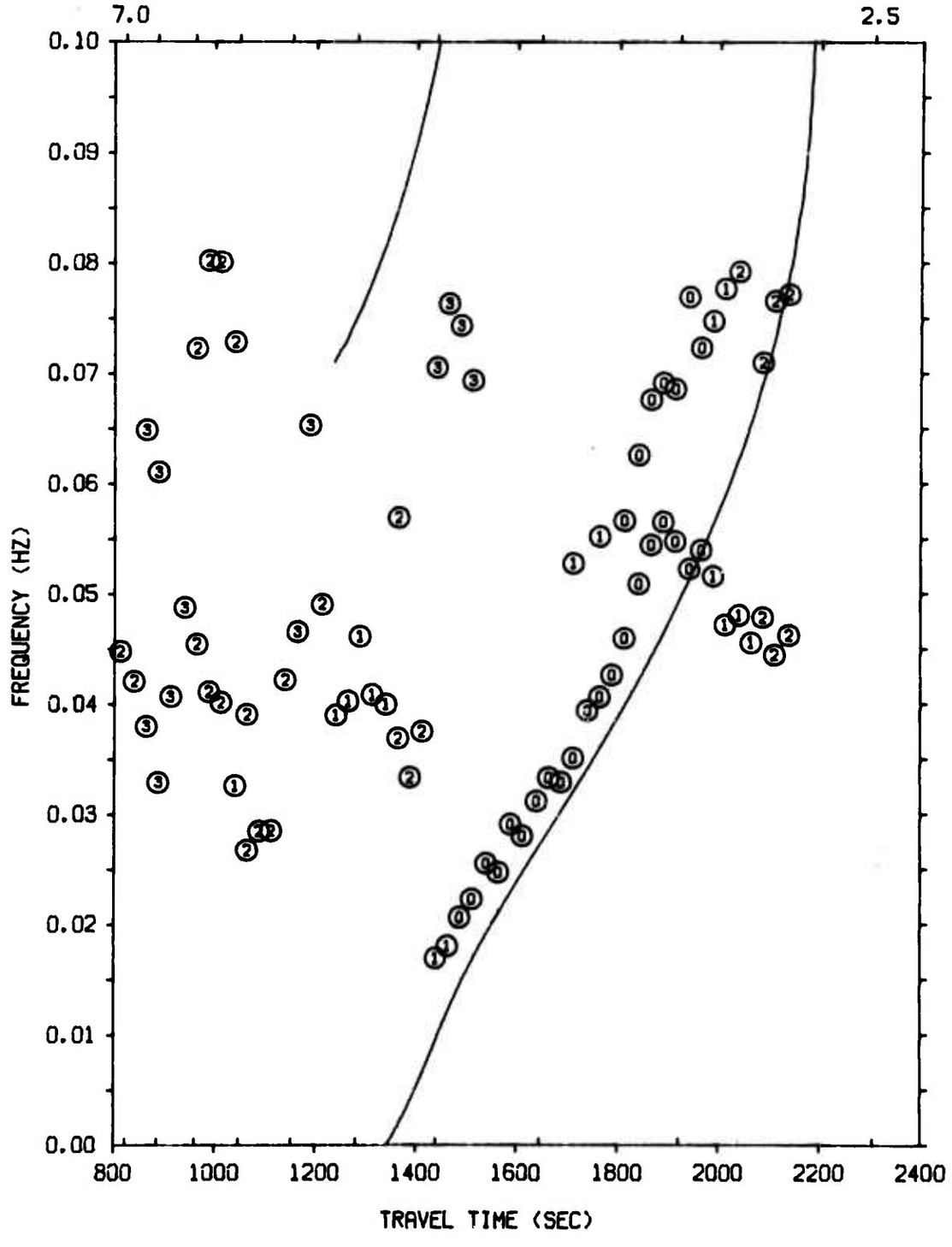

Figure IV-28. Experimental Dispersion Curve for L-01

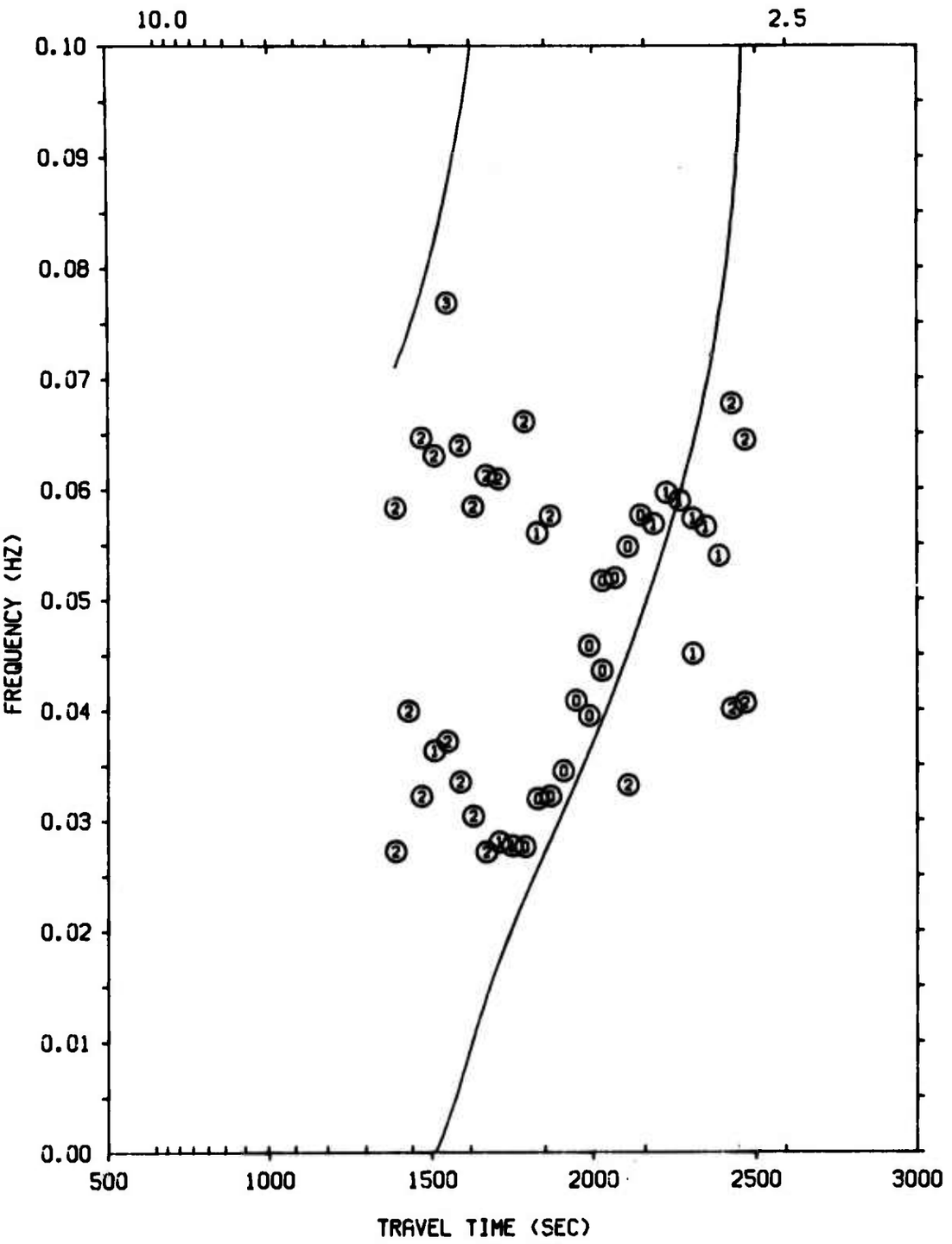

Figure IV-29. Experimental Dispersion Curve for EPX-14649

The group velocity dispersion of EPX-18387, Figure IV-30, is rather confused with four or five separate short sections present. The envelope of the surface waves is strongly and rapidly modulated, causing sum and difference frequencies and the multivalued dispersion. The path of this event is within a few degrees azimuth of L-01. The complicated dispersion must be caused by the continental section of travel northwest across eastern Russia.

The three points between 0.05 Hz and 0.06 Hz at 2300 seconds lie directly on the curve expected for M_{21} energy if the M_{21} energy suggested by L-01 discussed above is not an artifact. Unfortunately, the record duration of this event is too short to obtain an indication of noise behavior.

The results and conclusion obtained from the analysis of the European group are:

- Higher mode energy in the form of possible leaking mode and M_{21} is seen in event L-01. If the suspected M_{21} mode is actually present, then that mode is in poor agreement with what is expected from the LASA model and the propagation suggests a more oceanic crustal model.
- EPX-18387 has a confused M_{11} dispersion. However, there is evidence of M_{21} energy which would lie on the curve suggested by the possible M_{21} energy of L-01.

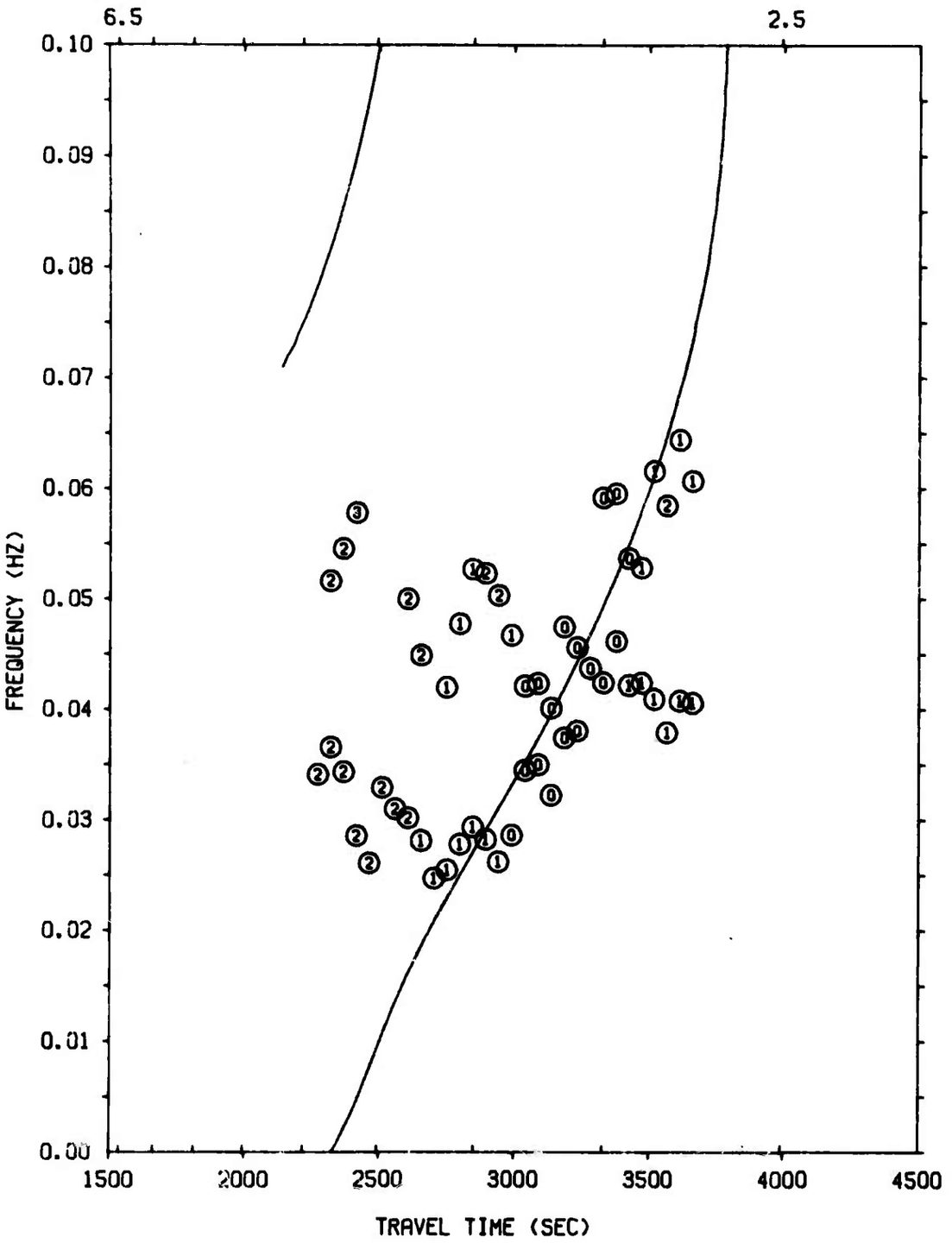

Figure IV-30. Experimental Dispersion Curve for EPX-18387

SECTION V
CONCLUSION

Maximum entropy spectral analysis has been shown to be an effective method for computing group-velocity frequency curves of seismic events. The procedures used for this report are able to detect spectral components accurately down to signal-to-noise ratios estimated at around 3 or 4. This is probably much better than that obtained by similar methods for at least two reasons. First, the spectra are not obscured by the spectral window effects attendant to the usual Fourier analysis. Second, the method gives good frequency estimates even with a small amount of data.

The analysis of the LASA long-period seismograms produced only a few instances of possible higher mode energy. These modes were tentatively identified as PL "leaking" modes and M_{21} modes. Positive identification was not possible because of the lack of substantiating evidence. The group-velocity curves calculated from a LASA crustal model were originally included in the travel time plots as an aid to identification of the M_{11} and M_{21} modes. This was only partially successful. The measured group velocity of Rayleigh waves usually were within a few tenths of a km/sec of that predicted by the LASA model. The few instances of possible M_{21} waves did not agree at all with the LASA prediction in frequency but did arrive about when expected. If in the future higher mode identification is attempted by this type of comparison, a realistic crustal structure for the entire propagation path must be used.

The earthquakes having indication of higher mode all had either continental or nearly continental paths, being either from the Gulf of California or Europe. It appears that continental-path events and large signal-to-noise ratio events at smaller distances are more likely to have observable higher mode waves. There are two probable causes. First, inelastic attenuation is

greater at higher frequencies. Since the higher modes encompass a higher frequency band than does the fundamental Rayleigh mode, they are selectively attenuated and usually are unobservable at teleseismic distances. Second, the higher modes for many crustal structures will be outside the passband (on the high frequency side) of the long-period seismometer. For thicker (e.g., continental) crusts, the higher modes are shifted downward in frequency, thus increasing the chances of observation.

Neither of these causes for non-observation of higher modes is useful from the standpoint of discrimination. It appears at this point that no useful higher mode discriminant is available at teleseismic distance. However, it is still quite likely that higher modes will provide useful discriminants at shorter (regional) distances.

SECTION VI

REFERENCES

1. Oliver, Jack and Maurice Ewing, 1957: Higher modes of continental Rayleigh waves, Bull. Seism. Soc. Am., v. 47, No. 3, July, p. 187-204.

2. Crampin, Stuart, 1965: Higher modes of seismic surface waves: second Rayleigh mode energy, J. Geophys. Res., v. 29, No. 20, 15 Oct., p. 5135.

3. Burg, J. P., 1967: Maximum entropy spectral analysis, Presentation at 37th Meeting of the Soc. of Exploration Geophysicists, Oklahoma City, Okla.

4. Burg, J. P., 1968: A new analysis technique for time series data, Presentation at the NATO Advanced Study Institute on Signal Processing with Emphasis on Underwater Acoustics, Enschede, Holland, Aug.

5. Oliver, Jack and Maurice Ewing, 1958: Normal modes of continental surface waves, Bull. Seism. Soc. Am., v. 48, Jan., p. 33-49.

6. Crampin, Stuart and Markus Bath, 1965: Higher modes of seismic surface waves: mode separation, Geophys. J., v. 10, p. 81-92.

7. Alexander, Shelton S.: Methods of mode separation of seismic surface waves, Contribution 1307, Div. of Geological Sciences, Calif. Institute of Technology, Pasadena, Calif.

8. Binder, F. H., 1970: A preliminary study of techniques for routine matched filtering of surface waves, Texas Instruments Incorporated Technical Rpt. No. 4, Contract F33657-70-C-0100, 27 Apr.

9. Laster, S. J., J. G. Foreman, and A. F. Linville, 1965: Theoretical investigation of modal seismograms for a layer over a half-space, Geophs., v. XXX, No. 4, Aug.

10. Texas Instruments Incorporated, 1967: Continuation of Basic Research in Crustal Studies, Final Report, Contract AF 49(638)-1588, AFOSR, 15 July.

11. Shubet, D. H., 1961: Determination of sedimentary thickness in the Mexican geosyncline by Rayleigh wave dispersion, J. Geophys. Res., vol. 66, No. 3, Mar.

12. Texas Instruments Incorporated, 1970: Statistical Discrimination, Quarterly Report No. 2, Contract F 33657-70-C-0311, 15 Apr.

UNCLASSIFIED

Security Classification

DOCUMENT CONTROL DATA - R & D

(Security classification of title, body of abstract and indexing annotation must be entered when the overall report is classified)

1. ORIGINATING ACTIVITY (Corporate author)
Texas Instruments Incorporated, Services Group,
P. O. Box 5621, Dallas, Texas 75222

2a. REPORT SECURITY CLASSIFICATION
Unclassified

2b. GROUP
None

3. REPORT TITLE
"Higher Mode Detection Studies"

4. DESCRIPTIVE NOTES (Type of report and inclusive dates)
Technical Report No. 3 30 November 1970

5. AUTHOR(S) (First name, middle initial, last name)
William H. Swindell

6. REPORT DATE
30 November 1970

7a. TOTAL NO. OF PAGES
98

7b. NO. OF REFS
12

8a. CONTRACT OR GRANT NO.
F 33657-70-C-0311

b. PROJECT NO.
VELA T/0702/B/ASD

c.

d.

9a. ORIGINATOR'S REPORT NUMBER(S)

9b. OTHER REPORT NO(S) (Any other numbers that may be assigned this report)

10. DISTRIBUTION STATEMENT
This document is subject to special export controls and each transmittal to foreign governments or foreign nationals may be made only with prior approval of Chief, AFTAC.

11. SUPPLEMENTARY NOTES
ARPA Order No. 624

12. SPONSORING MILITARY ACTIVITY
Advanced Research Projects Agency
Department of Defense
The Pentagon
Washington, D. C. 20301

13. ABSTRACT

This report presents results of applying a maximum entropy power spectrum analysis technique to detect higher order mode surface waves. The algorithm used partitioned each seismogram into time gates representing average group velocities, and spectral analysis was used to determine the periods of the data in the gates. The technique was tested successfully on artificial seismograms containing the Rayleigh and three higher modes of surface waves, with and without additive noise. Maximum entropy power spectrum analysis techniques were applied to an ensemble of 29 long-period seismograms obtained from LASA arrays. The long-period seismograms were of both continental and continental-oceanic paths. While several instances of possible higher mode waves were revealed by the analysis, no consistency was found in the occurrence of these modes. Major conclusions were that ME spectrum analysis provides finer details in seismogram spectra than are otherwise available and that it provides an effective method for computing group-velocity frequency curves.

DD FORM 1 NOV 68 1473

UNCLASSIFIED

Security Classification

14 KEY WORDS	LINK A		LINK B		LINK C	
	ROLE	WT	ROLE	WT	ROLE	WT
Discriminant						
Higher Mode						
Mchirp filtering						